Norwegian University
of Life Sciences

Master's Thesis 2019 60 ECTS
Faculty of Chemistry, Biotechnology and Food Science

Studying substrate specificity by site-directed mutagenesis of a novel lytic polysaccharide monooxygenase

Amanda Kristine Votvik
Master of Biotechnology

Studying substrate specificity by site-directed mutagenesis of a novel lytic polysaccharide monooxygenase

Master Thesis

Amanda Kristine Votvik

Protein Engineering and Proteomics Group

Faculty of Chemistry, Biotechnology and Food Science

The Norwegian University of Life Sciences (NMBU)

2019

The Norwegian University of Life Sciences SEP 2019

ACKNOWLEDGEMENTS

The research for this thesis was carried out in the Protein Engineering and Proteomics (PEP) group at the Faculty of Chemistry, Biotechnology and Food Science at the Norwegian University of Life Sciences, supervised by Professor Vincent G. H. Eijsink, Dr. Zarah Forsberg and Ph.D. candidate Anton Stepnov.

A special thanks to my first supervisor Anton Stepnov, an inspiring (and mad) scientist/boxer from Russia, for his dark humor and low tolerance for bullshit, which got me through the first months in the lab. You continue to motivate and make me laugh, for that and the above, I am forever grateful.

My upmost appreciation to Dr. Zarah Forsberg, for her countless advice, guidance, and encouragement. It truly has been an honor to have you as a supervisor;
thank you for believing in me.

My deepest gratitude goes to Professor Vincent Eijsink, for offering me the opportunity to write my thesis in the PEP group. His passion for science and immense knowledge of enzymology has truly inspired me. Thank you, for your honest feedback, patience, and support.

I also wish to thank all the people in, and around, the PEP group, who have helped me and shared their knowledge. I have really enjoyed my time at the lab, working with such accomplished and inspiring scientists.

Marius, your company at “Palasset” has been paramount.

Last but not least, my mom, Torill Pauline Walla. Thank you for always being there for me, I could never have done this without you.

Ås, July 2019

Amanda Kristine Votvik

SUMMARY

Cellulose and chitin are carbon-rich biopolymers which constitute the two largest biomass resources on earth. Conversion of these non-edible and renewable resources into useful products of value is essential to secure a sustainable bioeconomy. However, the efficient processing of cellulose and chitin is hampered by their recalcitrant nature.

To exploit the energy-rich composition of these homopolymers, different microorganisms have evolved specialized enzyme systems which include enzymes referred to as lytic polysaccharide monooxygenases (LPMOs). LPMOs are copper-dependent enzymes, which in the presence of an external electron donor, catalyzes cleavage of the glycosidic linkages in recalcitrant polysaccharides through an oxidative and somewhat enigmatic reaction mechanism. LPMOs display relatively flat substrate binding surfaces which enables them to bind to the planar surface of crystalline polysaccharides. Various structural motifs, of conserved surface exposed residues found on the substrate binding face, are believed to contribute the specific oxidizing activity of LPMOs toward different polysaccharides.

Seven LPMO encoding genes are found within the genome of the Gram-negative soil bacterium *Streptomyces coelicolor*. Among these LPMOs, various specificities for substrate and regioselectivities have been identified such as C1- or C1/C4-spesific cellulose oxidizing enzymes, and enzymes which display activity both toward cellulose (C1/C4) and chitin (C1). One of these enzymes which have not been characterized yet, called *Sc*LPMO10D, exhibits a catalytic domain with conserved motifs specific for both chitin- and cellulose oxidizing LPMOs. In addition, *Sc*LPMO10D exhibit a C-terminal domain that have been predicted to covalently anchor the catalytic domain to the cell wall, an unusual feature which may classify *Sc*LPMO10D within a novel clade of Auxiliary Activity Family 10 (AA10) enzymes.

In this study, *Sc*LPMO10D was characterized as a chitin oxidizing enzyme with particular specificity toward β-chitin. Taking advantage of its sequence similarity to cellulose-oxidizing

AA10s, five surface-exposed residues were targeted for site-directed mutagenesis in an attempt to change the substrate specificity toward cellulose. Out of the six mutants produced, none displayed activity toward cellulose. However, out of two mutants with retained activity on β-chitin, one displayed an initial rate of catalytic activity which exceeded the wild type enzyme.

SAMMENDRAG

Cellulose og kitin er karbonrike biopolymerer som utgjør to av de største biomasse-ressursene på jorden. Enzymatisk omdanning av disse ikke-spiselige og fornybare ressursene, til nyttige produkter av verdi, regnes som et avgjørende steg for å sikre en bærekraftig bioøkonomi. Kostnadseffektiv prosessering av kitin, men aller mest cellulose, er derfor et viktig mål innen industriell bioteknologi; et mål som foreløpig er hindret av deres tungt nedbrytbare oppbygning.

For å utnytte den energirike sammensetningen av disse homopolymerne, har forskjellige mikroorganismer utviklet intrikate enzymsystemer som blant annet inkluderer enzymer, kalt lytiske polysakkarid-monooksygenaser (LPMOer). LPMOer kobberavhengige enzymer som, ved hjelp av en ekstern elektrondonor, katalyserer spalting av glykosidbindingene til forskjellige polysakkarider, via en oksidativ og noe gåtefull reaksjonsmekanisme. Detter er blant annet mulig fordi LPMO-enzym har en relativt flat substratbindende overflate som gjør dem i stand til å binde til de krystallinske flatene til kitin og cellulose. Ulike strukturelle motiver, bestående av høyst konserverte aminosyrer lokalisert på den substratbindende overflaten til LPMO-enzymer, antas å spille en viktig rolle for den spesifikke katalytiske preferanse for forskjellige polysakkarider.

Genomet til den Gram-negative jordbakterien *Streptomyces coelicolor,* koder for syv forskjellige LPMO-enzymer. Blant disse, har enzymer med forskjellige preferanser for både substrat og karbon-oksiderende selektivitet blitt identifisert. Mens noen viser spesifisitet for cellulose og oksidering av C1-karbonet i glykosidbindinger, kan andre både oksidere C1 og C4 i cellulose, i tillegg til C1 i kitin. Et annet enzym blant disse syv LPMOene, som tidligere ikke har blitt karakterisert, er *Sc*LPMO10D. Dette spesielle LPMO-enzymet har et katalytisk domene med konserverte motiver som ellers har blitt utpekt som spesifikke for enten kitin- eller cellulose-oksiderende LPMOer. *Sc*LPMO10D viser også et uvanlig C-terminalt domene, som har blitt predikert til å forankre det katalytiske domenet til celleveggen gjennom kovalent binding. Dette er en egenskap som skiller seg ut blant majoriteten av Familie 10 enzymer, innen karbohydrat-

aktive hjelpeenzymer (Auxiliary Activities Family 10, AA10), og kan derfor muligens resultere i dannelse av en ny klade.

I dette studiet ble *Sc*LPMO10D karakterisert som et kitin-oksiderende enzym, med særlig spesifisitet overfor β-kitin. Ved å utnytte sekvenslikheten *Sc*LPMO10D allerede deler med cellulose-oksiderende AA10-enzymer, ble fem aminosyrer på den substratbindene overflaten mutert med spesifikk hensikt for å modifisere *Sc*LPMO10D om til et cellulose-oksiderende enzym. Av seks produserte mutanter, viste ingen aktivitet på cellulose. Men, av to mutanter som beholdt aktivitet på β-kitin, viste en mutant en innledende katalytisk aktivitet som overgikk villtypen.

TABLE OF CONTENTS

ACKNOWLEDGEMENTS ..... **I**

SUMMARY ..... **II**

SAMMENDRAG ..... **I**

TABLE OF CONTENTS ..... **I**

ABBREVIATIONS ..... **V**

1. INTRODUCTION **1**

1.1 THE FUTURE BIOECONOMY 1

1.2 CARBOHYDRATES 4

1.2.1 Cellulose *5*

1.2.2 Chitin *7*

1.2.3 Microbial degradation of recalcitrant polysaccharides *10*

1.2.4 Degradation of recalcitrant polysaccharides by free enzyme systems *11*

1.3 LYTIC POLYSACCHARIDE MONOOXYGENASES 14

1.3.1 Early history of LPMO discovery *14*

1.3.2 Classification, occurrence and substrate specificity *16*

1.3.3 Global structure, catalytic site and modularity *19*

1.3.4 Catalytic mechanism *21*

1.3.5 Further aspects of catalytic activity *25*

1.3.6 Determinants of substrate-binding and oxidative regioselectivity *28*

1.4 AIMS OF THIS STUDY 29

2. MATERIALS **31**

2.1 LABORATORY EQUIPMENT 32

2.2 CHEMICALS AND BUFFERS 34

2.3 SELF-MADE BUFFERS AND STOCK SOLUTIONS 35

2.4 BACTERIAL STRAINS 36

2.5 KITS 36

2.6 SUBSTRATES 38

2.7 ENZYMES AND PROTEIN 38

2.8 SOFTWARE AND ONLINE APPLICATIONS 39
2.9 PRIMERS 40

3. METHODS 41

3.1 CULTIVATION OF *ESCHERICHIA COLI* 41
3.1.1 Antibiotics 41
3.1.2 Agar and cultivation media 42
3.1.3 Cultivation in small volumes 43
3.1.4 Long-term storage of bacterial cultures 43
3.2 PRODUCTION OF MUTANTS 44
3.2.1 Primer design 44
3.2.1.1 Primer preparation 45
3.2.2 Plasmid isolation 45
3.2.3. QuikChange II XL Site-Directed Mutagenesis 47
3.2.4. Transforming chemically competent cells 48
3.2.5. Verification of directed mutations 49
3.3 EXPRESSION, PURIFICATION AND PREPARATION OF ENZYMES 50
3.3.1 Overexpression expression 50
3.3.2 Osmotic shock extraction 51
3.3.3 Sodium dodecyl sulfate polyacrylamide gel electrophoresis (SDS-PAGE) 52
3.3.4 Buffer-exchange and concentrating protein solutions with centrifugal filters 53
3.3.5 Anion-Exchange Chromatography 54
3.3.6 Size-Exclusion Chromatography 56
3.3.7 Direct photometric measurement of protein (A280) 57
3.3.8 Saturating LPMOs with copper 58
3.3.9 Determination of protein purity using SDS-PAGE 60
3.4 ENZYME CHARACTERIZATION 60
3.4.1 LPMO activity assays 60
3.4.1.1 Wild type activity assay 60
3.4.1.2 Other LPMO-activity assays 61
3.4.1.3 H_2O_2-supplemented activity assay 62
3.4.2 MALDI-TOF mass spectroscopy analysis of oxidized products 63
3.4.3. PRODUCT ANALYSIS BY ION CHROMATOGRAPHIC SYSTEM (ICS) 64
3.4.4 Thermal shift assay 66
3.4.5 Binding assay 67

3.4.5.1 Wild type binding assay with chitin substrates 67
3.4.1.2 Combined binding and activity assay, wild type and mutants 68
3.4.6 Bradford assay *69*
3.4.7 Hydrogen peroxide assay *70*

4. RESULTS & DISCUSSION 73

4.1 CHARACTERIZATION OF WILD TYPE *SC*LPMO10D 73
4.1.1 Production of wild type ScLPMO10D *74*
4.1.1 Substrate specificity and product profile *75*
4.1.2 Binding assay with α- and β-chitin *78*
4.2 RATIONAL DESIGN AND SITE-DIRECTED MUTATION 79
4.2.1 Homology modeling *80*
4.2.2 Sequence analysis *81*
4.2.3 Structural alignment and final mutant designs *82*
4.2.4 Site directed mutagenesis *84*
4.3 PRODUCTION OF *SC*LPMO10D MUTANTS 86
4.3.1 Expression and extraction *86*
4.3.2 Purification *88*
4.3.3 Copper saturation and final yield *93*
4.5 INVESTIGATION OF MUTATIONAL EFFECTS 96
4.5.1 Activity of wild type ScLPMO10D and its mutants *96*
4.5.1 Apparent melting temperatures *97*
According to the results from the Thermal Shift Assay (Fig 4.14), all mutants and wild type enzyme seems to bind copper (except for the missing value for 4b-apo). Although the mutants displayed a lower Tm than the wild type, there is not a significant difference in melting temperature between them. The results from Thermal Shift Assay are dependent on many factors which can be *97*
4.5.2 Binding β-chitin *99*
4.5.3 H_2O_2 production *100*
4.5.5 H_2O_2 supplemented activity *102*

..... 104

6. REFERENCES 105

7. APPENDICES X

APPENDIX A X

APPENDIX B XI

ABBREVIATIONS

A_{280} / A_{260} /A_{595}	Absorbance of ultraviolet light at e.g., 280 nm
AA	Auxiliary activity
AEC	Anion Exchange Chromatography
Å	Ångström (0.1 nanometers)
CAZy	Carbohydrate-Active Enzyme
CBM	Carbohydrate-Binding Module
CBP	Chitin-binding protein
CDH	Cellobiose dehydrogenase
DNA	Deoxyribonucleic Acid
Da	Dalton
dNTP	Deoxynucleotide Triphosphate
DP	Degree of Polymerization
EDTA	Ethylenediaminetetraacetic Acid
GH	Glycoside Hydrolase
Glc	Glucose
GlcNAc	*N*-Acetylglucosamine
GlcN	Glucosamine
HPAEC-PAD	High-Performance Anion Exchange with Pulsed Amperometric Detection
ICS	Ion Chromatography System
IPTG	Isopropyl b-D-1-thiogalactopyranoside
kDa	Kilo Dalton
LB	Lysogeny Broth
LPMO	Lytic Polysaccharide Monooxygenase
MALDI-ToF	Matrix Assisted Laser Desorption/Ionization-Time of Flight
MS	Mass Spectrometry

MSA	Multiple Sequence Alignment
PASC	Phosphoric-Acid Swollen Cellulose
PCR	Polymerase Chain Reaction
PDB	Protein Data Bank
rpm	Rotation per minute
SDS-PAGE	Sodium Dodecyl Sulfate-Polyacrylamide Gel Electrophoresis
SEC	Size Exclusion Chromatography
TB	Terrific Broth

1. INTRODUCTION

1.1 The future bioeconomy

The necessity of a green industrial revolution has become increasingly evident in the past decade. Fossilized carbon reservoirs (e.g. petroleum, gas, and coal) are finite resources, which have required millions of years to compose, and thus bound to run out eventually. Nevertheless, global economy continues to rely primarily on hydrocarbons to meet the growing demand for fuel, energy, and chemicals (International Energy Agency, 2018), which is potentially steering civilization toward an economic dead end. While shifting to renewable alternatives is urgent due to economic concerns, continuing use of non-renewables also has critical environmental implications. Extensive burning of fossil fuels is causing dangerously poor air-quality in densely populated regions and contributes to global climate change via immense CO2 emissions (Vanholme et al., 2013; Perera, 2017). In addition, petroleum-derived debris (e.g. plastics and synthetic fibers) is accumulating at an exponential rate in terrestrial and marine ecosystems, where it pollutes the environment, causes harm to animal species, and enters the human food chain as microplastic particles (Barnes et al., 2009; Geyer et al., 2017; Cox et al., 2019).

Increased global awareness regarding the above issues has elevated the economic and scientific interest in biofuels, biodegradable materials, and other bio-based goods. Bio-based economy, or bioeconomy, is an economic model focusing on exploiting vacant biomass recourses, like non-edible biomass and byproducts from agriculture, aquaculture and food production, which can be processed into food, fuel, and other valuable products (Fig. 1.1). A key concept within the bioeconomy is the utilization of biological principles and processes for industrial and commercial purposes. For example, biorefineries use enzyme technology to convert plant biomass into fermentable mono-sugars, which thereafter can be transformed into biofuels (e.g. bioethanol) or other chemicals through microbial fermentation. The majority of today's bioethanol production relies on first-generation feedstocks that are easy to process, i.e., food crops like sugarcane and

corn. However, cultivation of edible feedstocks compromises food production by battling for cropland, water supply, and other limited resources such as phosphorous (Rulli et al., 2016; Hein, 2012). Second-generation feedstocks, such as lignocellulose (i.e. plant fiber), on the other hand, can be derived as non-edible plant residues from an expanding food-crop production.

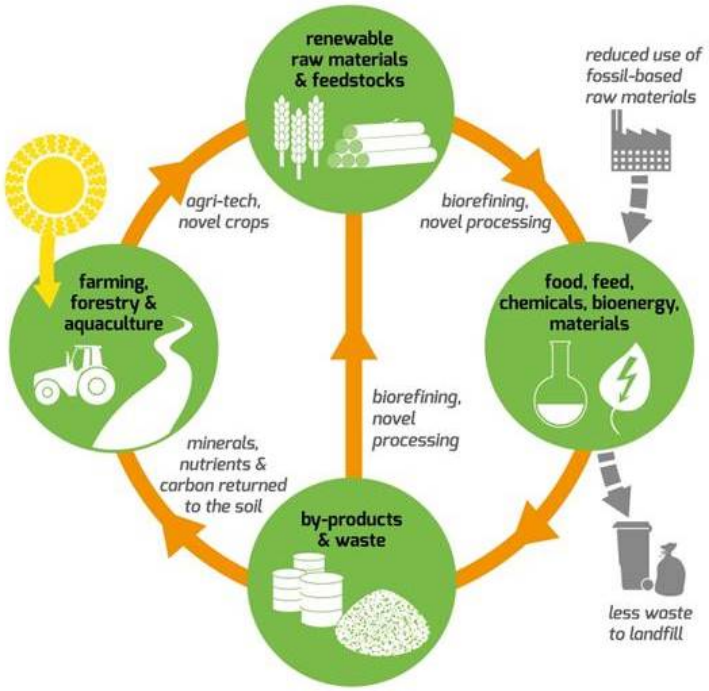

Figure 1.1. Basic concept of a bioeconomy. The picture shows a schematic introduction to how exploiting renewable biomass resources, derived from farming, forestry, and aquaculture, can yield valuable products, reduce waste, and relieve reliance on fossil-based raw materials. The figure was taken from (https://www.biovale.org/the-bioeconomy/).

In addition to being ubiquitous in nature, chitin-rich and lignocellulosic materials are continuously produced in vast amounts as non-edible byproducts in the aqua-, agricultural-, and forest industry. These two polysaccharides are considered as the two most abundant biomass resources on earth. While cellulose is the main constituent in plant fiber, chitin can be obtained

from exoskeletons of insects and crustacean species. Both cellulose and chitin consist of long polymers of hexose sugars, which share high structural resemblance. Their abundance and chemical composition represent a tremendous potential for innovation and economic growth. Being a homopolymer of fermentable glucose, cellulose is an ideal carbon source for production of biofuels and other valuable chemicals. Cellulose can also be processed into nanofibrillated cellulose, a sought-after material with exceptional physicochemical properties suitable for producing hydrogels, biosensors, supercapacitors, and flexible transparent displays (Hu et al., 2018; Moreau et al., 2019). Derivates of chitin have unique biochemical properties, such as the ability to form films, and combine biodegradability and non-toxicity, with a wide variety of interesting biological activities, including antibacterial-, immunoenhancing- and antitumoral activity (Elieh-ali-komi & Hamblin, 2016; Kravanja et al. 2019). Chitin derivates have further proven useful in other fields, such as wastewater detoxification (Bhatnagar et al., 2014), crop yield improvement (Sharp, 2013), and food packaging (Harish Prashanth & Tharanathan, 2007), just to mention a few.

Cost-effective processing of lignocellulosic and chitin-rich biomass is challenging. In Nature, chitin and cellulose form crystalline structures that, in addition to being highly insoluble, exist in co-polymeric heterogenous structures that make them exceedingly resistant to enzymatic depolymerization. Their recalcitrant characters present a tough challenge in commercial bioprocessing, where, for example the efficiency of enzymatic saccharification of cellulose is a major economic bottle neck. Today, relatively harsh physical and chemical pretreatments are used to isolate chitin and cellulose from raw biomass and increase their accessibility to hydrolytic enzymes (Baruah et al., 2018; Devi & Dhamodharan, 2018). These pretreatments have many potential disadvantages, such as the generation of non-desirable side products and a decrease in overall yield and potential profit (Balan, 2014; Wagner et al., 2018).

Carbohydrate-Active enzymes (CAZymes) are Nature's own catalytic tools for synthesis, modification, and degradation of structural biomass polysaccharides (Cantarel et al., 2009). To resolve environmental issues and secure a sustainable bioeconomy, it is essential to invest in

research that focuses on the utilization of CAZymes for cost-effective biomass conversion. Studies of CAZymes and have already contributed to advancement within enzyme-technology and substantial cuts in processing expenses (Alvira et al., 2013). However, the production of second-generation biofuels and other valuable products from cellulose still require further innovation and improvements to become profitable (Balan, 2014; Kurita, 2001; Elieh-ali-komi et al., 2016). Several approaches to enhance CAZyme-technology are currently under thorough investigation, including optimization of enzyme systems, mining for novel enzyme activities, and engineering of beneficial enzyme properties.

1.2 Carbohydrates

Carbohydrates, or saccharides, are biomolecules of three or more carbons that include at least one alcohol group and one carbonyl group. The term "carbohydrate" stems from the 19th century when carbohydrate in the form of glucose $C_6H_{12}O_6$, was believed to be a hydrate of carbon $C_6(H_2O)_6$ (Hon, 1994). After further investigation, saccharides were found to contain either an aldehyde or a ketone and thus being aldehydes (e.g. glucose) or ketones (e.g. fructose), respectively (Fig 1.2).

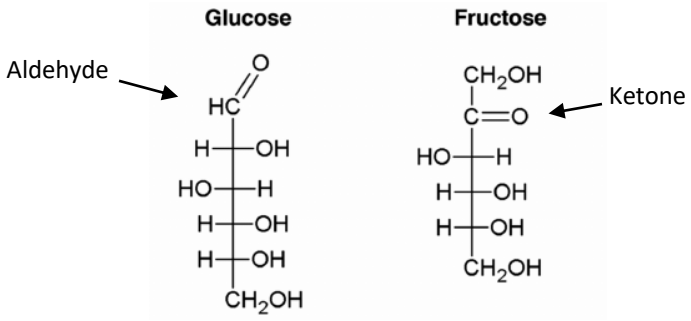

Figure 1.2. Open ring representation of glucose and fructose. The figure illustrates the aldehyde and ketone characteristics of carbohydrates. The picture was taken and modified from (Charrez et al., 2015) and modified for the purpose of this thesis.

The basic units of carbohydrates are simple sugar molecules (i.e. monosaccharides), which can further combine via α- or β-glycosidic bonds, to form di-, oligo-, and polysaccharides. Oligo- and

polysaccharides are synthesized by glycosyl transferases into a wide range of linear or branched structures with different chemical and physical properties. The structural and chemical diversity among carbohydrates are a result of numerous possible combinations of monosaccharide units, glycosidic linkages, and chemical modifications (e.g. acetylation). Carbohydrates are of great biological importance. Being the main source of energy for most living things, carbohydrates are stored by organisms in the form of glycogen (i.e. animals) and starch (i.e. plants), in addition to making up key structural components, such as cellulose in plants and chitin in e.g. arthropods.

1.2.1 Cellulose

Cellulose is a long linear polysaccharide built out of thousands of β-1,4-linked D-glucopyranose (i.e. glucose, Glc) monomers, which predominantly occur in a stable chair conformation. In the cellulose polymer, every second glucose unit is rotated 180° relative to the adjacent monomer, making cellobiose (Glc_2) the repeating unit (Fig. 1.3, right). Polymers are synthesized by cellulase synthase in plants and bacteria, making up the most stable biopolymer on earth with an estimated half-life of 22 million years (Wolfenden et al., 1998).

As the main constituent in the cell wall of plants, cellulose provides structural rigidity and protection against pathogens. Its rigidity and strength come from intra- and inter-chain hydrogen bonding, in which intra-chain hydrogen bonds provide rigidity to each polymer, and inter-chain hydrogen bonds tie polymers together into two-dimensional sheets (Shen et al. 2009). Formation of sheets usually occurs spontaneously at a degree of polymerization (DP) of eight or higher, as the affinity towards other cellulose polymers surpasses the affinity for the surrounding aqueous solution (Brown, 2014). Sheets aggregate further and stack on top of each other, in a parallel or antiparallel fashion, to form crystalline microfibrils held together by inter-sheet hydrogen bonds and hydrophobic interactions (Beckham et al., 2011). Crystalline mirofibrils have hydrophobic planes, which result from highly organized polymers with strict positioning of hydrogen- (i.e. axial) and hydroxyl groups (i.e. equatorial). Close inspection shows that the crystalline regions of microfibrils are interspaced with amorphous (i.e. less organized) patches, which are areas that are particularly exposed to enzymatic hydrolysis (Bertran & Dale, 1985). On a higher level of

organization, however, cellulose microfibrils closely associate with hemicelluloses and become entangled into a matrix reinforced with lignin, which provides as a resilient shield against microbial attack (Fig. 1.3, left).

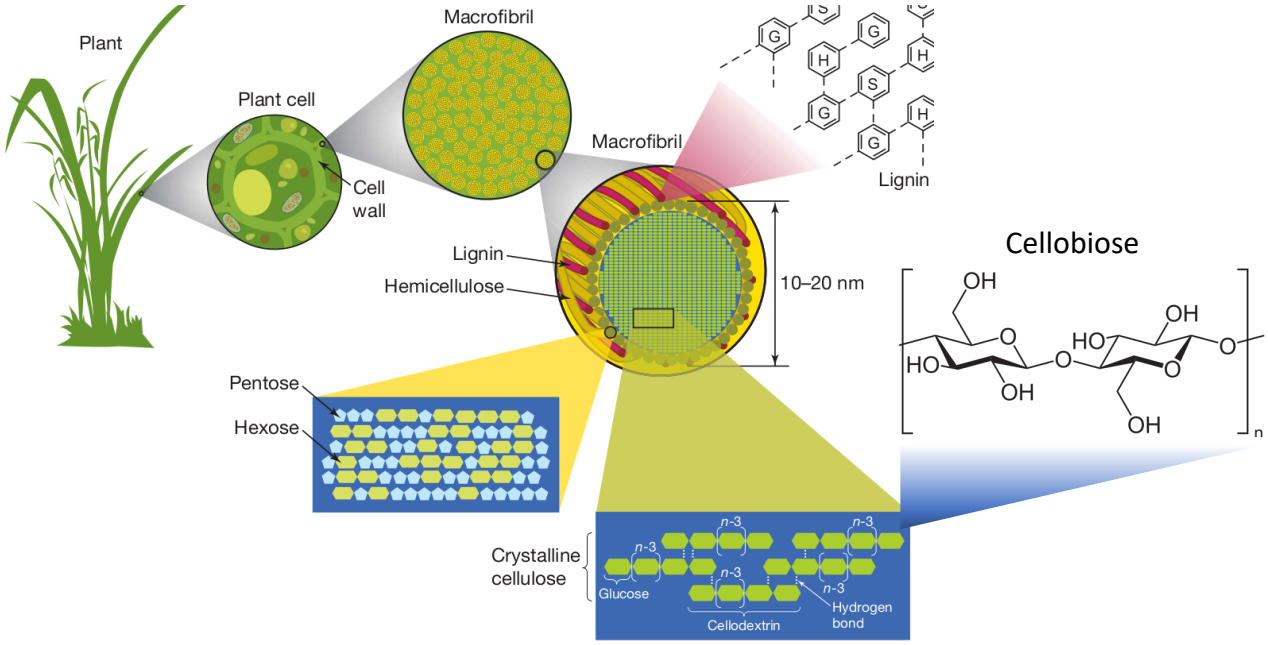

Figure 1.3. Structure of cellulose derived from plants. This figure illustrates the hierarchical organization of plant derived cellulose; from the smallest repeating unit cellobiose (right), to the crystalline microfibrils (i.e. 10-20 nm), which are covered by hemicellulose (i.e. branched heteropolymers of different monosaccharides) and lignin (i.e. cross-linked phenolic polymers), and further combined into recalcitrant macrofibrils (left). The figure is constructed of two pictures, taken from (http://resizeandsave.online/dappy-May_27_5.html) and (https://en.wikipedia.org/wiki/Cellulose#cite_note-1.aken).

Cellulose can exist in different crystalline forms, thus being a polymorph. Out of seven known polymorphs only two are common in Nature, termed cellulose Iα and Iβ. These native forms usually occur together in mixed ratios that vary depending on the source (Vanderhart & Atalla,

1984). Whereas the Iα form is most common in algae and bacteria, Iβ usually dominates in higher plants. Both polymorphs have parallel oriented sheets. However, stacks of Iβ-sheets pack more densely than Iα-sheets due to differences in inter-chain hydrogen bonding patterns, which also gives the two forms distinct structural characteristics that enable discrimination (Nishiyama et al., 2002 & 2003). Cellulose Iβ can be converted into cellulose Iα but not the other way around, thus indicating Iα to be more thermodynamically stable (Gilbert & Kadla, 1998). Various chemical and physical treatments of native cellulose (Iα & Iβ) can further generate five artificial forms called cellulose II, III_I, III_{II}, IV_I, and IV_{II} (Gilbert & Kadla, 1998). Pretreatments of lignocellulosic biomass generally disrupt the cellulose-hemicellulose-lignin assembly and decrease the crystallinity of the microfibrils. Phosphoric acid swollen cellulose (PASC) is an example of chemically pretreated cellulose with a lowered crystallinity that is widely used as a model substrate in characterization of carbohydrate-active enzymes (Wood et al., 1988).

1.2.2 Chitin

Chitin is a common structural component in several organisms and is especially plentiful in the fungal cell wall and external skeletons of arthropod species (e.g. insects and crustaceans). As an unbranched and nitrogenous polysaccharide, chitin is composed of *N*-acetyl-D-glucosamine (GlcNAc) subunits, linked together by β-1,4 glycosidic bonds. Every second GlcNAc subunit is turned 180° relative to its neighbors, creating the repeating unit *N,N'*-diacetylchitobiose $(GlcNAc)_2$ (Fig. 1.4). The monomeric structures of chitin and cellulose are closely related; the only difference being that the hydroxyl group on the second carbon in cellulose is substituted with an *N*-acetyl group in chitin (Carlström, 1957). Like cellulose, chitin polymers are strengthened and linked together by intra- and inter-chain hydrogen bonds, making up highly crystalline and insoluble nanofibrils (Kameda et al., 2005; Fig. 1.4). However, the higher structural organization of chitin differs significantly from cellulose. In the crustacean cuticle, for example, crystalline chitin nanofibrils closely associate with protein and calcium carbonate to form mineralized chitin-protein fibrils, which further assemble into twisted plywood structures (Raabe et al., 2005; Younes & Rinaudo, 2015).

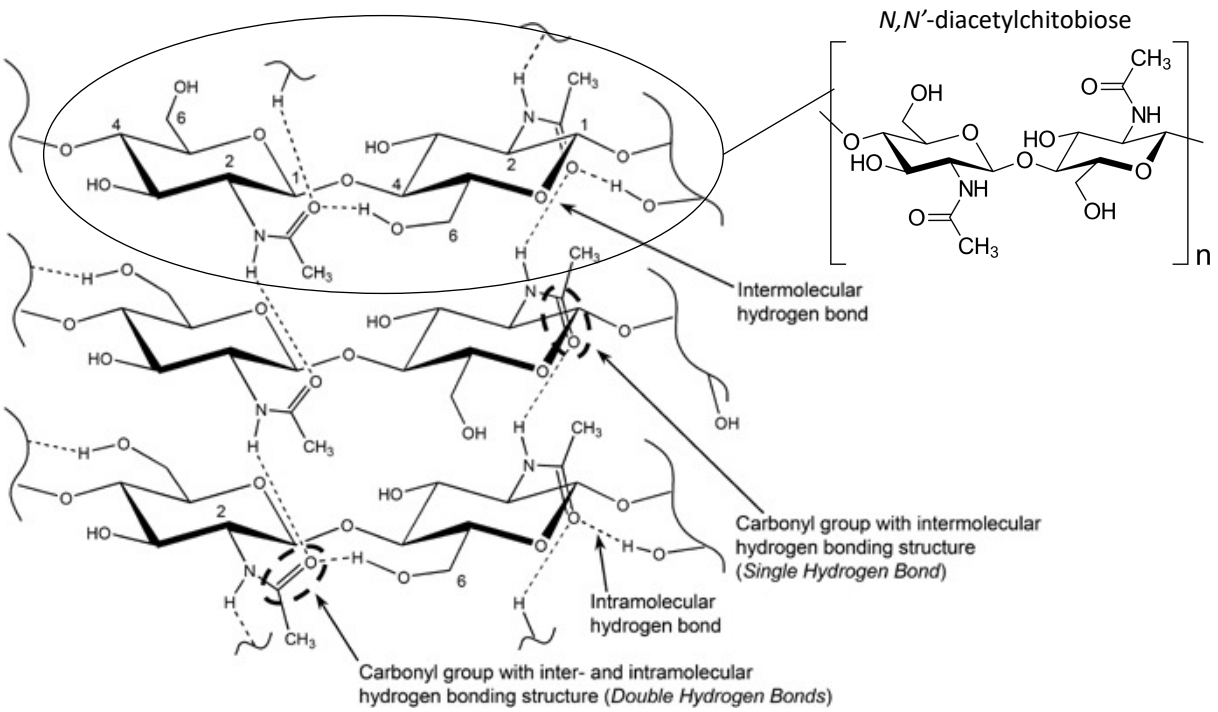

Figure 1.4. Chemical structure and repeating unit of chitin. The figure displays a diagram of inter- and intramolecular hydrogen bonds in α-chitin (left), and the repeating unit of chitin polymers (right). There are two types of C=O hydrogen bonds found in chitin: intermolecular hydrogen bonding (Single Hydrogen Bond) and a combination of intermolecular and intramolecular hydrogen bonding (Double Hydrogen Bonds). This figure is an assembly of two illustrations taken from (Kameda et al., 2005) and (https://de.wikipedia.org/wiki/Chitin), respectively.

Native chitin occurs in three crystalline forms, designated α-, β-, and γ-chitin, which can be discriminated both by chain orientation (Fig. 1.5) and patterns of inter- and intramolecular hydrogen-bonds (Kameda et al., 2005). α-chitin is the most abundant form, especially plentiful in the external skeleton of insects and crustaceans. The antiparallel chain orientation allows α-chitin to form intersheet hydrogen bonds and solidify into a particularly compact and rigid structure (Minke & Blackwell, 1978). β-chitin, which can be obtained from squid pen, has parallel oriented chains. Intersheet hydrogen bonds are absent in β-chitin because the parallel chain orientation allows fewer intermolecular interactions. Thus, β-chitin is less compressed but more flexible, compared to α-chitin. The looser packing further allows β-chitin to absorb water molecules and

swell in aqueous solvents, which makes it more exposed to enzyme activity (Saito et al., 2000). The third and least common form, γ-chitin, is composed of a mixture of both parallel and antiparallel chains (Roberts, 1997; Rinaudo, 2006). γ-chitin has been identified in the cell wall of mushrooms (Elieh-ali-komi & Hamblin, 2016).

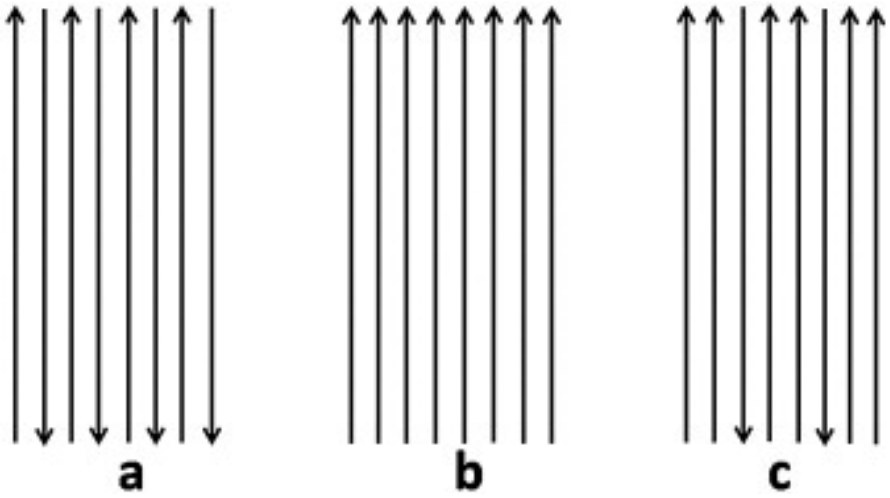

Figure 1.5. Chain orientation of the different chitin polymorphs. The picture displays α-chitin (a), β-chitin (c),and γ-chitin (c). Taken from: (Anitha et al., 2014).

Polymers of chitin are highly insoluble but can be converted into a soluble derivative called chitosan through enzymatic or chemical deacetylation (i.e. removal of *N*-acetyl groups) (Khattak et al. 2019). Unlike chitin, polymers of chitosan have free amine groups (NH_2), which in diluted aqueous acidic solvents can be protonated (NH_3^+), promoting solubility (Franca et al., 2008). Complete deacetylation of chitin is difficult to achieve. The term chitosan is used for polymers where the degree of deacetylation is such (i.e. at least 35 - 40%) that the polymers can be dissolved in a dilute acidic medium (Franca et al., 2011). Chitosan thus usually contains a mixture of both GlcNAc and glucosamine (GlcN).

1.2.3 Microbial degradation of recalcitrant polysaccharides

Cellulose and chitin are omnipresent and abundant biopolymers, which in addition to being exceedingly resistant to depolymerization, represent a rich source of organic carbon. Consequently, a diverse group of heterotrophic microorganisms have evolved diverging enzymatic strategies specialized in deconstructing and utilizing these recalcitrant polysaccharides as a source of energy. Such microorganisms are represented within the kingdoms of protozoa, fungi, and bacteria, and are ubiquitous in the biosphere (e.g. found in water sediments, soils, compost, gut of plant-eating insects and animals, and in general anywhere appropriate biomass is available), where they play an essential role in the global carbon cycle.

Cellulose and chitin are omnipresent and abundant biopolymers, which, in addition to being exceedingly resistant to depolymerization, represent a rich source of organic carbon. Consequently, a diverse group of heterotrophic microorganisms have evolved diverging enzymatic strategies specialized in deconstructing and utilizing these recalcitrant polysaccharides as a source of energy. Such microorganisms are represented within the kingdoms of protozoa, fungi and bacteria, and are ubiquitous in the biosphere (e.g. found in water sediments, soils, compost, gut of plant-eating insects and animals, and in general anywhere where appropriate biomass is available). Such microorganisms play an essential role in the global carbon cycle.

Microorganisms rely primarily on the concerted action of various hydrolytic CAZymes, such as chitinases and cellulases, to efficiently depolymerize chitin and cellulose. Over billions of years, microbes have adapted to various environmental conditions (e.g. pH, temperature, salinity, oxygen level) and evolved distinct hydrolytic strategies, optimized for their respective ecological niches. Anaerobic and aerobic bacteria, for example, employ contrasting strategies based on large often cell-attached enzyme complexes (cellulosomes) and cocktails of free secreted enzyme, respectively (Lynd et al., 2002, Swiontek Brzezinska et al., 2013). In addition, anaerobic microbes are often associated with other organisms (i.e. mixed microbial communities) that enhance their access to digestible polysaccharides (Kato et al., 2004).

The digestive systems of plant-eating animals host diverse communities of anaerobic bacteria, many of which contain large clusters of co-regulated genes, referred to as polysaccharide utilization loci (PULs) (Bjursell et al., 2006). These PULs encode membrane-associated proteins needed for polysaccharide depolymerization and sugar transport, which together form systems of closely associated enzymes that ensure minimal loss of products to surrounding competitors. One single species genome can contain several different PULs, diverging in genetic composition and carbohydrate specificity (Martens et al., 2008). Most cellulolytic anaerobes, however, employ large multi-enzyme complexes called cellulosomes (Schwarz, 2001), which usually anchor to the cell wall and digest insoluble polymers in the vicinity of their proprietor. In short, a cellulosome consists of a scaffolding protein with so-called cohesin domains that binds multiple dockerin-containing CAZymes via cohesin-dockerin interactions, and thus assembling a powerful cellulolytic multi-enzyme (Borne et al., 2013).

While anaerobes employ strategies specialized in conserving energy, aerobes can generate significantly more energy (i.e. ATP) through cellular respiration with O_2 as the final electron acceptor. Oxygenated environments further allow microbes to utilize reactive oxygen species (ROS) to decrease biomass recalcitrance. Aerobic bacteria and fungi employ free enzyme systems, in which numerous individual CAZymes are secreted into the surroundings upon detection of a suitable food source. The free enzyme strategy is found in both cellulolytic and chitinolytic microorganisms, and is particularly well-described for e.g. the cellulolytic fungus *Trichoderma reesei* (Bischof et al., 2016) and the chitinolytic bacterium *Serratia marcescens* (Vaaje-Kolstad et al., 2013).

1.2.4 Degradation of recalcitrant polysaccharides by free enzyme systems

The chitinolytic system of *S. marcescens* has been proposed as a model system for enzymatic conversion of recalcitrant polysaccharides, because it is simple and efficient, while containing all known major enzyme activities (Vaaje-Kolstad et al., 2013; Fig. 1.6). The efficiency of the chitinolytic machinery of *S. marcescens* comes from its complementary enzyme activities that act

together in synergy, which means that the sum of their cooperative action is greater than the sum of their individual actions combined (Wood & Garcia-Campayo, 1990).

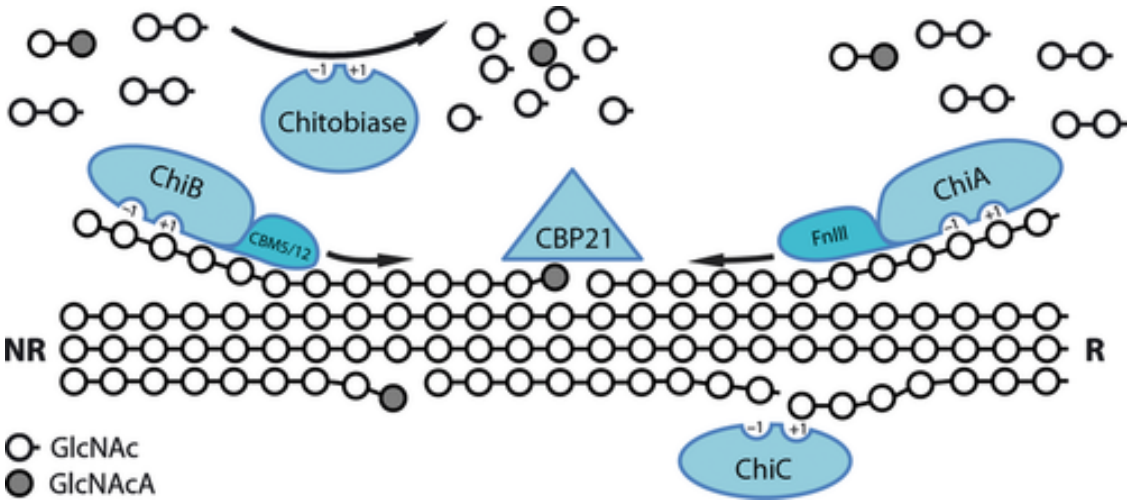

Figure 1.6. Simplified model of the free chitinolytic system of *S. marcescens*. ChiA and ChiB are processive exo-acting chitinases, which convert chitin polymers into chitobiose $(GlcNAc)_2$, acting from either the reducing (labeled R) or non-reducing end (labeled NR), respectively. The endochitinase ChiC generates random cuts in amorphous regions, while the lytic polysaccharide monooxygenase CBP21 oxidizes glycosidic linkages in highly crystalline areas. When CBP21 oxidatively cleaves glycosidic bonds of chitin polymer, the C1-oxidized products spontaneously convert into more stable aldonic acids (GlcNAcA). The chitobiase further hydrolyses soluble di- and oligosaccharides to GlcNAc monomers. Units of GlcNAc are shown as white circles, while GlcNAcA (oxidized products) appears in gray. Note the additional modules of ChiA and ChiB, which are substrate specific binding domains, important for substrate recognition. The figure was taken from (Vaaje- Kolstad et al., 2013).

As mentioned in the previous section, microbial depolymerization of polysaccharides mostly relies on the concerted action of glycosyl hydrolases (GHs), which comprise a diverse group of CAZymes that cleave glycosidic bonds using hydrolytic reaction mechanisms (Davies & Henrissat, 1995). GHs are often named after their substrate specificity (e.g. cellulases and chitinases) and their mode of action, either cleaving glycosidic linkages randomly (i.e. endo-

activity) or acting only on free chain ends (i.e. exo-activity). Exo-acting chitinases and cellulases are often processive, which implies that they attach to free chain ends and catalyze multiple hydrolytic events along the same chain before disassociating from their substrates (Payne et al., 2012). Non-processive chitinases and cellulases, on the other hand, have to reattach for each catalytic event.

The substrate-binding surfaces of processive and non-processive GHs ted to show different architectures. Processive enzymes exhibit deep substrate-binding clefts or tunnels, through which they can thread single polysaccharide chains. Non-processive enzymes display more shallow clefts and may be able to accommodate distorted chains associated to an amorphous polysaccharide fibril. A third type of glycosyl hydrolase (e.g. chitinolytic or cellulolytic β-glucosidases), has a smaller and pocked-like binding site, which is only fit to accommodate dimeric sugars (Davies & Henrissat, 1995). Processive GHs may show opposite directionalities such as e.g. ChiA and ChiB of *S. marcescens* (Fig. 1.6), which are specific for either the reducing or non-reducing end of chitin polymers, respectively.

While processive glycosyl hydrolases generally represent the major driving force of polysaccharide depolymerization in Nature (Beckham et al., 2014), the processive enzymes of free enzyme systems are usually promoted by additional enzyme activities (Horn et al., 2012). As processive activity releases extensive amounts of soluble disaccharides, β-glucosidases (called Chitobiase in the case of chitin) are needed to further convert these into mono sugars, which can then be ingested by the microbe. Notably, many microbes may ingest soluble oligomers and dimers before further digestion. The non-processive GHs are responsible for targeting amorphous regions, where they cleave distorted chains randomly and generate free chain ends for attack by processive enzymes. Recalcitrant regions of highly organized polymers are disrupted by lytic polysaccharide monooxygenases (LPMOs), which are the most recent discovery related to the free enzyme systems of recalcitrant polysaccharide degrading organisms (Vaaje-Kolstad et al., 2010). Unlike GHs, LPMOs are redox enzymes that exhibit relatively flat substrate-binding surfaces. The planar topology of LPMOs allows them to bind strongly to crystalline surfaces,

where they are able introduce specific chain-breaks in the scissile bond by using an oxidative reaction mechanism (Vaaje-Kolstad et al., 2010). After the highly organized regions have been distorted by LPMO activity, these regions become more accessible to hydrolytic enzymes. As a result of the action of these hydrolytic enzymes, polymer chains in distorted areas are peeled off. Thus, new crystalline binding sites for LPMO activity are generated. Of note, both GHs and LPMOs may contain non-catalytic carbohydrate-binding modules (CBMs), which enhance substrate recognition and substrate binding.

By combining the complimentary enzyme activities described above, cocktails of synergistically acting catalysts can be produced and utilized for e.g. full degradation of recalcitrant polysaccharides in biorefineries.

1.3 Lytic polysaccharide monooxygenases

Lytic polysaccharide monooxygenases are monocopper enzymes that catalyze the cleavage of recalcitrant polysaccharides by oxidizing one of the scissile carbons of the glycosidic bond (Vaaje-Kolstad et al., 2010; Beeson et al., 2012). Found within all domains of life, LPMOs exhibit vast sequence diversity and display several substrate specificities. While their role in the depolymerization of recalcitrant polysaccharides is universally recognized, they may have additional functions related to bacterial pathogenicity (Paspaliari et al., 2015; Agostoni et al., 2017), virulence of viruses (Chiu et al., 2015), and metamorphosis of arthropod species (Sabbadin et al., 2018).

1.3.1 Early history of LPMO discovery

Before the 21st century, microbial degradation of polysaccharides was believed to be exclusively hydrolytic (e.g. cellulases and chitinases). The first to indicate otherwise was Reese et al. (1950), publishing the C_1C_x hypothesis (Fig. 1.7.). The C_1C_x hypothesis postulate that an unknown enzymatic activity (C_1) is required in advance of hydrolytic action (C_x), to degrade crystalline cellulose properly. Following, Eriksson et al. (1974) described an oxidative enzyme from *Sporotrichum pulverulentum* that displayed a synergistic effect on the hydrolytic degradation of

cellulose. Eriksson and colleagues further stated that their findings agreed with the former C_1C_x hypothesis.

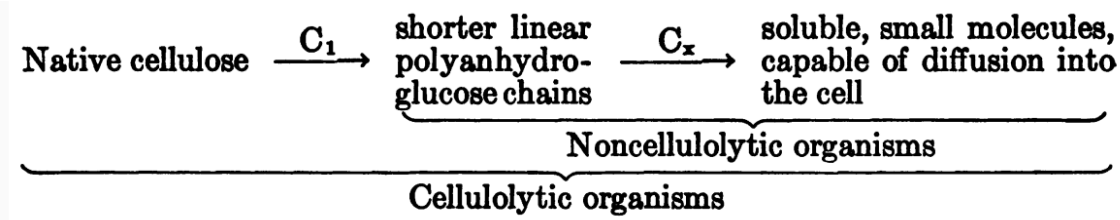

Figure 1.7. C1Cx hypothesis. The scheme illustrates the observations leading to the formulation of the C1Cx hypothesis. The figure was taken from (Reese et al., 1950).

In the early 1990s, a fungal protein (i.e. Cel1) of unknown activity was linked to digestion of cellulose, based on the observation of cellulose-induced expression and the presence of a C-terminal domain associated with fungal cellulases (Raguz et al., 1992). Cel1 was shown to bind strongly to crystalline cellulose, but no hydrolytic activity was detected (Armesilla et al., 1994). Later, sequence similarities between Cel1 and a protein suspected to have a weak endo-1,4-beta-D-glucanase activity (i.e. EGIV, today known as Cel61A), resulted in the formation of the Glycoside Hydrolase Family 61 (GH61), in the CAZy database (Saloheimo et al., 1997; Karlsson et al., 2001). Parallel to the discovery of GH61, a group of bacterial Chitin-Binding Proteins (CBPs) with no apparent catalytic activity caught attention (Schnellmann et al., 1994; Kolbe et al., 1998; Suzuki et al., 1998; Schrempf, 1999; Folders et al., 2000; Chu et al., 2001). Among the investigated CBPs was a 21 kDa chitin-binding protein derived from *S. marcescens* called CBP21 (Watanabe et al., 1997). CBP21 and the other CBPs were initially annotated as family 33 Carbohydrate-Binding Modules (CBM33s), and conserved aromatic residues, were believed to be responsible for binding chitin (Zeltins & Schrempp, 1997).

Moving into the 21st century, Vaaje-Kolstad and coworkers revealed the structure of CBP21, being the first CBM33 structure to be published (Vaaje-Kolstad et al. 2005a). The structure

revealed that a majority of the aromatic residues, which were previously believed to be involved in binding, rather resided in the interior of the protein. Using site-directed mutagenesis, Vaaje-Kolstad et al. further showed that conserved polar surface residues were important for chitin-binding. Not long after, CBP21 was shown to increase the efficiency of the hydrolytic machinery of *S. marcescens* while, apparently, lacking an individual catalytic activity (Vaaje-Kolstad et al., 2005b). A striking structural similarity between CBP21 and a GH61 enzyme (Cel61B) was unveiled a few years later (Karkehabadi et al., 2008). The structural linkage between CBM33s and GH61s was followed by the discovery of a functional connection, when it was shown that several GH61s enhanced the activity of cellulase (Harris et al., 2010). Finally, a breakthrough came when CBP21 was proven to be a redox enzyme (Vaaje-Kolstad et al., 2010). Vaaje-Kolstad and colleagues demonstrated that, in the presence of divalent metal ions and a reducing agent, CBP21 was able to oxidize and break glycosidic bonds in crystalline chitin in a dioxygen-dependent reaction. Soon after, another CBM33 protein (CelS2) was reported to display oxidative activity towards cellulose (Forsberg et al., 2011), followed by the demonstration that several GH61 enzymes do the same (Quinlan et al., 2011; Phillips et al., 2011; Langston et al., 2011; Westereng et al., 2011). After additional studies, all of which confirmed a functional and structural connection between CBM33s and GH61s, Horn et al. (2012) introduced the term "lytic polysaccharide monooxygenase" (LPMO) to collectively describe their catalytic activity. Not long after, the CAZy database created a novel class called Auxiliary Activities (AA), in which the GH61s and CBM33s were reclassified into AA families 9 and 10, respectively (Levasseur et al., 2013). More details concerning these discoveries and recent insights, follow in the subsections below.

1.3.2 Classification, occurrence and substrate specificity

Based on sequence similarities, LPMOs are currently classified within Auxiliary Activity families AA9-AA11 and AA13-AA16, in the CAZy database (Levasseur et al., 2013). The three latest additions AA14-AA16, were discovered quite recently (Couturier et al., 2018; Sabbadin et al., 2018; Filiatrault-Chastel et al., 2019). Fig. 1.6 gives an overview of families AA9-AA11 and

AA13-AA15, with their respective substrate specificities, oxidative regioselectivities, and additional domains (Forsberg et al. 2019). Notably, a majority of characterized LPMOs have only been screened against a minority of possible substrates (Forsberg et al., 2019).

Family AA9 (previously GH61) consists of fungal enzymes, characterized to oxidize glycosidic linkages in cellulose (Quinlan, et al., 2011), hemicelluloses (Agger et al., 2014), cellulose-oligosaccharides (Isaksen et al., 2014), and xylan (Frommhagen et al., 2015). Family AA10 LPMOs, formerly known as CBP33s, predominantly originate from bacteria but are also found among viruses, archaea, and eukaryotic organisms. AA10s exhibit specificity for either chitin (Vaaje-Kolstad et al., 2010), cellulose (Forsberg et al., 2011), or both (Forsberg et al., 2014a). Family AA11 is dominated by chitin-active enzymes of fungal origin (Hemsworth et al., 2014), with one exception being an AA11 sequence identified in an uncultured bacterium (CAZy, 2019a). Family AA13 and AA14 both consist of fungal enzymes, characterized to oxidize starch (Lo Leggio et al. 2015) and crystalline xylan (Couturier et al., 2018), respectively. AA15s have so far been identified in viruses, algae, oomycetes, and several invertebrates (i.e. insects, crustaceans, mollusks, and cnidaria) (Sabbadin et al., 2018). Interestingly, AA15 is the first family to hold LPMOs of animal origin. Out of two characterized AA15 enzymes (as of June 2019), one is active on chitin, and another on both on chitin and cellulose (Sabbadin et al., 2018). As the newest addition to the CAZy database, AA16s have been found in both fungi and oomycetes (Filiatrault-Chastel et al., 2019), and the only characterized member displays oxidative activity on cellulose.

Of note, LPMOs acting on β(1-4) glycosidic bonds may oxidize C1 or C4, whereas some produce mixtures of C1- and C4-oxidized products, as outlined in Fig. 1.6.

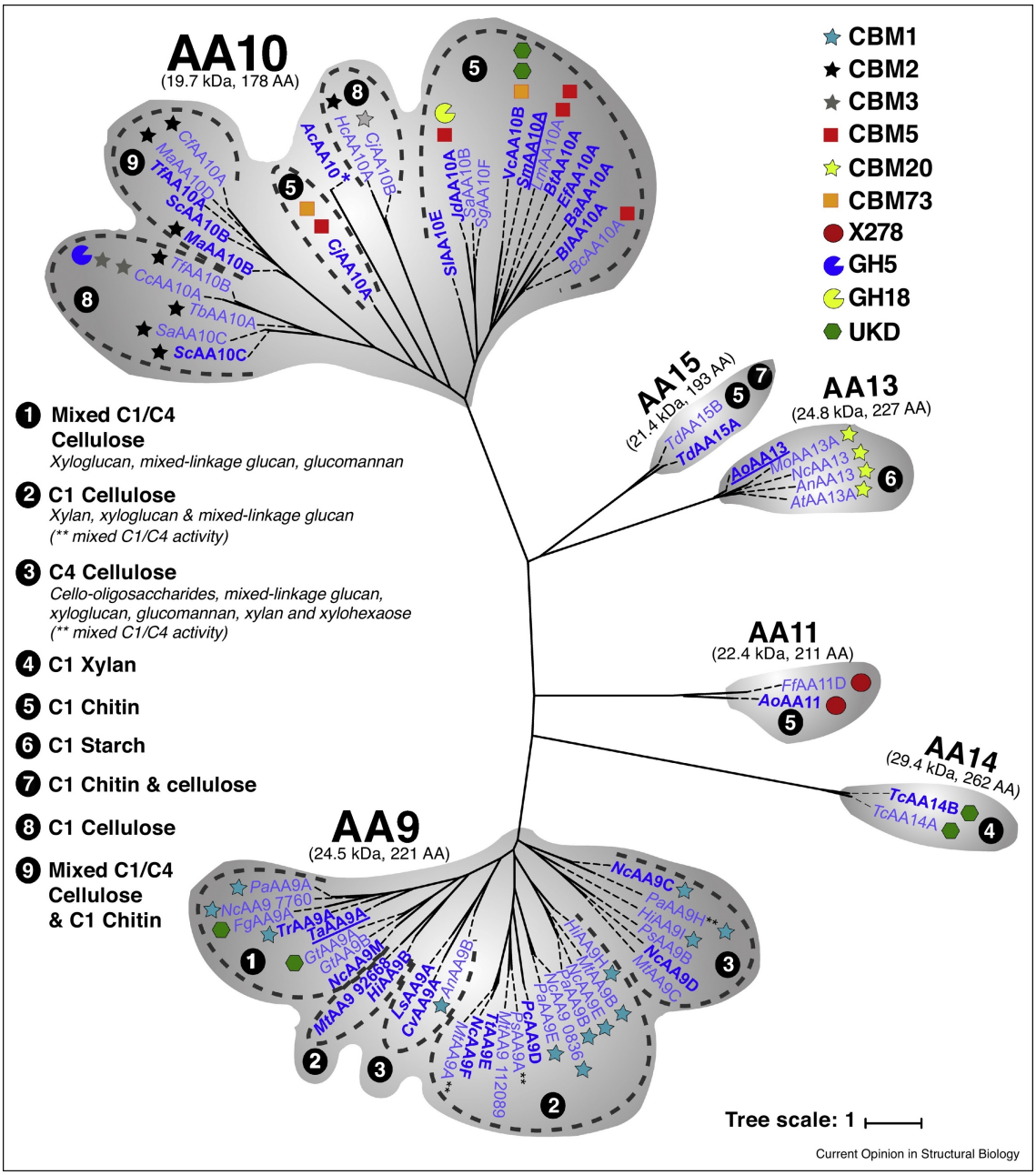

Figure 1.6. Phylogenetic tree of Auxiliary Activity families. The picture displays a phylogenetic tree, featuring a selection of functionally characterized LPMOs from AA families 9-11 and 13-15. Names in bold signify LPMOs with known three-dimensional structures. Symbols behind names indicate the presence of additional domains, like CBMs, GHs, and unknown domains (UKD). The circled numbers (1-9) assign substrate specificity and oxidative regioselectivity (C1, C4, or mixed C1/C4) to each cluster. Family AA16 is missing because of its recent discovery. The figure was taken from (Forsberg et al., 2019).

1.3.3 Global structure, catalytic site and modularity

Lytic polysaccharide monooxygenases share a high degree of structural similarity while displaying relatively low sequence identity, both between and within families (Book et al., 2014; Hemsworth et al., 2014; Lo Leggio et al., 2015; Vaaje-Kolstad et al., 2017), adhering with the common perception of tertiary structures being more related to function than to amino acid sequence. Today, most knowledge about LPMOs and their structural features extends from studies on enzymes from families AA9 and AA10, which also constitute the largest families in the CAZy database.

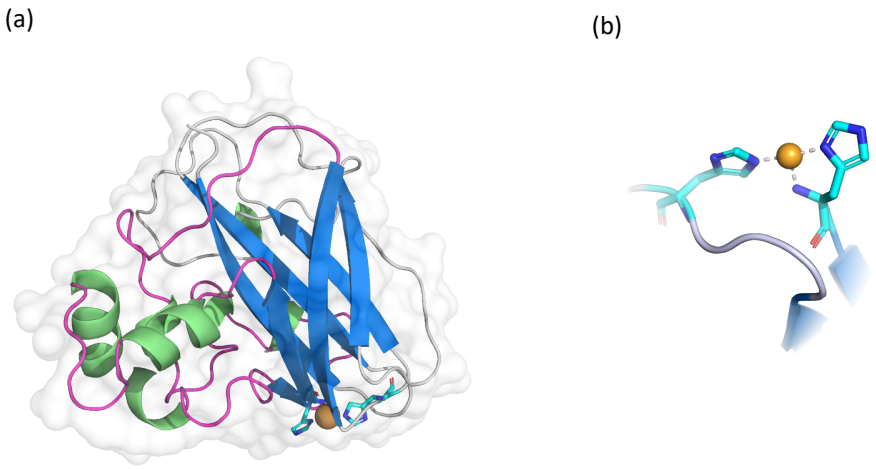

Figure 1.7. Global structure and catalytic site of LPMOs. Panel (a) shows the overall structure in cartoon representation, including a β-sandwich core structure (blue), α-helices (green), loops (light gray),a catalytic motif (side chians shown as cyan sticks) and a copper co-factor (light organge sphere). In addition, the the loop which is often referred to as loop 2, has been highlighted in pink. The molecular surface is shown as a transparant shadow. Note the flat substrate-binding surface and the triangular shape of the tertiary structure. The catalytic motif (b) consist of two conserved histidine residues, coordinating Cu(I) with three nitrogen ligands in a trigional (T-shaped) geometry. Both figures are made in PyMol, using a homology model of *Sc*LPMO10D (section 4.2.1).

The immunoglobulin-like core structure of LPMOs is formed by a skewed β-sandwich fold, consisting of 7-9 antiparallel β-strands that are connected via loops of varying lengths (Vaaje-Kolstad et al., 2017; Fig. 1.7a). Some longer loops may include short α-helices and contribute to

substantial portions of the relatively flat substrate-binding landscape (Karkehabadi et al., 2008; Harris et al., 2010; Li et al., 2012; Vaaje-Kolstad et al., 2012; Wu et al., 2013; Hemsworth et al., 2014; Lo Leggio et al., 2015). Disulfide bridges are common but not an entirely conserved feature, which form strong covalent linkages between secondary structures and loops, and thereby contributes to the overall stability of the protein (Vaaje-Kolstad et al. 2012; Tanghe et al., 2017). The long loop connecting β-strands 1 and 3, commonly referred to as loop 2 (L2), makes up most of the structural diversity within families AA9 and AA10. Varying in length, conformation and number of α-helices, L2 constitutes up to half of the putative substrate-binding surface of AA10s (Fig. 1.7a), where it is thought to play an essential role in polysaccharide recognition and catalytic regioselectivity (Book et al., 2014; Forsberg et al., 2014a; Forsberg et al., 2016; see also section 1.3.6).

The catalytic center of the LPMOs is located on a planar face and includes a solvent exposed type II copper center (Fig. 1.7b), in which mononuclear copper is coordinated by two histidine residues (one of which being the N-terminal residue). Being essential for LPMOs catalytic function, the two copper-binding histidines form a highly conserved structural motif, called the histidine brace (Quinlan et al., 2011; Hemsworth et al., 2013).

As illustrated in Fig. 1.6 (section 1.3.2), modularity is a relatively common feature among LPMOs. Approximately 30% of the family AA10 enzymes in the CAZy database exhibit additional domains (Horn et al., 2012), including carbohydrate binding modules (i.e CBM2, CBM3, CBM5, and CBM73), glycosyl hydrolases (i.e. GH5 and GH18), and domains of unknown function (Forsberg et al., 2019). CBMs are non-catalytic binding modules with discrete folds that display specific carbohydrate-binding activity, and thus promote the productive binding of their associated catalytic domain to specific polysaccharides. They also represent the majority of additional domains associated with LPMO structures and are thought to have been evolutionary beneficial for enzymes operating in water-rich environments (Várnai et al., 2013). In modular CAZymes, including LPMOs, domains usually connect via flexible linker/spacer regions of varying length. Linker regions generally display low-complexity sequences, typically

dominated by disorder-promoting (e.g. proline and serine) and disorder-neutral residues (e.g. aspartic acid and threonine) (DePristo et al., 2006; Meng & Kurgan, 2016). The flexibility of the linkers is believed to enhance performance of multi-domain proteins; however, this flexibility hampers structural studies of full-length proteins, and thus makes it difficult to gain insight into functional connotations (i.e. domain interactions and overall enzyme functionality) (Courtade et al., 2018).

1.3.4 Catalytic mechanism

In 2010, Vaaje-Kolstad and coworkers defined CBP21 as a redox enzyme capable of releasing C1-oxidized oligosaccharides from crystalline chitin (Vaaje-Kolstad et al., 2010). Examination of oxidized products was enabled by using isotope labeled dioxygen ($^{18}O_2$) and water ($H_2{}^{18}O$) in separate reactions, which revealed incorporation of two oxygen atoms; one originating from dioxygen and another from water (Fig. 1.8).

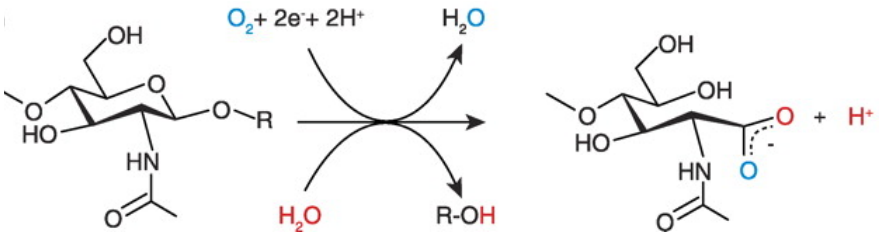

Figure 1.8. The oxidizing reaction of CBP21. The reaction scheme gives a simple overview of the incorporation of oxygen during C1-oxidative cleavage of a chitin polymer, in which one oxygen is derived from molecular oxygen (blue) and another from water (red). Figure taken from (Vaaje-Kolstad et al., 2010).

Additional assays further showed that the reaction depended on divalent metal ions and the presence of a reducing agent (Vaaje-Kolstad et al., 2010). Today, it is clear that , LPMOs are strictly copper dependent enzymes, which require reduction of the copper cofactor by an external electron donor, such as gallic acid (Quinlan et al., 2011), cellobiose dehydrogenase (Phillips et al., 2011) lignin (Westereng et al., 2015), or a photosynthetic pigment (Cannella et al., 2016), to catalyze the oxidative cleavage of scissile glycosidic bonds in recalcitrant polysaccharides.

Monooxygenases are defined as enzymes that catalyze the displacement of single oxygen atoms from molecular oxygen into organic substrates (Torres Pazmiño et al., 2010). To overcome spin-forbidden reactions between O_2 and substrate, monooxygenases often utilize inorganic cofactors (e.g. transition metals) and external electron donors, to bind and thereafter activate dioxygen. Phillips et al. (2011) were among the first to point out the monooxygenase activity of LPMOs, in a publication, in which they called the enzymes polysaccharide monooxygenases (PMOs) and further proposed a reaction mechanism built on principles of well-studied copper monooxygenases (Klinman et al. 2006; Solomon et al. 2011). In subsequent years, the theory of an O_2-dependent LPMO mechanism prevailed and several catalytic mechanisms, all following the monooxygenase paradigm (Fig. 1.9, equation a), have been suggested (Beeson et al., 2015; Walton & Davis, 2016). Although diverging on the timing of electron and proton transfers, the proposed LPMO mechanisms generally rely on the activation of molecular oxygen to generate either Cu(II)-superoxide or Cu(II)-oxyl (i.e. strong reactive oxygen intermediates), which abstract a hydrogen from the substrate. While there is still missing crucial experimental evidence related to the mechanism of O_2 activation by substrate-associated LPMOs, extensive data (i.e. computational, crystallographic, and biochemical) have confirmed O_2 activation by unbound LPMOs (Kjaergaard et al., 2014; Hangasky et al., 2018), which, interestingly, may lead to the formation of hydrogen peroxide (H_2O_2) (Kittl et al., 2012; Isaksen et al., 2014).

The formation of H_2O_2 by LPMOs, which happens in the presence of reductant when substrate is absent, has earlier been regarded as a futile side reaction. Naturally, it came as a big surprise when Bissaro et al. challenged the monooxygenase paradigm and described a series of experiments that all pointed to H_2O_2 as the native co-substrate of LPMOs (Bissaro et al., 2017; Bissaro et al., 2018b; Fig. 1.9, equation b). If Bissaro and his colleagues are correct, enzymes currently known as lytic polysaccharide monooxygenases could be better described as peroxygenases.

Hitherto, there is unison consensus on the initial one electron reduction of LPMO-Cu(II) to LPMO-Cu(I) that primes the enzyme for catalysis, but exactly how LPMOs catalyze the

oxidative cleavage of glycosidic bonds remains somewhat enigmatic. Figure 1.9 gives a general overview of the currently proposed O_2- (a) and H_2O_2- (b) dependent oxidative mechanisms. In both putative pathways, the activated enzyme binds and reduces an oxygen species (i.e. O_2 or H_2O_2, respectively), to yield a highly reactive oxygen species bound to the copper. This highly reactive intermediate abstracts a hydrogen from one of the scissile bond carbons and thereby generates a substrate radical that becomes hydroxylated. Such hydroxylation destabilizes the glycosidic bond and results in a spontaneous elimination reaction (Beeson et al., 2012),

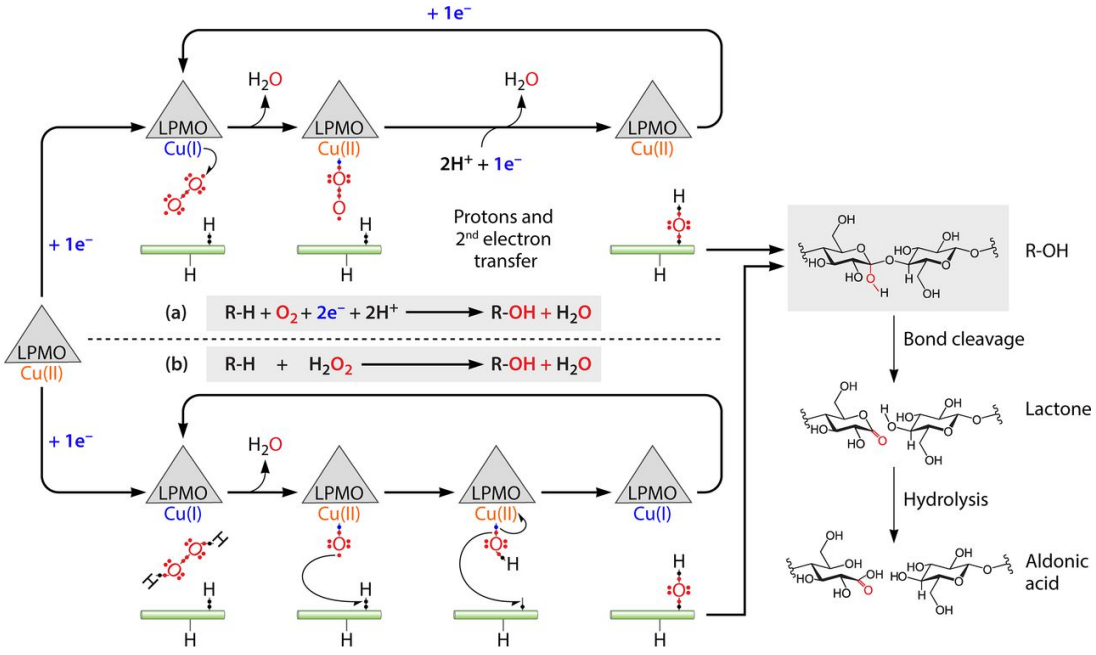

Figure 1.9. Reaction pathways for LPMO reactions with O_2 (a) or H_2O_2 (b) as co-substrate. Both pathways are initiated by reduction of the copper co-factor, from Cu(II) to Cu(I), which primes the enzyme for further catalysis. Subsequent to activation, the O_2 pathway (a) further requires delivery of a second electron and two protons to carry out one catalytic cycle, whereas in the H_2O_2 pathway (b), the co-substrate itself is adequate both to complete turnover, leaving the enzyme in the reduced ("primed") state, ready for another catalytic event. Despite obvious differences, both pathways also rely on the activation of an oxygen species (i.e. O_2 and H_2O_2, respectively) to hydroxylate either the C1 or C4 carbon of the scissile bond. The scheme to the right shows a C1-hydroxylated product that undergoes a spontaneous reaction, which eliminates the glycosidic bond and generates a lactone that further hydrolyzes into its respective aldonic acid. This figure was taken from (Bissaro et al., 2018).

Which is possibly unassisted by the enzyme (Wang et al., 2018). In case of the latter, some researchers consider it to be inappropriate to use the term “lytic” to describe LPMO functionality, and thus prefer the description PMO over LPMO (Beeson et al., 2015). Depending on the substrate and regioselectivity of the enzyme, either the C1 or C4 carbon of the scissile bond will be hydroxylated, yielding a 1,5-δ-lactone and a 4-ketoaldose, respectively (Fig. 1.10). These products will exist in a pH-dependent equilibrium with their corresponding hydrates, aldonic acid and geminal diol (or gemdiol), respectively, where alkaline pH will favor the hydrated form (Isaksen et al., 2014). Notably, LPMOs that produce mixtures of C1- and C4-oxidized products will also generate double oxidized products, i.e. oligomers that have both chain ends oxidized, as well as non-oxidized products. The latter could explain why some studies detected an apparent weak hydrolytic activity for LPMOs (Westereng et al., 2017). Such weak apparent activity could also be detected for C4-oxidizing LPMOs since such LPMOs will generate products with normal reducing ends, which will appear as cellulase products in common cellulase activity assays that are based on detecting newly formed reducing ends. Of note, C4-oxidized products have never been detected for chitin-active LPMOs.

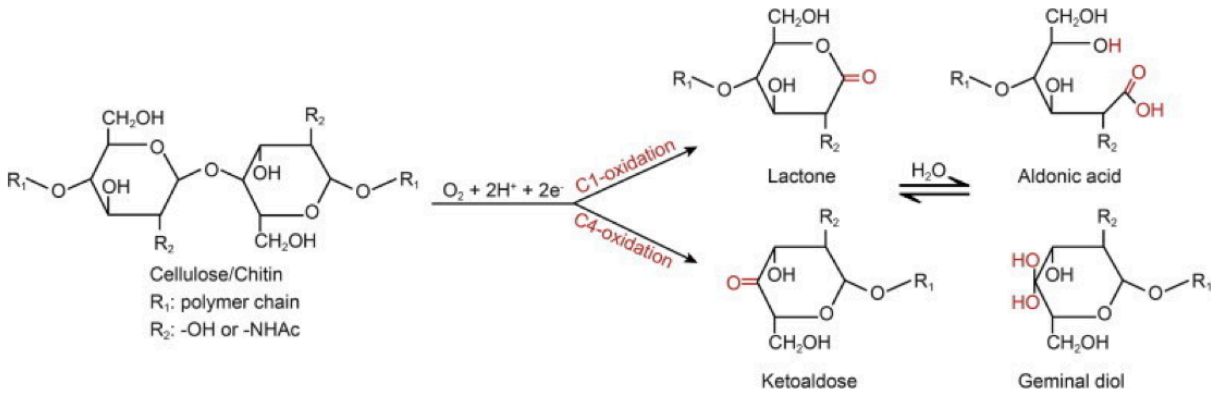

Figure 1.10. Oxidized products generated by LPMOs. The reaction scheme illustrates the formation of lactone and ketolase through by C1- and C4-oxidation, respectively, both which will exist in a pH-dependent equilibrium with their respective hydrates aldonic acid and geminal diol. The picture was taken from (Loose et al., 2014).

Following priming reduction, the O_2 driven mechanism depends on the delivery of an additional electron and two protons to complete the catalytic cycle (Fig. 1.9; O_2 pathway). However, direct delivery of the second electron from an electron donor to the copper cofactor during catalysis seems challenging as the enzyme would be tightly bound to the substrate at this moment (Courtade et al., 2016; Bissaro et al., 2017). To resolve the controversial "second electron conundrum", the existence of aromatic systems for electron storage or transfer (e.g. electron tunneling and electron transport chains) has been suggested (Solomon et al., 2014; Beeson et al., 2015; Walton & Davies, 2016). However, such systems have yet to be identified in LPMOs. In the H_2O_2 driven reaction (Fig. 1.9; H_2O_2 pathway), the enzyme is able to catalyze multiple reactions after the initial one-electron priming of the copper ion, until an occasional re-oxidation of the copper cofactor occurs, in which reactivation by an external electron donor is required (Bissaro et al., 2018b). This scenario has been supported by observations of supra-stoichiometric product formation (i.e. relative to the reductant) in reactions with exogenous H_2O_2 and low amounts of reductant (Bissaro et al., 2017; Müller et al., 2018). Bissaro et al. (2017) further showed that H_2O_2-scavenging enzymes such as Horseradish peroxygenase, inhibit LPMO activity under standard reaction conditions (i.e. with O_2 and reductant). They also reported a clear catalytic preference for H_2O_2, which was demonstrated ed in an experiment with $H_2{}^{18}O_2$, in the presence of ten-fold surplus of molecular oxygen (i.e. $^{16}O_2$). Several subsequent studies support the peroxygenase premise (Hangasky et al., 2018; Kuusk et al., 2018; Müller et al., 2018; Wang et al., 2018; Hegnar et al., 2019).Withal, elucidating reaction intermediates still awaits experimental verification, and the role of H_2O_2 as an LPMO co-substrate therefore remains under discussion (Bissaro et al., 2018b; Chylenski et al., 2019; Eijsink et al., 2019; Forsberg et al., 2019; Hangasky et al., 2019).

1.3.5 Further aspects of catalytic activity

The lower the reduction potential a reducing, the more efficiently it can drive an LPMO reaction (Kracher et al., 2016). LPMOs generally display varying preferences for reducing agents based on their active site architecture and associated LPMO-Cu(II)/Cu(I) reduction potentials, which

can range from 155-326 mV, but lie around 250 mV for most LPMOs (Frommhagen et al., 2016 & 2018b). Because the stability and redox properties of reducing agents further depend on both temperature and, particularly, pH, the performance of a specific LPMO-reductant system will also depend on these parameters (Kracher et al. 2016; Frommhagen et al., 2018a). Ascorbic acid, which has a relatively low reduction potential (i.e. around -0.1 mV at pH 6.0), is commonly utilized in experiments with LPMOs. However, potent reductants like ascorbic acid may also reduce free transition metals such as Cu^{2+}, which thereafter may react with O_2 or H_2O_2 (Fig. 1.11).

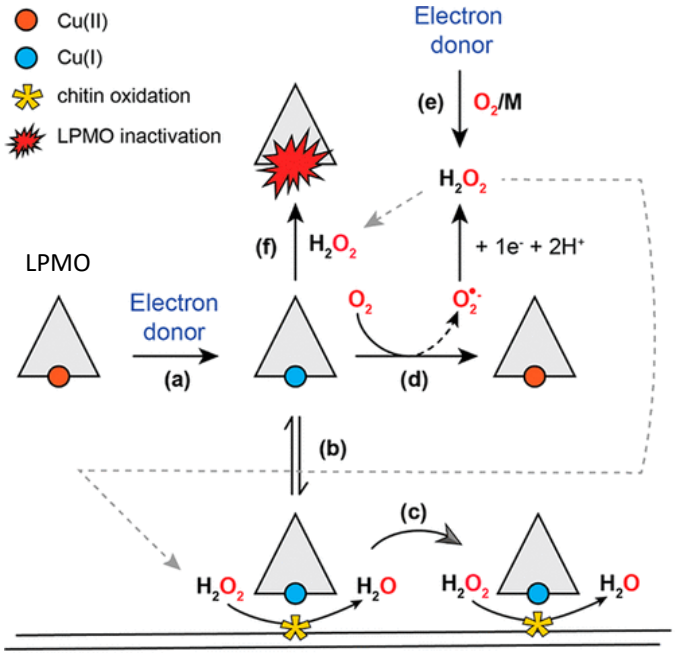

Figure 1.11. Off-pathway reactions in H_2O_2-driven LPMO catalysis. In the absence of a reducing agent, LPMOs will be in their inactive state with an oxidized (red) copper. Upon one-electron reduction by an external reducing agent (a), the enzyme becomes primed for catalysis (b and c). Primed enzymes may generate H_2O_2 from O_2 and thus display oxidase activity (d). H_2O_2 can also be produced by reducing agents through autoxidation of O_2, which is catalyzed by free transition metals (M) in the solution (e). Highly reactive oxygen species can be formed if primed LPMOs react with H_2O_2 in the absence of a substrate, which exposes the active-site histidines to oxidation, leading to inactivation of the LPMO (f). The figure was taken from (Loose et al., 2018) and slightly modified.

Illustrated by Fig. 1.11, LPMOs are prone to autocatalytic inactivation during catalysis. This was first shown for reactions with excess amounts of H_2O_2 (Bissaro et al., 2017). When activated LPMOs are not protected by the "caged" environment formed by productive binding to a substrate, Bissaro et al. (2017) propose that the reduction of H_2O_2 by LPMOs may result in oxidative attack on one of the active-site histidines, and thus lead to self-inactivation. While studies on copper-binding have shown that LPMOs bind Cu(I) with higher affinity than Cu(II) (Quinlan et al., 2011; Aachmann et al., 2012), another study has suggests that reduction of the copper cofactor increases the affinity of LPMOS toward cellulose (Kracher et al., 2018). Thus, the system seems tailored for directing the reduced LPMO, which is prone to inactivation, to the substrate, and thereby ensure that reactions with H_2O_2 are productive and do not damage the enzyme. The N-terminal histidine of fungal LPMOs (i.e. AA9s) is post-translationally modified to carry a τ-methylation (i.e., methylation of Nε2), which seem to protect these enzymes from autocatalytic oxidation (Petrović et al., 2018). Other protective strategies, *in vivo* or *in vitro*, may include utilization of ROS-scavenging enzymes (e.g. catalase) to control oxidative stress (Scott et al., 2016), the use of less potent reducing agents with reducing potentials ≥ +160mV (Hegnar et al., 2019), regulating the excess of free copper using chaperone proteins (Chaplin et al., 2016), or controlled electron delivery via redox enzymes like cellobiose dehydrogenase (Phillips et al., 2011; Loose et al., 2016).

Importantly, while some claim that autocatalytic inactivation is specific for H_2O_2-driven reactions (Hangasky et al., 2018, 2019), available kinetic data clearly show that similar inactivation processes also happen in O_2-driven reactions (Loose et al., 2018; Müller et al., 2018; Eijsink et al., 2019; Chylenski et al., 2019). This can either mean that the O_2- and H_2O_2-driven reactions have similar stability challenges, or support the claim that O_2-driven reactions in fact are limited by the in situ generation of H_2O_2 and that the only true catalytic activity of an LPMO is that of a peroxygenase (Bissaro et al., 2017& 2018).

1.3.6 Determinants of substrate-binding and oxidative regioselectivity

As mentioned in section 1.3.3, the substrate-binding surface of LPMOs is shaped by elongated loops, which often referred to as L2, L3, LS (short loop), and LC (long C-terminal loop) (Vaaje-Kolstad et al., 2005a; Aachmann et al., 2012; Li et al., 2012; Wu et al., 2013)

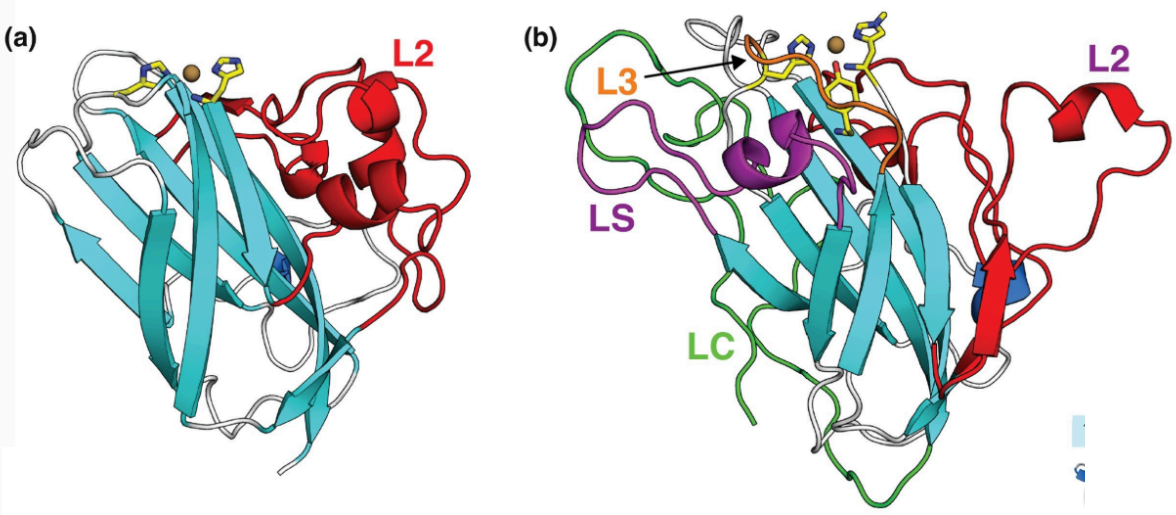

Figure 1.12. LPMO-loops important for substrate binding. Illustration (a) and (b) show the typical fold of an AA10 (CBP21, PDB: 2BEM) and AA9 (NcLPMO9M, PDB: 4EIS), respectively. Loops that contribute to the substrate-binding surface (L2, L3 LS and LC) are indicated. Note that NcLPMO9M, which is an C1/C4 cellulose oxidizing AA9 enzyme, have a relatively short L3 loop that is generally more prominent in C4 oxidizing AA9s (Vu et al., 2014). This picture was taken from (Vaaje-Kolstad et al., 2017).

1.4 Aims of this study

While some fungal genomes encode more than 30 *lpmo* genes, bacterial genomes contain considerable fewer *lpmo* genes, often only one or two, and maximally less than 10. Actinomycetes, a taxonomic subgroup within the phylum Actinobacteria, tend to have relatively complex CAZyme repertoires, which include a high number of LPMOs, compared to bacteria of other phyla (e.g. Firmicutes and Proteobacteria) (Takasuka et al., 2013). Actinomycetes are Gram-positive aerobes with high CG-content (Ventura et al., 2007) and make up considerable proportions of aquatic and soil microbiomes, where they play an essential role in the turnover of organic matter (Saini et al., 2015). Their ability to efficiently degrade polysaccharide biomass in a broad range of environmental conditions (i.e. pH, temperature, salinity), makes Actinomycetes attractive for bioprospecting of novel carbohydrate-active enzymes such as LPMOs.

Originally, this study focused on five novel *lpmo* genes identified through bioinformatic analysis of sequencing data derived from a marine water-samples, with the aim to discover exotic LPMOs originating from Actinomycetes. The plan was to succeed in expressing at least one of them and carry out a thorough characterization. However, after two months of failed expression trials and no detection of LPMO activity, the project was abolished. Instead, the research was focused on a novel Actinomycete LPMO which had already been successfully expressed, namely *Sc*LPMO10D from *Streptomyces coelicolor.*

The novel *Sc*LPMO10D enzyme display a rather unusual amino acid sequence. Compared to previously characterized LPMOs, *Sc*LPMO10D has an additional C-terminal domain which is predicted to covalently anchor the catalytic domain to the cell wall (Fig. 1.16). The cell wall of Gram-positive bacteria consists of several layers of peptidoglycan, which is covalently and noncovalently decorated with teichoic acids, polysaccharides, and proteins (Marraffini et al., 2006). The C-terminal domain of *Sc*LPMO10D features a common cell wall sorting-motif, namely LPxTG, which is known to be targeted for cleavage and covalent coupling to the

peptidoglycan layers by sortase enzymes (Boekhorst et al., 2005). Interestingly, *Sc*LPMO10D and other AA10 enzymes identified to display C-terminal domains with LPxTG motifs are clustered upon phylogenetic investigation (Fig. 1.17; Frosberg et al., 2018), which may suggest that this feature has evolved to fulfill a distinct function.

Nevertheless, as indicated in Figure 1.16, the *Sc*LPMO10D enzyme investigated in this research is a truncated version of the full-length enzyme. The C-terminal domain and GD-linker was removed to be able to specifically study the catalytic activity of the enzyme and to avoid enzyme aggregation during expression. Therefore, bear in mind that the truncated version will be referred to as the wild type enzyme throughout this thesis, only to distinguish it from its mutated versions.

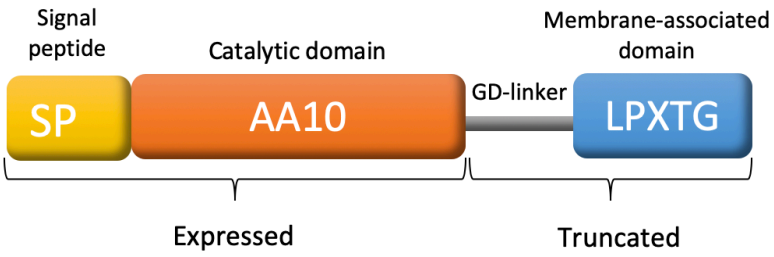

Figure 1.16. Modularity of the ScLPMO10D enzyme. The figure displays a schematic overview of the different domains identified in the amino acid sequence of *Sc*LPMO10D. The non-matured protein displays an N-terminal signal peptide (SP) which needs to be removed to generate a functional enzyme. In the mature protein, the catalytic N-terminal module features an AA10 domain which is fully functional, followed by a C-terminal domain with a LPxTG sorting-motif. The N-terminal and C-terminal domains are connected through a linker region especially rich in glycine and aspartic acid residues. The brackets indicate what part of the full-length enzyme investigated in this thesis.

In addition to belonging to a novel clade of LPMO10s of unknown substrate specificity predicted to be anchored to the cell wall, *Sc*LPMO10D share conserved structural features with both chitin- and cellulose-oxidizing LPMOs. During the first phase of this research, *Sc*LPMO10D was

determined to be a chitin C1-oxidizing enzyme. Notably, a large number of *Streptomyces* species are able to grow on plant biomass, but relatively few have been found to efficiently depolymerize crystalline cellulose (Takasuka et al., 2013). In the next phase of the project, a rational approach was utilized in an attempt to engineer *Sc*LPMO10D into a cellulolytic enzyme. Besides trying to alter the substrate specificity, the aim was to obtain information about specific structural determinants predicted to be important for substrate interactions.

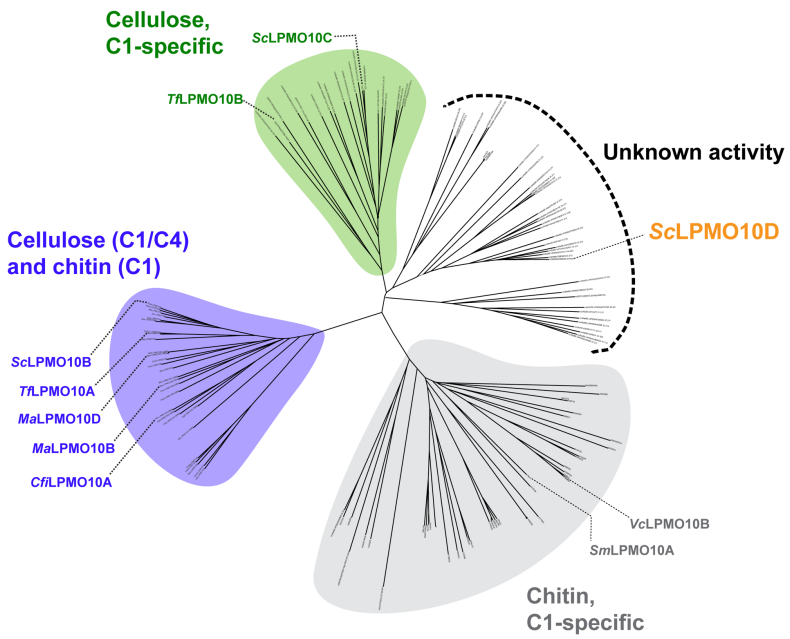

Figure 1.17. Phylogenetic tree constructed from 130 LPMO10-sequences. Enzymes with green labels have been characterized as strict C1 cellulose oxidizers, whereas purple labels indicate enzymes with known C1/C4-oxidizing activity on cellulose and C1-oxidizing activity on chitin, and grey labels indicate enzymes known to oxidize C1 in chitin. The fourth, non-colored cluster contains uncharacterized enzymes with unknown activity. A smaller cluster within the cluster of unknown activities have been found to employ C-terminal domains which have been predicted to be covalently anchored to the cell wall in Gram-positive bacteria. Among the enzymes of this smaller cluster is the enzyme described in this thesis, *Sc*LPMO10D, highlighted in orange. The figure was taken from (Forsberg et al., 2018), and slightly modified for the purpose of this thesis.

2. MATERIALS

2.1 Laboratory equipment

Table 2.1. Laboratory equipment.

EQUIPMENT	SPECIFICATION	SUPPLIER
Anion-Exchange Chromatography	ÄKTA pure™ protein purification system	GE Healthcare
	HiTrap® Q FF. 5 ml column	GE Healthcare
Antifoaming agent	Antifoam 204	Sigma
Automatic pipettes	Finnpipette F2 Pipettes, single channel pipettes	Thermo Scientific
Balances	Sartorius basic	Sartorius
	Microbalance	Sartorius
Biosafety cabinet	Safe 2020 Class II	Thermo Fisher
Blue-cap bottles	1000 ml, 500 ml, 250 ml, 100 ml, and 50 ml	VWR
Centrifuges	Avanti™ J-25 Centrifuge	Beckman
	5418R	Eppendorf
	mySPIN™ 6 Mini Centrifuge	Thermo Fisher
	Haerus Multifuge	Thermo Fisher
Centrifuge rotors	JA10, JA25.50	Beckman
Centrifuge tubes	500 ml, 25 ml	Nalgene
Centrifuge filters for protein concentration	Amicon Ultra-15 10K	Merck Millipore
Cryotubes	2 ml	Sarstedt
Electrophoresis equipment	Grant QBD2, sample boiler	Grant
	Mini PROTEAN® TGX Stain-Free™ Gels	Bio-Rad
	Mini-PROTEAN® Tetra Cell vertical mini gel electrophoresis system	Bio-Rad
	PowerPac 300, power supply	Bio-Rad
	Gel Doc EZ Imager	Bio-Rad
	BenchMark™ Protein Ladder	Thermo Fisher
Eppendorf tubes	1.5 ml - Axygen®	VWR
Falcon tubes	15 ml, 50 ml	
Filters	Filter Upper Cup 250 ml bottle top filter 0.2 µm, PES membrane	VWR
	MultiScreenHTS GV Filter Plate, 96 well, 0.22 µm	Merck Millipore

	Filtropur S 0.2 syringe filter, PES membrane	Sarstedt
Freezer (-18 ℃)		Bosch Whirlpool
Freezer (-80 ℃)	Ultra-Low	SANYO
Fume hood	Mc6	Waldner
Glass equipment		Schot-Duran/VWR
HPLC-PAD	Dionex™ CarboPac™ PA1, analytical and guard columns.	Thermo Scientific
	Dinoex™ ICS 3000 Ion Chromatography System	Thermo Scientific
	Dinoex™ Gold Disposable Electrode, carbohydrate certified	Thermo Scientific
HPLC system		Thermo Scientific
Incubator systems	Eppendorf Thermomixer C	Eppendorf
	Heratherm™ Refrigerated Incubator	Thermo Fisher
	Multitron Standard Incubator	Infors HT
	Heated bath circulator	Thermo Scientific
	LEX-48 Bioreactor	Harbinger
Inoculation toothpick	Regular, wood	Sarstedt
Magnetic stirrer		VWR
MALDI-ToF MS	Nitrogen laser, 337 nm	Bruker Daltonics
	MTP 384 target plate ground steel BC	Bruker Daltonics
	Ultraflex MALDI-ToF/ToF instrument	Bruker Daltonics
Multiskan™FC Microplate Photometer		Thermo Scientific
Pasteurpipettes	Plastic: 5 ml, 10 ml	VWR
PCR system	SimpliAmp™ Thermal Cycler	Thermo Scientific
PCR tubes	0.2 ml	VWR
Petri dish	9 cm	Heger
pH benchtop meter	FiveEasy™ Plus	Mettler Toledo Sentron
Pipette tips	Next Generation Pipette Tips	VWR
Refrigerator (4 ℃)		Whirlpool
RSLC	Dionex™ UltiMate™ 3000 RSLC system	Thermo Fisher
	Rezex™ RFQ-Fast Acid H+ (8%) 7.8 x 100 mm column	Phenomenex

Size-Exclusion Chromatography	ÄKTAprime™ Plus chromatography system	GE Healthcare
	HiLoad™ 16/600, Superdex™ 75 prep grade	GE Healthcare
Sonicator bath	Transonic 460/H	Elma
Spectrophotometer	AG Biophotometer	Eppendorf
Syringe filters	0.22 µm, 0.45 µm	Sarsted
Syringes	50 ml, 20 ml, 10 ml, 2 ml	Merck
Thermal Shift Analysis	MicroAmp™ Optical 96-Well Reaction Plate	Thermo Fisher
	MicroAmp® Optical Adhesive Film	Thermo Fisher
	Step-One Plus™ Real-Time PCR System	Applied Biosystems
Thermomixer	Comfort C	Eppendorf
Ultrasound bath	Transsonic 460/H	Elma
Cuvettes	Eppendorf® UVette®, 2 × 10 mm	Eppendorf
	BRAND® standard disposable cuvettes, 4.5 × 23 mm	Brand
	µCuvette® G1.0	Eppendorf
Vacuum manifold		Millipore
Vortexer	Vortex-2 Genie MS 3 basic	Scientific Industries IKA
Weighing boats	Disposable, plastic	VWR
Whirlmixer	Vortex-Genie 2 MS 3 Basic	Scientific Industries IKA

2.2 Chemicals and buffers

Table 2.2. Chemicals and buffers

CHEMICAL	FORMULA	SUPPLIER
Agar agar		Merck Millipore
Ampicillin sodium salt	$C_{16}H_{18}N_3NaO_4S$	Sigma-Aldrich
Bacto™ Yeast Extract, granulated		Merck
Bacto™ Tryptone (peptone from casein)		Merck
Copper(II) sulfate	$CuSO_4$	VWR

Distilled water, dH_2O (Milli-Q quality)	H_2O	Merck Millipore
Ion-free water, FLUKA TraceSELECT®	H_2O	Sigma-Aldrich
Ethylenediaminetetraacetic acid (EDTA)	$C_{10}H_{16}N_2O_8$	Sigma-Aldrich
Ethanol 96 %	C_2H_5OH	VWR
Glycerol 85 %	$C_3H_5O_3$	VWR
Hydrogen chloride	HCl	Sigma-Aldrich
L-Ascorbic acid	$C_6H_8O_6$	Sigma-Aldrich
Magnesium chloride	$MgCl_2$	VWR
Matrix solution, 2.5-dihydroxybenzoic acid	$C_7H_6O_4$	Bruker Daltonics
NuPAGE™ LDS Sample Buffer 4×		Thermo Fisher
NuPAGE™ Sample Reducing Agent 10×		Thermo Fisher
Potassium phosphate dibasic	K_2HPO_4	Sigma-Aldrich
Potassium phosphate monobasic	KH_2PO_4	Sigma-Aldrich
Sodium chloride	NaCl	Sigma-Aldrich
Sodium hydroxide	NaOH	VWR
Sodium phosphate dibasic	HNa_2O_4P, H_2O	Sigma-Aldrich
Sodium phosphate monobasic	H_2NaO_4P, $2H_2O$	Sigma-Aldrich
Tris-Glycine-SDS Buffer 10×		Bio-Rad

2.3 Self-made buffers and stock solutions

Table 2.3. Self-made buffers and solutions. All solutions were stored at room temperature, unless indicated otherwise

BUFFER / STOCK SOLUTION	CONTENT
Ascorbic acid 100 mM	88.06 mg Ascorbic acid Add Trace select water to 5 ml, store aliquots at -20 °C.
Sodium phosphate buffer 0,5 M, pH 6.0	12.192 g Sodium phosphate dibasic 59.543 g Sodium phosphate monobasic Add dH_2O to 1000 ml, adjust pH, filtrate through 0.2 µm filter.

Spheroplast buffer	100 ml Tris-HCl 1 M, pH 8.0 171 g Sucrose 1 ml EDTA 0.5 M, pH 8.0 Add dH_2O to 1 L, filtrate through 0.2 µm filter, store at 4 °C.
Tris-HCl 1 M, pH 8.0	121.1 g Tris-Base Add dH_2O to 1000 ml, adjust pH, filtrate through 0.2 µm filter.
Tris-HCl 50 mM NaCl 200 mM, pH 8.0	50 mL 1 M Tris-HCl pH 8.0 11.69 g NaCl Add dH_2O to 200 ml, adjust pH, filtrate through 0.2 µm filter.
Tris-HCl 1 M, pH 9.0	121.1 g Tris-Base Add dH_2O to 1000 ml, adjust pH, filtrate through 0.2 µm filter.
Tris-HCl 50 M, pH 9.0	50 ml 1 M Tris-HCl pH 9.0 Add dH_2O to 200 ml, adjust pH, filtrate through 0.2 µm filter.
Tris-HCl 50 mM NaCl 1 M, pH 9.0	50 ml 1 M Tris-HCl pH 9.0 58.44 g NaCl Add dH_2O to 200 ml, adjust pH, filtrate through 0.2 µm filter.

2.4 Bacterial strains

Table 2.4. Bacteria Strains.

BACTERIA STRAIN	SPECIFICATION	SUPPLIER
One Shot® BL21 Star™ (DE3)	Chemical competent *E. coli* cells for protein expression	Life Technologies
One Shot® TOP10	Chemical competent *E. coli* cells for plasmid production	Life Technologies

2.5 Kits

Table 2.5. Kits.

KIT	CONTENT	SUPPLIER
Amplex® Red Hydrogen Peroxide/ Peroxidase Assay Kit	5 x reaction buffer (0.25 M sodium phosphate, pH 7.4) Amplex® Red (154 µg) Dimethyl sulfoxide (DMSO) 10 U Horseradish peroxidase (HRP)* Hydrogen peroxide (H_2O_2)	Thermo Scientific
NucleoSpin® Plasmid QuickPure Kit	Resuspension Buffer A1 (with RNase) Lysis Buffer A2 Neutralization Buffer A3 Wash Buffer AQ (with EtOH) Elution Buffer AE QuickPure Columns Collection Tubes (2 ml)	Macherey-Nagel
Protein Thermal Shift™ Dye Kit	Protein Thermal Shift™ Buffer Protein Thermal Shift™ Dye	Life Technologies
QuikChange® II XL Site-Directed Mutagenesis	*Pfu*Ultra High-Fidelity DNA polymerase (2.5 U/µl)* 10 reaction buffer *Dpn* I restriction enzyme (10 U/µl)* dNTP mix	Agilent Technologies

*One U (µmol/min) referrers to the amount of enzyme needed to catalyze the conversion of one micromole of substrate per minute under the specified conditions of the respective assay (Terminology of bioanalytical methods, IUPAC Recommendations 2018).

2.6 Substrates

Table 2.6. Polysaccharide substrates.

SUBSTRATE	SOURCE	SPECIFICATIONS	SUPPLIER
α-chitin	Shrimp shell	Dried and milled (~400 µm particle size, ash 1.7 %, 4.7 % moisture)	Sea garden
β-chitin	Squid pen	Dried and milled (~400 µm particle size)	France chitin, Marseille, France
Avicel® PH-101	Cellulose	~50 µm particle size	Sigma-Aldrich
PASC	Avicel® PH-101	Phosphoric acid swollen cellulose	Made in-house (Wood et al., 1988)
BMCC	Bacteria	Bacterial microcrystalline cellulose	Wien (BOKU university)

2.7 Enzymes and protein

Table 2.7. Enzymes and proteins used for analysis, processing of samples or analysing molecular weight.

ENZYME	ORIGIN	PRODUCER
CBP21 (SmAA10A)	(Vaaje-Kolstad et al., 2005)	Inhouse
CelS2-N (ScLPMO10C without CBM2)	(Forsberg et al., 2014)	Inhouse
ChiA	(Vaaje-Kolstad et al., 2013)	Inhouse
Chitobiase	(Loose et al., 2014)	Inhouse
ScLPMO10D (Without C-terminal domain)	Unpublished study, inhouse	This study
ScLPMO10D-2a		This study
ScLPMO10D-2b		This study
ScLPMO10D-3a		This study
ScLPMO10D-3b		This study
ScLPMO10D-4a		This study
ScLPMO10D-4b		This study
TfCel6A		Inhouse

2.8 Software and online applications

Table 2.8. Software and online servers

SOFTWARE	APPLICATION	SUPPLIER / WEB ADDRESS
ÄKTA Prime™ Plus chromatography system	Anion-exchange chromatography	ÄKTA
CLC DNA Workbench	Sequencing	CLCbio
Chromeleon 0.7	Analysis of oxidized product	Chromeleon
ESPript 3.0	MSA modification	http://espript.ibcp.fr/ESPript/ESPript/
ExPASy ProtParam tool	Calculations of pI, MW and ε	https://web.expasy.org/protparam/
FlexControl Version 3.4 Software	MALDI-ToF MS	Bruker Daltonics
FlexAnalysis Version 3.4 Software	MALDI-ToF MS	Bruker Daltonics
Image Lab™ Version 6.0.1	Visualization of gels and quantification of protein purity	BioRad
MUSCLE	Multiple sequence alignment	https://www.ebi.ac.uk/Tools/msa/muscle/
Protein BLAST	Sequence analysis	https://blast.ncbi.nlm.nih.gov/Blast.cgi?PROGRAM=blastp&PAGE_TYPE=BlastSearch&LINK_LOC=blasthome
PyMOL Molecular Graphics System, Version 2.2	Mutant design and analysis	Schrödinger
SkanIt	Multiskan™ FC Microplate Photometer	Thermo Scientific
StepOne™ Software v2.2	Real time PCR	Applied Biosystems
SWISS-MODEL	Homology Modelling	https://swissmodel.expasy.org/
QuikChange Primer Design tool	Primer design for site-directed mutagenesis	https://www.agilent.com/store/primerDesignProgram.jsp
Unicorn 5.20 Workstation Software	Protein purification	GE Healthcare
WebLogo 3	Analyzing conserved residues	http://weblogo.berkeley.edu/logo.cgi

2.9 Primers

TABLE 2.9. Designed primers for site-directed mutagenesis of *Sc*LPMO10D

USAGE	REVERSE (R) & FORWARD (F) PRIMERS	5' to 3'
Site-directed mutagenesis	G81S-R	CGCCGCGTTGCTAATACGGATACCGTTCCAAT
	G81S-F	ATTGGAACGGTATCCGTATTAGCAACGCGGCG
Site-directed mutagenesis	K135P-R	ACTTTAAAGGTGCCCGGGTGCGGCGCGGTCAC
	K135P-F	GTGACCGCGCCGCACCCGGGCACCTTTAAAGT
Site-directed mutagenesis	D74N-R	GGATACCGTTCCAATTGTACAGCGCCTGGGT
	D74N-F	ACCCAGGCGCTGTACAATTGGAACGGTATCC
Site-directed mutagenesis	D74N_N76F-R	TGCTAATACGGATACCGAACCAATTGTACAGCGCCTGGGTGC
	D74N_N76F-F	GCACCCAGGCGCTGTACAATTGGTTCGGTATCCGTATTAGCA
Site-directed mutagenesis	T131W-R	GCCCGGGTGCGGCGCCCACACACGATACTTGAA
	T131W-F	TTCAAGTATCGTGTGTGGGCGCCGCACCCGGGC
Site-directed mutagenesis	T131Q-R	GCCCGGGTGCGGCGCCTGCACACGATACTTGAA
	T131Q-F	TTCAAGTATCGTGTGCAGGCGCCGCACCCGGGC
Site-directed mutagenesis	V130D-R	CGGGTGCGGCGCCTGATCACGATACTTGAAGGT
	V130D-F	ACCTTCAAGTATCGTGATCAGGCGCCGCACCCG
Sequencing	*Sc*LPMO10D_seq-R	TTTAGAGGCCCCAAGGGGTT
Sequencing	*Sc*LPMO10D_seq-F	GATCTCGATCCCGCGAAATT

3. METHODS

3.1 Cultivation of *Escherichia coli*

E. coli is a Gram-negative, facultative anaerobe, which naturally resides in the large intestine of warm-blooded animals. Today, *E. coli* is a well-studied model for prokaryotic organisms, which is widely utilized in the fields of biotechnology, biochemistry, molecular biology, and genetics. Known for its rapid growth rate, with a generation time down to 20 min, and ability to grow with or without oxygen, *E. coli* further allows the usage of relatively simple transformation procedures. Consequently, specialized strains have been developed for different purposes such as gene cloning and heterologous protein expression. In this thesis, *E. coli* One Shot® TOP10 cells were used to generate high copy numbers of plasmids (pRSET-B vector constructs with *lpmo* genes), while E. coli BL21 Star™ (DE3) cells were used for heterologous expression of the wild type enzyme and its mutants (Table 2.4).

3.1.1 Antibiotics

The β-lactam antibiotic ampicillin (Amp) is a common antibiotic and resistance to this antibiotic is used as a selection marker in gene cloning and protein expression in *E. coli*. Amp is an irreversible inhibitor of the transpeptidase enzyme and kills bacteria through the inhibition of cell wall synthesis (Wilke et al., 2005). The pRSET-B expression vector encodes the enzyme β-lactamase, which hydrolyzes the β-lactam ring of Amp and thereby inactivates it. Thus, cells that have successfully taken up pRSET-B (i.e. transformants) become resistant against Amp and may therefore grow in medium with a defined concentration of Amp, while other strains will not be able to grow.

Ampicillin stock solution (100 mg/ml):

- 1 g sodium ampicillin

Dissolve the ampicillin salt in a final volume of 10 ml of dH_2O. Filtrate the solution with a prewashed 0.22 µm sterile filter and store the finished ampicillin stock solution in aliquots at -20 °C, for one year shelf life.

3.1.2 Agar and cultivation media

Lysogenic broth (LB)

Liquid medium:

- 10 g Bacto™ Tryptone
- 5 g Bacto™ Yeast Extract
- 10 g NaCl

The solid ingredients were dissolved in 800 ml dH_2O and the volume was thereafter adjusted to 1 liter with dH_2O before autoclaving at 121 °C for 20 min. To prepare media for cultivation of transformants, ampicillin was added to a final concentration of 100 µg/ml.

Agar plates:

- 10 g Bacto™Tryptone
- 5 g Bacto™ Yeast Extract
- 10 g NaCl
- 15 g Agar

Solid ingredients were dissolved and suspended in 800 ml dH_2O and the volume was thereafter corrected to 1 liter with dH_2O, followed by autoclaving at 121 °C for 20 min. The autoclaved medium was cooled down to ~ 55 °C before 500 µl ampicillin solution (*100 mg/ml)* was added in a sterile bench. The ampicillin was gently mixed with the medium without making any air bubbles. While the medium was still liquified, it was poured into petri dishes and cooled further down. After the medium had solidified (after ~ 20 min), the resulting agar plates were stored upside-down at 4 °C.

Terrific broth (TB)

Phosphate solution:

- 11.57 g KH_2PO_4
- 62.7 g K_2HPO_4

The chemicals were mixed and dissolved in dH_2O to a final volume of 0.5 liter, followed by autoclaving at 121 °C for 20 min.

Liquid medium:

- 12 g Bacto™ Tryptone
- 24 g Bacto™ Yeast Extract
- 4 ml 85 % (v/v) glycerol

The ingredients were dissolved in dH_2O to a final volume of 900 ml and thereafter partitioned into two 1 L blue-cork bottles, 450 ml in each. The bottles with medium were autoclaved at 121 °C for 20 min. Prior to usage, the liquid medium was supplemented with 50 ml of phosphate solution, 500 µl of ampicillin solution (giving a final concentration of 100 µg/ml), and 50 µl of antifoaming agent.

3.1.3 Cultivation in small volumes

All reagents and media used for cultivation were sterilized by either autoclaving or sterile-filtration (0.22 µm). All work with bacterial cultures and colonies was performed under sterile conditions. To initiate a new culture, a piece of a glycerol stock (section 3.1.4) or a single colony from an agar plate (section 3.2.4) was used to inoculate 5 ml of LB medium supplemented with 100 µg/ml ampicillin, followed by cultivation overnight at 37 °C in a shaking incubator (200 rpm).

3.1.4 Long-term storage of bacterial cultures

Long-term storage of cultures was accomplished by making glycerol stocks. Glycerol works as a cryoprotectant and prevents cell damage caused by freezing (Polge et al., 1949).

Glycerol stock:

- 1 ml overnight culture
- 300 µl 85% glycerol (v/v), autoclaved

After gently mixing of the culture with glycerol in a cryogenic tube, the resulting glycerol stock was stored at -80 °C.

3.2 Production of mutants

Site-directed mutagenesis is an invaluable technique for characterizing the relationship between protein structure and protein function. For this purpose, two main mutants with five mutations each were rationally designed as described in section 4.2. Optimized mutagenic primers (Table 2.9) were designed (section 3.2.1) and used to generate the desired mutations (Table 4.1). To produce the first mutations (section 3.2.3), an inhouse pRSET-B vector construct with the gene encoding the catalytic domain of *Sc*LPMO10D (Appendix A), was utilized as a template. To generate additional mutations, already mutated plasmids were used as templates. The mutated plasmids were transformed into One Shot® TOP10 chemically competent *E. coli* cells via heat shock (section 3.2.4). After plasmid amplification in TOP10 cells, plasmids were isolated using the protocol described in section 3.2.2. Mutated plasmids were further sequenced to verify that the desired mutations had been incorporated (section 3.2.5), before additional site-directed mutations were generated.

3.2.1 Primer design

Site-directed mutagenesis requires two primers, one forward primer and one reverse primer, each containing the desired mutation. The oligonucleotide primers, each complementary to the opposite strands of the vector (e.g. encoding *Sc*LPMO10D variants), are extended during temperature cycling by DNA Polymerase. The designed primers should be approximately 25-45 base pairs long with the point mutation in the center of the primer. The ends of the primers need to be rich in GC-content to stabilize the binding to the vector. Importantly, the melting temperature (Tm) should be > 78 °C which can be ensured by for example designing primers

with GC-content higher than 40%. The sequence of a primer should also not display complimentary stretches that may lead to secondary structures, also referred to as false priming.

The online primer design application of Agilent Technologies (Table 2.8) was used to design optimized primers based on the factors described above. The mutagenic primers are given in Table 2.9.

3.2.1.1 Primer preparation

The primers (Table 2.9), which came in dehydrated form, were dissolved in dH_2O to make stock solutions with a concentration of 100 pmol/µl. Working solutions (10 pmol/µl) were prepared by diluting 5 µl of the stock solution in 45 µl dH_2O in new Eppendorf tubes. All primer solutions were stored at -20 ºC when not used.

3.2.2 Plasmid isolation

Plasmids (pRSET-B) of *Sc*LPMO10D variants were isolated from One Shot® E. coli TOP10 cells using the NucleoSpin® Plasmid QuickPure Kit and following its protocol for isolation of high-copy plasmid DNA from *E. coli*. All reaction steps were conducted at room temperature and centrifugation was conducted with 11 000 x g.

Materials

- NucleoSpin® Plasmid QuickPure Kit
- Centrifuge 5418 R
- 3 ml of overnight cell culture

Method:

The bacterial culture was transferred to a 1.5 ml Eppendorf tube and centrifugated for 30 seconds, before discarding the supernatant. This was done in two turns, to make a cell pellet from 3 ml culture. Thereafter, the harvested cell pellet was resuspended in 250 µl resuspension buffer (A1 supplemented with RNase). The resuspension buffer helps the cells to maintain an optimal pH in the following steps, and the added RNase digests bacterial RNA after cell lysis. To preform cell

lysis, 250 µl alkaline lysis buffer (A2) was mixed carefully with the solution by inverting the now closed tube 6-8 times. The lysis buffer contains sodium dodecyl sulfate (SDS) which disrupts the cell membrane and denatures proteins, and sodium hydroxide (NaOH) which helps to break down the bacterial cell wall. NaOH is also responsible for denaturing double-stranded DNA, transforming both genomic and plasmid DNA into single-stranded DNA. The sample was incubated at room temperature for no longer than five minutes, or until the lysate appeared clear. Afterwards, 300 µl neutralization buffer (A3) was added to stop the reaction and neutralize the resulting lysate, carefully mixing the ingredients by inverting the tube 6-8 times until the solution appeared completely colorless. Addition of neutralization buffer result in renaturation of both genomic and plasmid DNA. However, only the plasmid DNA renatures in its correct conformation due to its circular nature, while the longer genomic DNA is unable to renature correctly, and thus ends up as precipitate. The mixture was centrifuged for 10 minutes to separate the precipitated genomic DNA from the soluble plasmid DNA. The cleared supernatant with plasmid DNA was thereafter loaded onto a NucleoSpin® QuickPure column placed in a 2 ml collection tube and centrifuged for one minute. The plasmid DNA had been conditioned to bind to the silica membrane of the column, and the flow-through in the collection tube was therefore discarded. Contaminations like salts, metabolites, nucleases, and soluble macromolecular cellular components were removed through a single washing step with 450 µl washing buffer (AQ). After centrifugation for three minutes, the flow-through was discarded and the silica membrane was dried by centrifuging the tube for three more minutes. The QuickPure column was thereafter placed in a clean 1.5 ml Eppendorf tube and 50 µl elution buffer (AE) was added to the column. The elution buffer (AE) is composed of a Tris buffer with slightly a basic pH (8.5), which ensure stable storing conditions for plasmid DNA. Following a one-minute incubation at room temperature, the plasmid was eluted into the clean tube by centrifugation for one minute.

Plasmid DNA concentrations were further assessed by measuring A_{260}, using a µCuvette® G1.0 cuvette and small sample volumes of 3 µl. The elution buffer (AE) was used to calibrate the spectrophotometer. All isolated plasmids were stored at -20 °C until further use.

3.2.3. QuikChange II XL Site-Directed Mutagenesis

Single and multiple point mutants were generated using the QuikChange II XL Site-Directed Mutagenesis Kit. In this method, *PfuUltra* High-Fidelity DNA polymerase and a PCR thermal cycler is used to replicate the double strands of plasmid DNA, using two synthetic primers (forward and reverse) containing the desired mutations. After denaturation of the template DNA, the mutagenic primers anneal to complimentary sequences on their respective template strands. The temperature is thereafter adjusted to an optimal temperature for *PfuUltra* DNA polymerase, which extends the primers into full-length plasmids. After PCR, newly amplified plasmids are treated with the endonuclease *Dpn* I, which specifically target deoxyadenosine methylase (dam) methylated DNA. The DNA synthesized *in vivo* by One Shot® *E. coli* TOP10 cells is dam methylated and thus susceptible to digestion by *Dpn* I, while the mutated plasmids which have been synthesized *in vitro*, are left intact. The mutated plasmids will contain staggered nicks, but these are sealed *in vitro* after the plasmids have been transformed into competent *E. coli* cells.

Materials:

- QuikChange II XL Site-Directed Mutagenesis Kit
- Designed primers (Table 2.9.)
- Isolated plasmid templates of *Sc*LPMO10D variants

Procedure:

The parental DNA templates were obtained from transformed One Shot® E. coli TOP10 cells as described in section 3.2.2. PCR reactions (50 µl) were prepared on ice in 0.2 ml PCR tubes according to Table 3.5. *PfuUltra* HF DNA polymerase was the last reagent added to the mixture. The reactions were subjected to thermocycling in a SimpliAmp™ Thermal Cycler, using the parameters outlined below (Table 3.6). Subsequent to PCR, 1 µl of *Dpn* I was added directly into the reactions. Mixing of the reaction was performed by gently pipetting the solution up and down, before the reactions were spun down (short spin up to 6000 rpm) and incubated at 37 °C overnight. The next day, mutated plasmids were transformed into One Shot® *E. coli* TOP10 cells, according to section 3.2.4.

Table 3.1. Optimized PCR reaction setup for QuikChange II XL Site-Directed Mutagenesis of *Sc*LPMO10 D variants. This table shows the optimized reagent composition which was used when general recommendations failed to generate mutations (Agilent technologies, 2016).

REAGENT	VOLUME
10x reaction buffer	5.0 µl
DNA template (Parental)	1.0 µl (>100 ng/µl)
Forward primer	2.5 µl (10 pmol/µl)
Reverse primer	2.5 µl (10 pmol/µl)
dNTP mix	1.0 µl
QuickSolution reagent	3.0 µl
dH_2O	34.0 µl
PfuUltra HF DNA polymerase	1.0 µl

Table 3.2. Optimized thermo cycler conditions for QuikChange II XL Site-Directed Mutagenesis of *Sc*LPMO10 D variants. The table shows the optimized PCR program used when general recommendations failed to generate mutations (Agilent technologies, 2016).

STEP	TEMPERATURE (C°)	TIME (min)	CYCLE
Initial denaturation	95	1	1
Denaturation	95	1	16
Annealing	55/65	1	
Elongation	68	7	

*2 minute/kb of plasmid length (pRSET-B ScLPMO10D is approximately 3.5 kb)

3.2.4. Transforming chemically competent cells

The mutated plasmids were transformed into One Shot® TOP10 chemical competent *E.coli* cells, to seal staggered nicks and amplify plasmid concentrations before sequencing and further

mutation. Plasmids with verified mutations were further transformed into One Shot® BL21 StarTM (DE3) cells for expression.

Materials:

- Chemical competent *E. coli*:
    - One Shot® BL21 Star™ (DE3), for expression
    - One Shot® TOP10, for plasmid amplification
- Isolated plasmids
- LB-media
- LB agar plates supplemented with ampicillin (100 µg/ml)
- 100 mg/ml Ampicillin

Method:

Competent cells were thawed on ice for 10 minutes. Thereafter, 50 µl of competent cells were carefully mixed with 5 µl of the *Dnp* I-treated PCR reaction and incubated on ice for 30 minutes. Transformation was induced when competent cells were incubated in a preheated water bath, at 42 °C for approximately 45 seconds (i.e. heat shock), before being cooled on ice for 2 minutes. Thereafter, 250 µl of preheated LB-media was added before one hour of incubation at 37 °C and 200 rpm. Transformants were distributed onto two agar plates supplemented with Amp (100 µg/ml) and incubated overnight at 37 °C.

Colonies were either cultivated as described in section 3.1.3 for plasmid amplification or used in large scale expression of *Sc*LPMO10D variants (section 3.3.1).

3.2.5. Verification of directed mutations

To verify that desired mutations had been generated and to out rule unspecific mutations, plasmid DNA was sequenced by GATC Biotech (Konstanz, Germany) using the LIGHTRun Sanger sequencing service.

Materials:

- 80-100 ng/µl purified plasmid DNA
- 5 ng/µl sequencing primers, forward and reverse (Table 2.9)
- dH_2O

Method:

The sequencing primers were put into two separate 1.5 ml Eppendorf tubes, one for each primer. Thereafter, solution of plasmid DNA was added before adding dH_2O to a total volume of 11 µl. The tubes were thereafter labeled and sent for sequencing.

3.3 Expression, purification and preparation of enzymes

Before the research in this thesis had started, the DNA sequence encoding the catalytic domain of *Sc*LPMO10D, which included a N-terminal signal peptide from CBP21, had been ligated into a pRSET-B expression vector. The signal peptide from CBP21 was utilized to ensure that the target protein would be directed to the periplasm. Notably, the inhouse pRSET-B vector used in this thesis seems to exhibit some sort of random mutation related to its T7-promotor, as it has been found to produce substantially amounts of target enzyme without any induction (i.e. IPTG). Therefore, all protein expression in this research was carried out without the need of induction.

3.3.1 Overexpression expression

For optimal expression of both wild type and mutant *Sc*LPMO10Ds, One Shot® *E. coli* BL21 Star (DE3) strains with respective plasmid constructs were cultivated in 500 ml of TB media. The TB media was prepared as described in section 3.1.2 and inoculated with one single colony form an agar plate or a small piece of glycerol stock. The cultures were incubated overnight at 30 ºC in a Harbinger bioreactor, which provides a combined aeration and mixing system for high-throughput protein expression in *E. coli*.

3.3.2 Osmotic shock extraction

The osmotic shock method is widely used for selective disruption of the outer membrane of Gram-negative bacteria to recover periplasm-directed proteins, a method also known as periplasmic extraction. The CBP21 signal peptide direct translocation of the *Sc*LPMO10D proteins to the periplasmic space before it is cleaved off. Thus, the *Sc*LPMO10D variants were extracted via the cold osmotic shock method (Neu & Heppel, 1965), aiming to release the target proteins from the periplasmic space while minimize contamination from cytoplasmic proteins, RNA, DNA, and other cytoplasmic substances. Firs, the periplasm is equilibrated to a high osmotic pressure using a hypertonic solution. Thereafter, rapid exposure to a low osmotic pressure causes water to quickly enter the periplasmic space, which increases the internal pressure of the periplasm and results in bursting of the outer membrane of the cell.

Materials:

- Spheroplast buffer (Table 2.3), ice cold
- Sterile dH_2O
- 20 mM $MgCl_2$
- JA10 and JA25.50 rotors
- Centrifugation bottles

Procedure:

Overnight cultures of One Shot® *E. coli* BL21 Star (DE3) in section 3.3.1 were transferred to two 500 ml centrifugation bottles, 250 ml of culture in each bottle. The cells were thereafter harvested by centrifugation for 10 minutes at 4 °C and 8 000 rpm. After discarding the supernatant (TB-medium), pellets were resuspended in 25 ml ice-cold spheroplast buffer which functioned as the hypertonic solution, and further transferred to 25 ml bottles. After approximately five minutes on ice, the cell suspensions were centrifuged for 10 minutes at 4 °C and 8 000 rpm. Following centrifugation, the supernatant (i.e. spheroplast buffer or sucrose fraction) was set aside and stored at 4 °C, while the remaining cell pellets were incubated at room temperature for 30 minutes. The pellets were then resuspended in 20 ml of ice-cold water, before

1 ml of 20 mM $MgCl_2$ was added to the solution. While the hypotonic water causes the outer membrane to burst, the $MgCl_2$ solution helps to stabilize the remaining spheroplast. Separation of cells and soluble proteins were done via centrifugation at 15 000 g (i.e. gravitational force) for 10 minutes.

Samples from the sucrose fraction, periplasmic fraction, and remaining cell pellet were analyzed through SDS-PAGE (section 3.3.3).

Since substantial amounts of target protein were found in both the periplasmic extract and the sucrose fraction, both were filtered through 0.22 µm sterile filters and stored at 4 °C until further use.

3.3.3 Sodium dodecyl sulfate polyacrylamide gel electrophoresis (SDS-PAGE)

Sodium dodecyl sulfate polyacrylamide gel electrophoresis (SDS-PAGE) is a widely utilized technique for analyzing heterogenous proteins in a solution. Being a variant of polyacrylamide gel electrophoresis, SDS-PAGE is based on the separation of charged molecules by their molecular masses in an electric field (Laemmli, 1970). The anionic detergent sodium dodecyl sulfate (SDS), combined with a reducing agent to reduce disulfide bonds, denature the proteins and provide them with a uniform negative charge. The denatured proteins can thereafter be separated based on their size through electrophoresis. Today, the use of precast gels and automated gel imaging systems allows safe and rapid visualization and analysis of protein samples in stain-free polyacrylamide gels.

Materials:

- Samples containing *Sc*LPMO10D variants
- 200 µl SDS-PAGE working solution (2x), room temperate
    - 100 µl LDS sample buffer (4x)
    - 40 µl sample reducing agent (10x)
    - 60 µl dH_2O

- Any kD™ Mini-PROTEAN® TGX Stain-Free™ Protein Gel, 10 wells
- BenchMark™ Protein Ladder
- 1 x TAE Running Buffer

Method:

Samples of 20 µl protein solution and 20 µl of SDS-PAGE working solution were prepared in 1.5 ml Eppendorf tubes. Of note, lithium dodecyl sulfate (LDS) was used as a sample buffer during this research, which like the traditional SDS sample buffer, is an anionic detergent (pH 8.4). The samples were heated up to 98 ºC for 10 minutes in a heating block to ensure fully desaturated proteins. The high temperature and LDS sample buffer help to unfold proteins, but only the reducing agent is able to reduce covalent disulfide bonds, and e.g. prevent dimerization of denatured proteins. The LDS sample buffer further confer the denatured proteins to similar charge-to-mass ratios, which enables separation through electrophoresis, as the proteins will migrate towards the anode at different speeds depending on their mass. After sample preparation, gels were placed in a gel-electrophoresis chamber and the chamber was filled with 1x TAE Running Buffer. To enable identification of bands containing target proteins, 10 µl of a BenchMark™ Protein Ladder was added to the first well. After loading samples carefully into separate wells, gels were run on 280 V (i.e. voltage) for 19 min. When the run had finished, the gels were transferred onto a Stain-Free Sample Tray and gel imaging was thereafter performed using a Gel Doc™ EZ Imager. This method exploits the intrinsic fluorescence of the aromatic amino acids of proteins to detect bands of migrated proteins. The gel was analyzed using the Image Lab™ software, from which bands corresponding to the molecular weights of the target proteins were identified using the known molecular weights of the protein ladder.

3.3.4 Buffer-exchange and concentrating protein solutions with centrifugal filters

The sucrose fractions were found to contain substantial amounts of target enzyme. To remove sucrose and other contaminants from the sucrose fraction, a simple buffer exchange procedure was followed. Sucrose is a known osmolyte that affect ionic strength of the aqueous solutions

(Gouffi et al., 1999). Thus, it is especially important to remove sucrose as it may interfere with the binding property of proteins during purification with ion exchange chromatography.

The concentration of sucrose in the sucrose fractions were calculated to be around 500 mM. Using an Amicon® Ultra-15 centrifugal filter with a 10 000 molecular weight cutoff (i.e. MWCO in kDa), the solution was concentrated and washed with 50mM Tris pH 9.0 several times, until the calculated concentration of sucrose was below 1.0 mM. The centrifuge was operated at 4300 g and 4 ºC. The buffer exchanged sucrose fraction was thereafter purified further with anion-exchange chromatography (section 3.3.5).

The same type of centrifugal filter was used to exchange buffer and concentrate fractions from anion-exchange purifications to 1.0 ml, before size-exclusion chromatography. With a molecular weight of around 19 kDa (Table 4.1), the *Sc*LPMO10D variants will be retained in centrifugal filter container, while aqueous solution containing molecules smaller than 10 kDa will go through the filter and end up in the collection container. Thus, concentrating the solution of target enzyme.

3.3.5 Anion-Exchange Chromatography

Purification of proteins by ion exchange chromatography (IEC) is based on separation of different proteins according to their affinity to a charged ion exchanger resin at a specific pH and or ion strength. IEC can further be divided into anion-exchange chromatography and cation exchange chromatography. The stationary phase (i.e. resin) in anion-exchange is positively charge and will thus bind negatively charged molecules, while the stationary phase in cation exchange is negatively charged and will bind positively charged molecules. The resin is typically constituted of either cellulose or agarose beads, which have been modified with either positively or negatively charged functional groups. Generally, when an aqueous sample with proteins is loaded onto the charged column resin, proteins with an opposite surface charge compared to the resin will bind, while proteins with neutral or similar surface charge compared to the resin will come out in the flow through. The surface charge of a protein is dependent on the summarized

contribution of charged surface-exposed residues at a particular pH, also referred to as the net charge. The isoelectric point of a protein (pI) is the pH value at which the protein has a net charge of zero (i.e. neutral charge). At pH values above their isoelectric point, proteins will carry a negative net charge, and therefore bind to a positively charged anion-exchanger. Likewise, pH values below their pI, will generate a positive net charge and therefore promote binding to a negatively charged cation exchanger. Separation of proteins bound to an ion exchange resin can be obtained by increasing the salt concentration (i.e. ionic strength) of the elution buffer, in a stepwise or linear gradient. Gradients of pH can also be employed, either combined with, or without a gradient of ionic strength. A change in pH works by affecting the charge of solvent-exposed residues based on the respective pKa values of their side groups (in addition to the -NaH_2 and -COOH of the N- and C-terminal, respectively). The gradient of salt works by gradually masking charged groups on the resin, from which proteins with weak and strong ionic interactions with the resin, will elute first and last, respectively.

In this research however, a rather opposite strategy was used for protein purification with anion-exchange chromatography (AEC), in which the target proteins were aimed at not binding to the column and thus come out in the flow through, while the majority of other proteins would bind to the resin. This was done by using a strong anionic stationary phase (i.e. quaternary amine), combined with a mobile phase of anionic pH of 9.0, which will generally give most proteins a negative net charge. For more details see section 4.3.2.

Materials:

- ÄKTApure™ cromatography system
- HighTrap Q Fast Flow 5 ml column
- Buffer A: 50mM Tris pH 9.0
- Buffer B: 50mM Tris pH 9.0 + 1M NaCl
- Periplasmic fractions of *Sc*LPMO10D variants

Method:

The system and column were washed with dH_2O, before being equilibrated with buffer A. After the monitored conductivity had stabilized, the monitored UV absorption (A_{280}) was calibrated to zero. The system was operated with a flow rate of 1.0 ml/min and the protein elution was monitored by recording absorbance at 280 nm. Eluates were collected in fractions of 0.5 - 3.0 ml. The sample was loaded onto the column and a broad peak emerged as the protein came out in the flow-through. After the target protein had been collected, a gradient of 0 - 50 % of buffer B was employed over 25 minutes, which eluted different proteins which had bound to the resin. As a final elution step, 100 % of buffer B employed.

After the column had been regenerated, it was filled with 20% ethanol before storing it at room temperature.

Fractions from the flow-through and peaks that had eluted at different salt concentration were further analyzed with SDS-PAGE. Fractions containing the target protein were pulled and concentrated according to section 3.3.4, before being further purified with size-exclusion chromatography (next section).

3.3.6 Size-Exclusion Chromatography

Size-exclusion chromatography (SEC), also referred to as gel filtration, generally separates macromolecules in a solution based on their size, but the geometry and weight of the molecules will have some extent effect on the separation. The SEC column is composed of a gel matrix (e.g. agarose) which is constituted of small spherical beads with pores of different sizes. While small proteins will diffuse through the pores, larger proteins will pass by the beads and move through the gel at a higher speed than the smaller proteins.

Materials:

- ÄKTAprime™ Plus chromatography system
- HiLoad 16/600 Superdex 75 PG, 120 ml column
- Running buffer: 50 mM Tris-HCl, pH 8.0 + 200 mM NaCl.

- Concentrated AEC fractions with *Sc*LPMO10D variants
- Sterilized syringe

Procedure:
The HiLoad 16/600 column connected to an ÄKTAprime™ Plus chromatographic system was washed with degassed dH_2O for 30 min. The column was thereafter equilibrated with buffer A, before calibrating the UV monitor (A_{280}) to zero, when the monitored conductivity had stabilized. The flow was always increased and decreased stepwise, and the pressure alarm was set to 0.35 MPa (i.e. millipascal). After stopping the flow, samples of 1.0 ml protein concentrate from the AEC purifications were injected into the sample loop, using a sterilized syringe. The sample was thereafter loaded onto the column by employing a flow rate of 1.0 ml/min, followed by one column volume (120 ml) of running buffer. Protein elution was monitored by recording absorbance at 280 nm and eluate were collected in fractions of 1-5 ml. Fractions presumed to contain the protein of interest were analyzed by SDS-PAGE according to section 3.3.3. The *Sc*LPMO10D variants always eluted after 60 - 70 minutes.

After two hours on Buffer A (i.e. 120 ml), the column was washed with degassed dH_2O for 20 minutes, before running the column on 20 % ethanol for two hours and thereafter storing it at room temperature.

Fractions containing *Sc*LPMO10D variants, which were verified by SDS- PAGE, were pooled and concentrated to approximately 1 ml using Amicon® Ultra-15 Centrifugal Filters with a MWCO of 10 kDa. After 1 ml was transferred into a 2.0 ml cryotube, approximately 1 ml of buffer was used to wash the sides of the filter and thereafter added to the cryotube to make a final volume of ~ 2.0 ml protein solution.

3.3.7 Direct photometric measurement of protein (A280)

Measurement of concentration in protein samples via directly measuring absorbance, is a fast and convenient method, in which no additional reagents or incubations are required. As the method, generally is based on the absorbance of tryptophan and tyrosine residues at 280 nm wavelength.

Calculation of protein concentration can be obtained following the Beer's law: $A = \varepsilon \times b \times c$. Beer's law states that the absorbance (A) is proportional to the concentration (c) of a solution which can absorb electromagnetic radiation. In the Beer's law equation, (b) represents the path length of the ultraviolet light, which in this research, always was 1.0 cm. The molar absorptivity coefficient ε (i.e. extinction coefficient), is a wavelength-dependent value that indicate how much light a given protein can absorb at a certain wavelength. The extinction coefficient for all proteins in this study can be found in Table 4.1.

Materials:

- AG Biophotometer
- Uvette® disposable cuvettes
- *Sc*LPMO10D variants

Procedure:

The A_{280} program of the spectrophotometer was employed. Protein samples were diluted with sample dH_2O to obtain absorbance values below 1.0, and dH_2O was used as a blank. To determine the protein concentration in mol/L, the average A_{280} value (n=3) was divided by the extinction coefficients of the respective proteins, which was determined using the ProtParam online tool. The calculated values were thereafter multiplied by the dilution factor and further divided by the molecular weight of the protein, giving the final protein concentration of *Sc*LPMO10D variants in mol/L.

3.3.8 Saturating LPMOs with copper

Desalting columns are commonly used for buffer exchange and cleanup of biological samples. By using a gravity protocol, there is no need for a purification system, and a simple cleanup of multiple samples can be done in parallel, using separate columns.

Materials:

- Purified *Sc*LPMO10D variants, in SEC running buffer (50 mM Tris-HCl pH 8.0 and 200 mM NaCl)

- 5 mM $CuSO_4$
- PD MiniTrap™ G-25 column
- Gravity protocol
- Storing buffer (50 mM Natrium phosphate pH 6.0)

Method:

To ensure copper-saturation, enzymea were incubated with a 3 x molar concentration of $CuSO_4$ compared to their respective enzyme concentration, for at least 30 min. The excess of copper, NaCl (i.e. from SEC buffer), and other low weight impurities (i.e. >5000 kDa biomolecules), were removed by applying samples onto separate PD MiniTrapTM G-25 columns and following the gravity protocol.

The column was equilibrated with 15 ml storing buffer before applying 500 µl of the copper-saturated enzymes. After the enzyme solution had gone completely into the column, 500 µl of storing buffer (without enzyme) was applied on the column to archive an enzyme solution of 1000 µl, which was collected into a 2.0 ml cryotube.

The concentrations of the copper-saturated and desalted protein solutions were determined by measuring A_{280} (section 3.3.7).

3.3.9 Determination of protein purity using SDS-PAGE

An SDS-PAGE gel was prepared, loaded with separate samples of the copper-saturated *Sc*LPMO10D variants which concentrations had been adjusted to a final concentration of approximately 1.5 mg/ml. The gel was run according to the method described in section 3.3.3. Using the Image Lab™ software, lanes and their corresponding bands were detected before running the Lane Profile application. The background was thereafter excluded, and the relative percentage of the target protein bands (band %), compared to the other bands in their respective lanes, were quantified by through the software application. The band percentage of each target-protein band were used as an estimate of the relative amount of *Sc*LPMO10D variants in the copper-saturated protein solutions, presented in a percentage of protein purity, which was further used to correct the protein concentrations measured with A_{280}. The new concentration was calculated by multiplying the respective purity factors of each protein with their measured concentrations, e.g. 0.8 x 300 µM = 240 µM. ¨

3.4 Enzyme characterization

In this research, several activity and binding assays were executed to investigate the activity of *Sc*LPMO10D and its mutants.

3.4.1 LPMO activity assays

3.4.1.1 Wild type activity assay

A fast activity assay was set up after periplasmic extraction of the wild type *Sc*LPMO10D to determine its activity and product profile of on cellulose (PASC) and β-chitin.

Materials:

- 200 µl Enzyme reactions:
    - 20 µl of crude PPE extract with *Sc*LPMO10D
    - 50mM Tris-HCl buffer, pH 8.0
    - 10 g/l β-chitin or 5 g/l PASC
    - 1.0 mM L-Ascorbic acid (samples without AscA for control reactions)

    - dH_2O
- Eppendorf Comfort Thermomixer

Method:

Enzyme reactions were started by adding 2 µl AscA into the reaction solutions, and thereafter incubated at 30 ºC in a Thermomixer with 800 rpm overnight. The next day, samples were analyzed with MALDI-Tof MS (section 3.4.2).

3.4.1.2 Other LPMO-activity assays

Several different activity assays were set up to analyze the substrate specificity of the mutated versions on cellulose (PASC, Avicel, and BMCC) and β-chitin.

As an initial experiment, reactions with PASC and β-chitin set up to analyze how of the substrate specificity of the mutants had been affected.

Materials:

- 2 x 300 µl enzyme reactions, final concentrations:
    - 1 µM enzyme
    - 50 mM Sodium phosphate buffer, pH 6.0
    - 10 g/l β-chitin or 3 g/l PASC
    - 1 mM ascorbic acid (samples without AscA for control reactions)
    - dH_2O
- Eppendorf Comfort Thermomixer

Method:

Enzyme reactions were started by adding 3 µl ascorbic into the reaction solutions, which was further incubated at 40 ºC in a Thermomixer with 800 rpm for 24 hours. Samples were taken after 1 and 24 hours and filtrated after collection to stop the reactions.

Oxidized products were thereafter analyzed with HPAEC-PAD, described in section 3.4.3.

3.4.1.3 H_2O_2-supplemented activity assay

An activity assay was set up to investigate if the lack of activity on β-chitin in some of the mutants could be regained upon addition of H_2O_2.

Materials:

- 2 x 200 µl enzyme reactions with final concentrations of:
  - 2 µl enzyme (50 µM)
  - 50 mM Sodium phosphate buffer, pH 6.0
  - 10 g/l β-chitin or 5 g/l PASC
  - 50 µM ascorbic acid (samples without AscA for control reactions)
  - dH_2O
- Addition of H_2O_2 stock solution in four different enzyme reactions with two replicates each (above):
  - 1 x 100 µM H_2O_2
  - 2 x 50 µM H_2O_2
  - 4 x 25 µM H_2O_2
  - 6 x 10 µM H
- Control reactions:
  - Without protein
  - Without reducing agent
  - With CelS2 (negative)
  - With *Sc*LPMO10D wild type (positive)
- Eppendorf Comfort Thermomixer
- 96-well filter plate
- V vacuum manifold

Method:

Enzyme reactions were started by adding ascorbic acid into the reaction solutions, and the samples were thereafter incubated at 30 ºC in a Thermomixer with 800 rpm. After 1 hour, the

reactions were incubated at 100 ºC for 15 minutes to stop all enzymatic activity. The samples (containing soluble and insoluble products) were thereafter incubated with 0.5 µM ChiA and 0.5 µM Chitobiase at 37 ºC and 800 rpm overnight, which released all oxidized products and converted them into chitobiose.

The total amount of oxidized products was assessed using UHPLC analysis accordingly:

Quantification of oxidized products was done using a Dionex Ultimate 3000 UHPLC system (Sunnyvale, CA, USA) rigged with a Rezex RFQ-Fast Acid H+ (8%) 7.8×100 mm column (Phenomenex, Torrance,CA) which was operated at 85 °C. Components of the samples were eluted isocratically by employing 5 mM sulfuric acid as a mobile phase. The eluted products were monitored by UV absorption at 194 nm. The Chromeleon 7.0 software was used to collect and analyze data. An in-house stock solution of oxidized N-acetyl-chitobiose, which had been prepared according to (Loose et al., 2014), was used as a standard when analyzing the samples.

3.4.2 MALDI-TOF mass spectroscopy analysis of oxidized products

Matrix Assisted Laser Desorption/Ionization-Time of Flight (MALDI-ToF) mass spectrometry is generally utilized as a non-quantitative method for analyzing the molecular weight and composition of organic molecules. Ionization by MALDI is achieved in two steps. First, the sample is mixed with a matrix solution, consisting of small organic molecules, directly on a metal plate. The matrix-sample mixture is dried, before being injecting the plate into the mass spectrometer. Under vacuum conditions, a laser is used to send multiple energy pulses onto the dried mixture, generating ionized sample molecules of different protonation states. The ionization of frail molecules such as oligosaccharides, requires soft ionization that allow them to be ionized without disintegration. By using a MALDI-matrix that provides both desorption and ionization, the pulsed energy is first absorbed by the matrix which thereafter transfer the energy indirectly to the sample molecules and thereby reduce fragmentation. Thereafter, a difference in applied potential generates a strong electric field which accelerates charged molecules from the sample into a mass analyzer, which provides a field-free flight tube where separation of ions can occur

before reaching a detector. Referred to as a Time-of-flight (TOF) mass analyzer, it determines the mass-to-charge ratio of ions by measuring the time it takes for the ions to reach the detector. Because smaller ions travel faster than larger ions, the separation caused by their difference in velocities can be used to determine their molecular weights.

MALDI-ToF was used to analyze the samples from section 3.4.1.1.

Materials:

- Ultraflex MALDI-TOF/TOF Mass Spectrometer
- MALDI TOF/MS 348 target plate ground steel TF
- DHB-mix: 2.5-dihydroxybenzoic acid (9 g/L^{-1}) dissolved in acetonitrile (1:3 v/v) and dH_2O
- LPMO-reaction samples

Method:

The samples were prepared by mixing 1 µl sample and 2 µl DHB-mix. The mix was applied to an MTP 384 target plate followed by drying under a steam of air. The samples were analyzed with an Ultraflex MALDI-ToF/ToF instrument from Bruker Daltonics (GmbH, Bremen, Germany) equipped with a Nitrogen 337 nm laser beam, using the FlexAnalysis software.

3.4.3. PRODUCT ANALYSIS BY ION CHROMATOGRAPHIC SYSTEM (ICS)

Products generated in LPMO reactions were analyzed by high performance anion-exchange chromatography (HPAEC) with pulsed amperometric detection (PAD).

Carbohydrates are weak acids that normally display pKa values in the range of 12 - 14. By exposing them to high pH values (i.e. > pKa), the hydroxyl groups of carbohydrates can be partially or fully converted into charged oxyanions, which further enables them to be selectively eluted as anions through high-performance anion-exchange chromatography (Corradini et al., 2012). The separation of oligosaccharides via HPAEC is often achieved by employing a constant

concentration of sodium hydroxide (NaOH), which makes the saccharides bind to the column, while a gradient of sodium acetate ($NaCH_3COOH$) is used to gradually elute the different oligosaccharides. When HPAEC is coupled PAD, a direct detection of the eluted carbohydrates is enabled by using carbohydrate specific wavelengths that oxidize carbohydrates on the surface of a gold working electrode in the highly alkaline solution, which further generates a current that can be measured (Rohrer, 1998; Thermo Scientific, 2017). Furthermore, because the generated current will be proportional to the concentration of the carbohydrates, HPAEC-PAD can be used to quantify the amounts of different oligosaccharides in a solution.

Materials:

- Dionex Bio-LC (ICS 3000) equipped with a CarboPac PA1 column
- Pulsed amperometric detector (PAD)
- Gold electrode, disposable
- Buffer A: Degassed 0.1 M NaOH
- Buffer B: Degassed 0.1 M NaOH, 1 M $NaCH_3COOH$ (NaOAc)

Method:

HPAEC-PAC was carried out using an ICS3000 system (Dionex, San Jose, CA, USA) which was set up with a CarboPac PA1 analytical column (2 × 250 mm) and guard column (2 × 50 mm), connected to an electrochemical detector that operated with a disposable gold electrode in a pulsed amperometric manner (PAD), using a carbohydrate specific waveform. Samples of 5 µl were injected on the column, which was operated with 0.1 M NaOH (buffer A) at a flow rate of 0.25 ml/min and a column temperature of 30 °C (Forsberg et al., 2011).

Oxidized products from each sample was eluted and separated using a stepwise gradient with increasing amounts of buffer B (1 - 4), followed by reconditioning of the column with buffer A (5 - 6), before the next sample was injected (Westereng et al., 2013): (1) 0 - 10 % B over 10 min. (2) 10 - 18 % B over 10 min. (3) 18 - 30 % B over 1.0 min. (4) 30 - 100 % B over 1 min. (5) 100 - 0 % B over 0.1 min. (6) 0 % B over 13.9 min.

The eluted chito-oligosaccharides were detected by PAD and the chromatogram was recorded using Chromeleon 7.0 (Dionex) software. Oxidized products were identified using a standard solution of oxidized N-acetyl-chitooligosaccharides with a degree of polymerization (DP) ranging from 1 to 6 (i.e. GlcNAc1A - $GlcNAc_5GlnNAc1A$), which had been prepared in-house according to (Loose et al., 2014).

3.4.4 Thermal shift assay

Thermal shift assay is a fast and simple method to detect protein-ligand interactions and investigate mutational effects on protein stability (i.e. thermostability). The method quantifies the denaturation temperature of a protein by using a dye that binds nonspecifically to hydrophobic surfaces, while displaying a fluorescence potential which is strongly quenched by water. Consequently, when an increasing temperature leads to unfolding of a protein it exposes hydrophobic surfaces which binds the dye and result in a fluorescence signal as water is excluded. However, this method will not work on proteins which is fibrillated by an increasing temperature instead of going to a molten globule.

Here, a Protein Thermal Shift™ Dye Kit was used to perform a thermal shift assay to investigate the thermal stability and ligand binding ability of the *Sc*LPMO10D mutants compared to the wild type.

Materials:

- StepOne™ Software v2.2
- MicroAmp™ Optical 96-Well Reaction Plate
- MicroAmp® Optical Adhesive Film
- Step-One Plus™ Real-Time PCR System
- 5 x 20 µl Reaction mix per enzyme (with or without EDTA)
    - 5.0 µl Protein Thermal Shift™ Buffer
    - 12.5 µl Enzyme solution (1.0 mg/ml enzyme + 50 mM Sodium phosphate buffer pH 6.0 +/- 10 mM EDTA)

- 12.5 µl Protein Thermal Shift™ Dye (8x), add last

Method:

The thermal shift assay was conducted a StepOnePlus™ Real Time PCR System. The protein reaction mix was added to the wells of a 96-well PCR plate. The plate was heated from 25 to 99 °C with a heating rate of 1 °C min^{-1}, and the fluorescence intensity was monitored with Ex/Em at 490/530 nm.

3.4.5 Binding assay

The substrate binding affinities of ScLPMO10D mutants and the wild type enzyme were examined by incubating the enzymes with various substrates, and with or without a reducing agent. Several binding assays were preformed, but only two representative assays are described here.

3.4.5.1 Wild type binding assay with chitin substrates

This procedure was used to compare the substrate affinity of the wild type enzyme toward α- and β-chitin. The assay was conducted at a relatively low temperature of 22 °C and in the absence of a reducing agent, to ensure stable binding conditions.

Materials:

- Comfort Thermomixer
- 96-well filter plate
- V vacuum manifold
- 3 x 600 µl reactions, in final concentrations of:
    - 5 µM copper-saturated wild type
    - 50 mM sodium phosphate buffer pH 6.0
    - 10 mg/ml β-chitin or α-chitin
- Blank reaction with buffer 50 mM sodium phosphate buffer pH 6.0
- Control reaction with 10 mg/ml substrate and 50 mM sodium phosphate buffer pH 6.0

- 5 µM copper-saturated wild type enzyme, without substrate, in 50 mM sodium phosphate buffer pH 6.0

Method:

Three parallels of 600 µl reactions were prepared for each substrate as directed above, and incubated at 22 °C and 1000 rpm, in the absence of a reducing agent. Samples taken after 5, 15, 30, 60, and 120 minutes, were filtrated immediately after collection, and stored at 4 ºC until further use. The amounts of unbound protein in filtrates were analyzed using the Bradford assay, as described in section 3.4.6.

3.4.1.2 Combined binding and activity assay, wild type and mutants

An activity assay was set up to analyze the mutational effects on substrate specificity toward β-chitin. Samples taken from these activity reactions were also used to analyze the binding affinity of the *Sc*LPMO10D variants, with and without activation by a reducing agent. Gallic acid was used instead of ascorbic acid in an attempt to reduce the enzyme-inactivation over time.

Materials:

- 800 µl enzyme reactions - with and without reductant (final concentrations):
    - 2 µM enzyme (50 µM)
    - 50 mM sodium phosphate buffer pH 6.0
    - 10 g/l β-chitin
    - 1.0 mM gallic acid
    - dH_2O
- 250 µl reactions - with and without reductant (final concentrations):
    - Blank reaction with 50 mM sodium phosphate buffer pH 6.0 and 1.0 mM gallic acid
    - Control reaction with 10 mg/ml substrate and 50 mM sodium phosphate buffer pH 6.0, and 1.0 mM gallic acid

  - 5 µM copper-saturated wild type enzyme, without substrate, in 50 mM sodium phosphate buffer pH 6.0 and 1.0 mM gallic acid
- Eppendorf Comfort Thermomixer
- 96-well filter plate
- V vacuum manifold

Method:

All samples were preincubated at 40 °C and 800 rpm, before the reactions with reductant were started by adding gallic acid to the reactions and all reactions were further incubated at the same conditions (i.e. 40 °C and 800 rpm). Samples were taken after 1, 2, 6, and 24 hours, filtrated immediately after collection and stored at 4 ºC until further use. The amount of unbound protein in filtrates were analyzed using Bradford assay (A_{595}), as described in section 3.4.6.

3.4.6 Bradford assay

The Bradford assay is a colorimetric method for measuring the concentration of protein in a solution, based on a shift in absorbance of Coomassie Brilliant Blue dye (Bradford, 1976). When the dye binds to protein it is converted from a cationic form (λmax = 470 nm) to a stable unprotonated blue form (λmax = 595 nm), which can be measured at A_{595} using a standard spectrophotometer.

Materials:

- Brilliant Blue G-250 dye reagent
- Disposable cuvettes
- Enzyme of interest
- BioPhotometer

Procedure:

Before measurement of the protein samples, a blank sample was prepared by mixing 800 µl of the respective sample buffer (or blank sample) with 200 µl dye reagent. After five minutes of incubation, the blank sample was used to calibrate the spectrophotometer at A_{595}.

Sample dilutions were performed by mixing 50 µl of protein solution with 750 µl dH_2O, before mixing the diluted samples with 200 µl dye reagent and incubating them for five minutes. After incubation, the absorbance at 595 nm was measured by using the Bradford micro application on the spectrophotometer. Sample A_{595} values were preferably calculated as the average value of three replicates. The average A_{595} values were thereafter converted into percentage of unbound protein according to the formula below.

$$\text{Percentage of free protein (\%)} = \frac{Avrage\ binding \div Substrate\ without\ protein}{Protein\ without\ substrate} \times 100$$

3.4.7 Hydrogen peroxide assay

As mentioned in the introduction, LPMOs have been observed to produce hydrogen peroxide (H_2O_2) in the absence of substrate (Kittl et al., 2012). When using the Amplex® Red assay to measure the H_2O_2 production of reduced LPMOs in absence of substrate, the generated H_2O_2 is utilized as a co-substrate by horseradish peroxidase (HRP) in a 1:1 stoichiometry to catalyze the conversion of Amplex® Red reagent into resorufin. Resorufin is both a chromogenic and fluorescent product (Kittl et al., 2012).

Materials:

- Multiskan™ FC Microplate Photometer
- Amplex® Red Dye kit, including H_2O_2 and horseradish peroxidase
- 96-well microplate
- 3 x 100 µl Reactions per *Sc*LPMO10D variant:
    - 40 µl Enzyme solution:
        - 3 µM final concentration of *Sc*LPMO10D variant
        - 5 µl 0.5 M Sodium Phosphate buffer, pH 6.0
        - Trace Select dH_2O to a final volume of 40 µl

- 50 µl Dye mix:
    - 1 µl Amplex Red (10 mM)
    - 5 µl HRP (100 u/ml)
    - 5 µl Buffer
    - 39 µl Trace Select dH_2O
- 10 µl Starting solution, last:
    - 500 µM Ascorbic acid
    - Trace Select dH_2O to a final volume of 10 µl

Method:

Reactions with enzyme solutions and dye mix were prepared as directed above and distributed in a 96-well microplate, before adding 10 µl of ascorbic acid (final concentration of 50 µM) to start the reactions. Three parallels (n=3) of each reaction were incubated for 30 min at room temperature and the H_2O_2 production was measured indirectly by monitoring the production of resorufin via A_{540}, using a Multiskan FC spectrophotometer. The measured A_{540} was thereafter converted to H_2O_2 concentrations, using a standard curve made with reactions of known H_2O_2 concentrations, ranging from 10-40 µM.

4. RESULTS & DISCUSSION

The results of this study have been organized into three main sections. The first section is dedicated to a relatively simple initial characterization of the wild type enzyme (section 4.1), whereas the second section addresses the rational design and production of mutant enzymes (section 4.2). The third section (section 4.3), describes results from the investigation of mutational effects on substrate specificity.

4.1 Characterization of wild type *Sc*LPMO10D

Prior to this work, the gene encoding *Sc*LPMO10D had been cloned by Zarah Forsberg and Bastian Bissaro. Sequence comparisons (Fig. 4.1) did not provide a clear suggestion concerning the substrate specificity of *Sc*LPMO10D, since some specificity-determining regions indicated cellulose-activity, whereas others indicated chitin-activity.

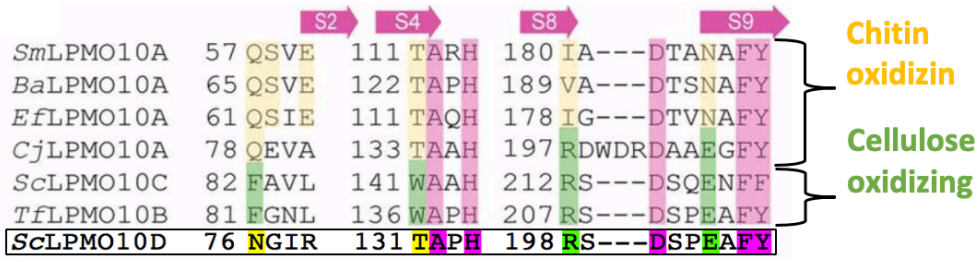

Figure 4.1. Deviating sequence characteristics of *Sc*LPMO10D. The pictures show details of a sequence alignment of chitin- and cellulose active LPMOs, highlighting conserved residues that may relate to substrate specificity. The alignments display sections associated with substrate-biding for selected LPMOs exhibiting either chitin or cellulose activity. Residues conserved in chitin-, cellulose-, or both chitin- and cellulose active LPMOs, are colored yellow, green, and pink, respectively. Note that the related stretches of sequence from ScLPMO10D (added to the bottom), display conserved residues that are either specific for cellulose- or chitin activity, which is a dual trait it shares with chitin active *Cj*LPMO10A. The corresponding stretches of sequence from *Sc*LPMO10D were identified via a structural alignment of a three-dimensional model of thie enzyme with *Sc*LPMO10C (PDB: 4OY7) and *Cj*LPMO10A (PDB: 5FJQ) in PyMOL. The figure was taken from (Forsberg et al., 2015), and modified for the purpose of this thesis.

4.1.1 Production of wild type ScLPMO10D

Due to a previous investigation of *Sc*LPMO10D, an *E. coli* strain containing an pRSET-B derived expression vector for production of the enzyme was in place. The expression vector contained a codon optimized gene (Appendix A) that encodes mature *Sc*LPMO10D coupled to the signal peptide from CBP21. Of note, the pRSET-B vector used here seems to have a random mutation within or related to the T7-promotor, which causes it to "leak" substantially, thus facilitating protein expression without induction (i.e. IPTG). The expression vector was transformed into chemically competent *E. coli* BL21 (DE3), the protein was expressed by cultivation overnight at 30°C, and a starting fraction for purification of *Sc*LPMO10D was prepared by periplasmic extraction, using an osmotic shock method (section 3.3).

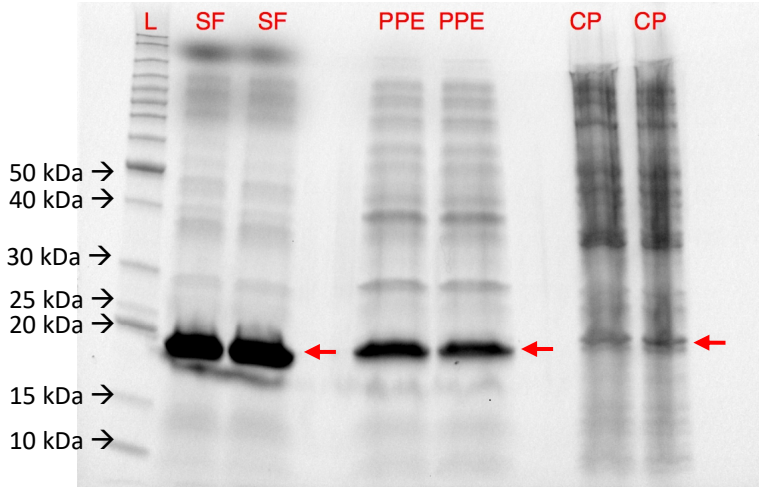

Figure 4.2. Periplasmic extraction of *Sc*LPMO10D, analyzed with SDS-PAGE. The first lane (L) displays a BenchMark™ Protein Ladder, of which molecular sizes ranging from 10 - 50 kDa is indicated to the left of the lane. The two next lanes display samples from sucrose fractions (SF), followed by one empty lane to prevent sample bleeding (i.e. mixing). The two next lines, display samples from the periplasmic fractions (PPE), followed by another empty line The two last lanes display samples from the remaining cytoplasmic fraction (CP). Bands corresponding to a molecular weight of ScLPMO10D (i.e. 19 kDa) are indicated by the red arrows.

Fig. 4.2 shows the presence of substantial amounts of *Sc*LPMO10D (19 kDa) in the periplasmic fraction (PPE) and even higher yields in the supernatant/sucrose fraction generated in the osmotic

shock procedure. The large amount of target enzyme in the sucrose fraction may result from cell lysis caused by rough handling during resuspension of cells in spheroplast buffer. However, since the overall band pattern for the supernatant was more similar to that of the periplasmic extract compared to a cell extract (Fig. 4.2), it is more likely that the proteins in the supernatant result from periplasmic-leakage, provoked by the osmotic dehydration caused by the hypertonic spheroplast buffer. Only a small fraction of *Sc*LPMO10D appeared in the cell pellet, which indicates that most of the target enzyme was soluble, and thus likely expressed and folded correctly. Results of the purification of the wild-type enzyme are not shown here, but representative results of the purification of two mutants are shown further below, in section 4.3. Using a starting culture of 500 ml, purification of the enzyme from both the supernatant and the periplasmic fraction yielded 69.3 g/l and 25.9 g/l of enzyme, respectively.

4.1.1 Substrate specificity and product profile

LPMO activity was tested using the periplasmic extract in reactions containing PASC or β-chitin and 1 mM ascorbic acid (AscA). Negative control reactions, i.e. reactions without AscA, were included. Reactions were incubated overnight at 30°C after which product formation was analyzed using MALDI-ToF MS. Several oxidized products were identified in the reaction with β-chitin (Fig. 4.3), whereas no masses corresponding to oxidized products were detected in the reactions with PASC (not shown).

Due to identical masses, it can be difficult to distinguish 1.5-δ-lactones and aldonic acids (i.e. C1-oxidized products) from 4-ketoaldoses and gemdiols (i.e. C4-oxidized product), respectively. Still MALDI-ToF MS analysis can give some insight as the hydrated gemdiols are more readily dehydrated during sample preparation than aldonic acids that further tend to form double adducts with e.g., sodium (Westereng et al., 2018). The formation of double adducts is the clearest discriminating factor and it is thus important to incubate samples at alkaline pH to drive the pH-dependent lactone/hydrate equilibrium toward aldonic acid formation (Loose et al., 2014). Figure 4.3 shows multiple signals representing double adducts of oxidized chitooligosaccharides, (i.e.

$DP3_{ox}$ - $DP9_{ox}$; M-H + $2Na^+$), which thus must be aldonic acids of C1-oxidized compounds with different degrees of polymerization.

While no C4-oxidized chitin products have been reported so far, LPMOs with specificity toward both cellulose (C1/C4) and chitin (C1) have a tendency to produce more deacetylated products (i.e. -42 Da per deacetylation) when acting on chitin (Forsberg et al., 2018). Such deacetylated products were not detected, which in addition to the negative results from the reaction with PASC, may imply that *Sc*LPMO10D is a C1-oxidizing enzyme with substrate specificity toward chitin. The lower spectrum in Figure 4.3 gives a detailed overview of the hexamer cluster, which shows signals for a 1,5-δ-lactone (i.e. $GlcNAc_5$1,5-σ-lactone) and an aldonic acid (i.e. $GlcNAc_5$GlcNAc1A) products, as various sodium and potassium adducts (i.e. M + Na^+, M + K^+, M - H + $2Na^+$, M - H + Na^+ + K^+, M - H + 2K). As expected under the alkaline conditions used (pH 8.0), there is a clear overrepresentation of aldonic acid chitooligosaccharide products.

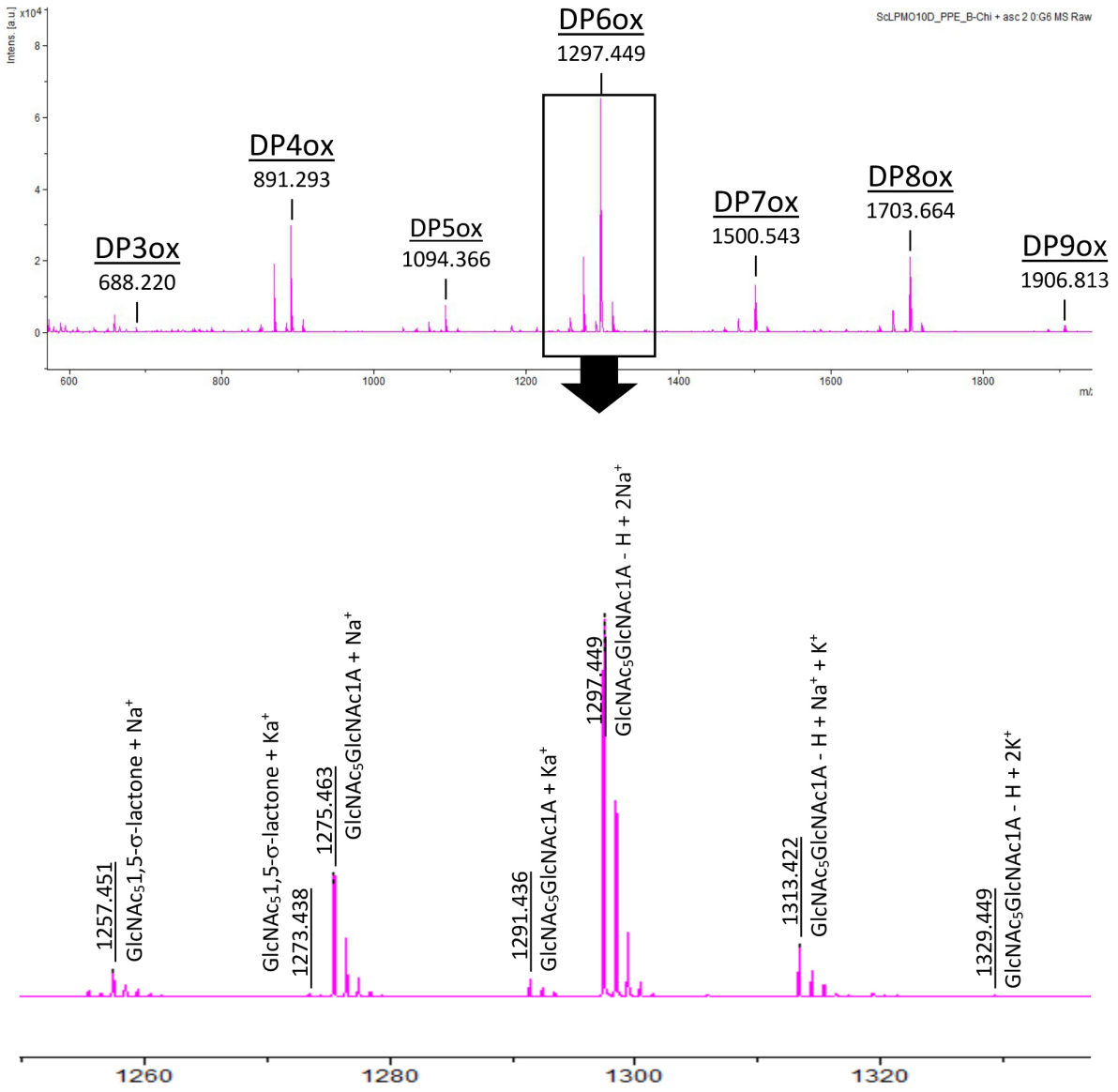

Figure 4.3. MALDI-ToF MS analysis of oxidized β-chitin products generated by *Sc*LPMO10D. The upper mass spectrum shows products generated by ScLPMO10D acting on 5.0 mg/mL β-chitin in 50 mM Tris-HCl (pH 8.0) with 1.0 mM ascorbic acid at 30 °C, after incubation overnight. Signals representing oxidized products with different degrees of polymerization (DP) appear in clusters due to the formation of both lactones and aldonic acids, with various sodium and potassium adducts. The larger labeled peaks represent double sodium adducts of aldonic acid chitooligosaccharides (i.e. $M - H^+ + 2Na^+$) and are marked with their degree of polymerization (i.e. DP3ox- DP9ox) and respective m/z values. The lower spectrum displays an enlargement of the hexamer cluster (i.e. DP6ox) in the upper spectrum. The various products are labeled with their respective adducts and m/z values (z = 1). $GlcNAc_5$1,5-σ-lactone represents the initial lactone product of a C1-oxidation and $GlcNAc_5GlcNAc1A$ represents its corresponding hydrate, the aldonic acid.

4.1.2 Binding assay with α- and β-chitin

Subsequent to purification and copper-saturation, the binding properties of purfied *Sc*LPMO10D were tested with α- and β-chitin (Section 3.4.5.1). Reactions were incubated at a relatively low temperature (22 °C) and in the absence of a reducing agent, to ensure stable binding conditions and to avoid catalytic reactions that could change the substrate and/or lead to autocatalytic enzyme damage (see section 1.3.5).

Fig. 4.3 shows binding of *Sc*LPMO10D-Cu(II) towards α- and β-chitin over time. After 15 minutes of incubation, 30 % of the enzyme had bound to β-chitin, whereas only 13 % of the enzyme had bound to α-chitin. Thus, *Sc*LPMO10D clearly has higher affinity for β-chitin compared to α-chitin. After the five first minutes, the binding rate (i.e. change in bound protein over time) toward β-chitin decreased, which may reflect saturation of binding sites suited for fast binding, whereas the subsequent slower binding rate may relate to less favored or more unspecific binding. Slow binding continued during the full length of the assay (up to 120 min) and seemed, in this time period, i.e. 15 – 120 min, somewhat faster for α-chitin compared to β-chitin. This could imply that *Sc*LPMO10D generally exhibits more unspecific binding towards unspecific binding towards α-chitin. Of note, unspecific binding hampers the catalytic activity of LPMOs and increases the chance of self-inactivation (Loose et al., 2018). The final percentages of bound enzymes in the reactions with either α- or β-chitin were 31% and 46%, respectively.

The apparently low binding affinity can be explained by two phenomena. Firstly, LPMOs in their oxidized Cu(II)-form display a significantly lower affinity toward substrate compared to the reduced Cu(I)-form (Kracher et al., 2018). Secondly, the reactions were made with a relatively high concentration of enzyme (5 μM) with respect to substrate (10 mg/ml); it is therefore possible that the specific binding capacity (i.e. threshold of specifically bound enzyme in μmol per gram of substrate) of *Sc*LPMO10D toward α- or β-chitin was exceeded by the high concentration of enzyme, but there is no data available to properly confirm this.

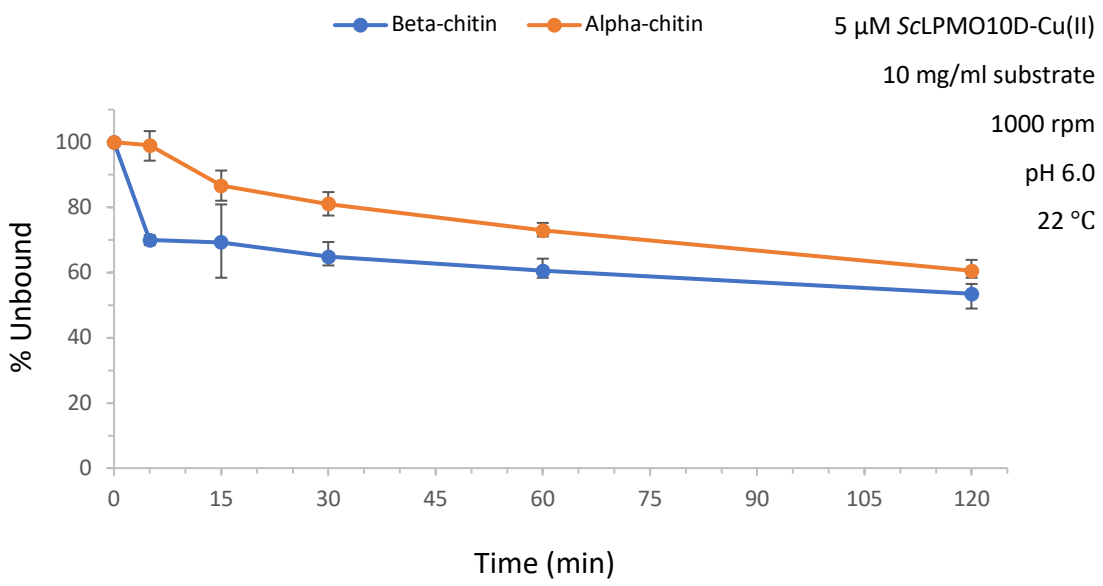

Figure 4.3. Binding assay with α-chitin and β-chitin. 5 uM *Sc*LPMO10D was incubated with 10 mg/ml substrate (i.e. α-chitin and β-chitin) in 50 mM $NaPO_4$ pH 6.0, at 22 °C and 1000 rpm, in the absence of a reducing agent. Samples, taken after 5, 15, 30, 60, and 120 minutes, were filtrated immediately after collection. The amounts of unbound protein in filtrates were analyzed using the Bradford assay (A_{595}). Results are shown as the mean percentage of unbound protein in three reactions (n = 3), with the with highest and lowest value indicated by error bars at each sample point, to give an impression of general the variation within samples. Note that the standard deviation for binding to β-chitin at 15 minutes is around ± 11%, which is much higher than at any of the other time points, and hence likely reflects a sampling error.

4.2 Rational design and site-directed mutation

Site-directed mutagenesis makes it possible to investigate structural determinants of substrate specificity in LPMOs through relatively simple enzyme characterization (e.g. binding and activity assays). As a starting point for rational design of *Sc*LPMO10D mutants, studies on structural determinants of polysaccharide specificity in AA10s were reviewed e.g., (Vaaje-Kolstad et al., 2017; Forsberg et al., 2016 & 2018; Loose et al., 2018). Thereafter, a homology model of *Sc*LPMO10D was generated (Fig. 4.5) to enable a structure-guided approach, in which a multiple sequence alignment (Fig. 4.6), a structural alignment (Fig. 4.7), literature data, and in-house information were utilized to target residues for site-directed mutagenesis.

4.2.1 Homology modeling

Being able to construct three-dimensional (3D) models of proteins with no available 3D structure, is helpful when planning experiments and analyzing experimental results. Because the 3D structure of *Sc*LPMO10D was not solved at the time, a structural model was generated by homology modeling using the Swiss-Model server (Waterhouse et al., 2018). The default template search function was used to find suitable template structures, from which *Cj*LPMO10A (PDB: 5FJQ) from *Cellvibrio japonicus* was chosen, based on shared substrate specificity (i.e. β-chitin), high sequence identity (i.e. 47 %) with *Sc*LPMO10D, and the shared sequence features displayed in Fig. 4.1. Structural templates with sequence identity above 40% generally generate structural models of decent quality (Fernandez-Fuentes et al., 2007). Swiss-Model provides a combined confidence estimate score to evaluate structural models, which is based on global (i.e. entire structure) and local (i.e. per residue) confidence scores, which are summarized in the absolute quality estimate QMEAN (Benkert et al., 2010). The QMEAN scoring system ranges from -4.00 to 1.00, where 1.00 represents the highest confidence score. The final model of *Sc*LPMO10D (Fig. 4.5) got an estimated QMEAN score of -2.32, which is not particularly good, but in general considered acceptable.

Interestingly, a chitin active AA10 enzyme (i.e. *Tma*12, PDB: 6IF7) originating from the fern *Tectaria macrodonta* (Yadav et al., 2019) shares a high sequence identity of 58 % with *Sc*LPMO10D, however, this structure was not available at the time.

Subsequent to the design, production and characterization of *Sc*LPMO10D variants, the crystal structure of *Sc*LPMO10D was determined, which can be reviewed in the appendices (Appendix B). Comments on the quality of the structural model, relative to the solved crystal structure, are provided in the discussion.

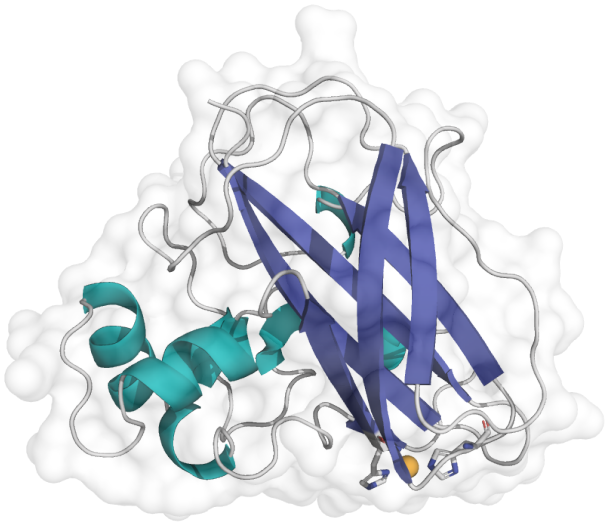

Figure 4.5. Structural model of *Sc*LPMO10D. The picture displays the structural model of *Sc*LPMO10D obtained through comparative modelling with *Cj*LPMO10A (PDB: 5FJQ) as a template. The model was made with the automated protein structure homology-modelling server SWISS-MODEL (Waterhouse et al., 2018) and visualized in cartoon representation with PyMOL (DeLano & Lam, 2005). The side chains of the tow catalytic histidines and the copper ion (orange sphere) are shown.

4.2.2 Sequence analysis

Comparative analysis of the sequences of AA10s with specificity toward either cellulose (C1), chitin (C1), or both cellulose (C1/C4) and chitin (C1) was conducted via a multiple sequence alignment (MSA). Well-studied AA10 enzymes with known structures were chosen as representative sequences and information on conserved residues was obtained from literature (Forsberg et al., 2016 & 2018; Loose et al., 2018). As depicted in Figure 4.6, *Sc*LPMO10D represents a typical cellulose active AA10 enzyme with a consensus sequence strongly associated with C1oxidizing specificity toward cellulose (i.e. residues highlighted in green and pink), while *Sm*LPMO10A represents a typical chitin-active enzyme with C1 regioselectivity (i.e. residues highlighted in yellow and pink), and *Sc*LPMO10D display conserved motifs from both. *Sc*LPMO10B, on the other hand, exhibit consensus sequence connected to C1/C4 regioselectivity (i.e. residues highlighted in blue) and otherwise conserved residues associated with either chitin

or cellulose activity. The residues highlighted in gray were found to show more variations but were still considered interesting targets because of possible contribution to substrate interaction.

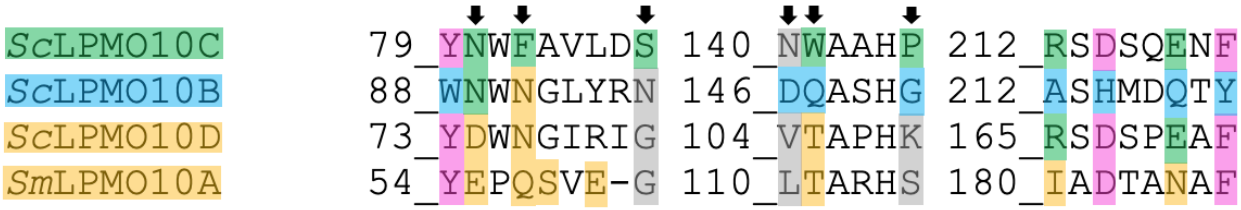

Figure 4.6. Sequence alignment for AA10 LPMOs with different substrate specitivity and regioselectivity. The figure shows a multiple sequence alignment of *Sc*LPMO10C (CelS2; C1, cellulose), *Sc*LPMO10B (C1/C4 cellulose & C1 chitin), *Sc*LPMO10D (C1 chitin as shown in this study), and *Sm*LPMO10A (CBP21; C1 chitin), limited to sections known to interact with substrate in family AA10 LPMOs. Residues (putatively) associated with different substrate specificity and regioselectivity are highlighted by colors: green (C1 cellulose); blue (C1/C4 cellulose and C1 chitin); yellow (C1 chitin); pink (C1 specific); gray (less concerved positions). The black arrows indicate positions in *Sc*LPMO10D targeted for mutation. The alignment was made with ClustalW format using the online MSA-tool MUSCLE (Edgar, 2004), launched by EMBL-EBI.

4.2.3 Structural alignment and final mutant designs

The information derived from the MSA and literature was further investigated through structural alignment in PyMOL (DeLano & Lam, 2005). Figure 4.7a displays the structural superposition of *Sc*LPMO10D (model) with *Sc*LPMO10C (CelS2), which is one of the best studied AA10 enzymes, with substrate specificity toward cellulose and with a C1 regioselectivity. In a recent study, Jensen et al. (2019) were able to engineer CelS2 into an enzyme with chitinolytic activity, in which Tyr79, Asn80, Phe82, Tyr111, and Trp141 were targeted for mutation. These five mutations are all located in loop 2 and affect substrate-binding in subsites -4 to -2, which are known to important for substrate binding by AA10s (Aachmann et al., 2012; Bissaro et al., 2018; see also Frandsen et al., 2016, who show similar data for an AA9). In Figure 4.7b, *Sc*LPMO10D is structurally aligned with *Sc*LPMO10B and *Ma*LPMO10A, both known to oxidize C1/C4 in cellulose and C1 in chitin. Residues important for the dual oxidative regioselectivity of

*Sc*LPMO10B and *Ma*LPMO10A have been described by Forsberg et al. (2018). After consulting the work of Forsberg et al. (2018) and Jensen et al. (2019), and based on the comparisons shown in Fig. 4.7, five residues in *Sc*LPMO10D were selected for mutation. At each position, one or two mutations were made intended to lead to cellulolytic C1 activity or to lead to a combination of chitin C1 and cellulose C1/C4 activity, as summarized in Fig. 4.7.

Notably, two of the selected residues, Gly81 and Lys135 had not been targeted for mutated in previous studies. These specific positions were selected among other candidates, to possible obtain novel information about residues which display a less obvious role in substrate binding and regioselectivity, among family AA10 enzymes.

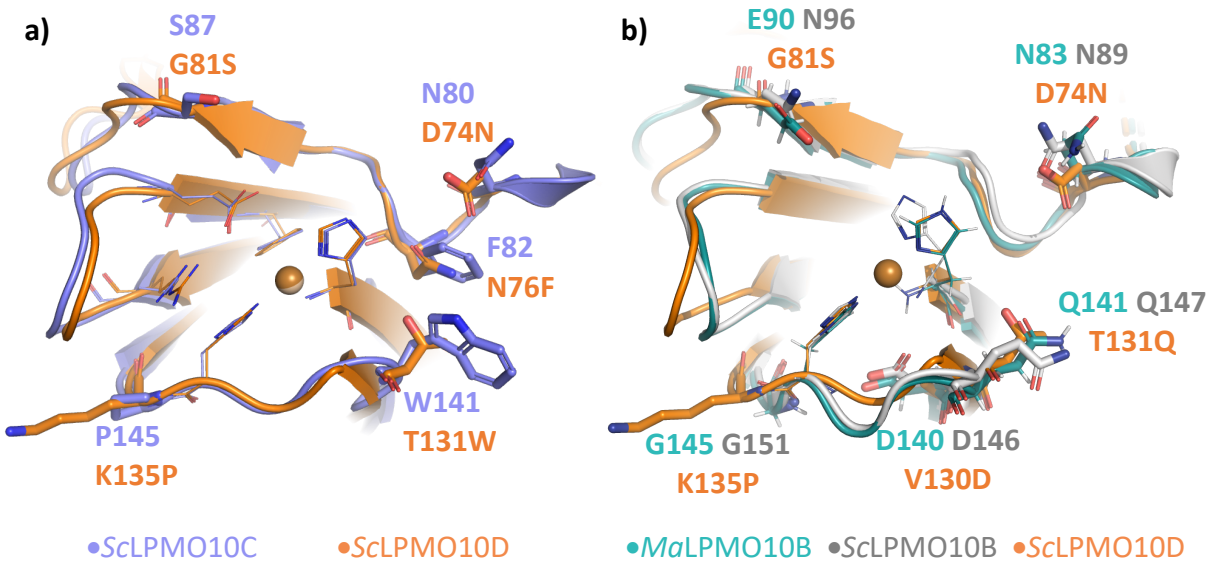

Figure 4.7. Structural alignments of LPMO catalytic centers. The picture shows structural superpositions of *Sc*LPMO10D (model), with either **a)** *Sc*LPMO10C (PDB: 4OY7) or **b)** *Sc*LPMO10B (PDB: 4OY6) and *Ma*LPMO10B (PDB: 5OPF). The labelled residues were targeted for site-directed mutagenesis with the aim of changing the substrate specificity to a) cellulose (C1), and b) cellulose (C1/C4) and chitin (C1). The first letter is the single letter code for the original amino acid in *Sc*LPMO10D, the number indicates the position in the sequence of *Sc*LPMO10D, and the letters after the numbers indicate the residue that was planned to be introduced in

*Sc*LPMO10D. The other labels indicate the corresponding residues in *Sc*LPMO10C (blue), *Sc*LPMO10B (gray) and *Ma*LPMO10B (Green).

4.2.4 Site directed mutagenesis

Due to time constraints, a limited set of mutant enzymes was targeted, including some with single mutations, and some with various combinations of mutations, as summarized in Table 4.1. The selected mutants were generated using the QuikChange II XL Site-Directed Mutagenesis Kit. Mutants with more than one mutation were made by using existing mutant plasmids (i.e. DNA) as templates, adding one mutation at the time and thereby generating different generations of mutants e.g., *Sc*LPMO10D-1b (D74N) → *Sc*LPMO10D-2b (G81S/D74N) → *Sc*LPMO10D-3b (G81S/D74N/K135P). For every mutation added, high copy numbers of plasmids needed to be generated, isolated, and their sequence were verified to establish the presence of the desired mutations and rule any out random events. While generating multiple mutations in this fashion is time consuming in itself, some mutations were more difficult to generate than others, which extended this phase of the project. Trouble shooting included variation of PCR conditions temperatures and cycling times (section 3.2.3), as false priming (i.e. secondary structure formation) and high melting temperatures were suspected to cause problems. Eventually, all mutant genes were successfully generated (Table 4.1).

Table 4.1. Overview and theoretical properties of *Sc*LPMO10D wild type and mutants. The table gives the name of each enzyme and its mutation(s), and includes calculated molecular weights (MW), isoelectric points (pI), and extinction coefficients (ε). Gray shading indicated mutants that were not expressed. The theoretical properties of proteins without signal peptide were calculated using the ExPASy Compute pI/Mw tool (Gasteiger et al., 2005).

NAME	SHORT NAME	MUTATIONS	MW (g/mol)	pI	ε
*Sc*LPMO10D-WT	WT	-	19145.27	7.11	33920
*Sc*LPMO10D-1a	1a	G81S	19175.30	7.11	33920
*Sc*LPMO10D-1b	1b	D74N	19144.29	7.85	33920
*Sc*LPMO10D-2a	2a	G81S/D74N/N76F	19207.38	7.85	33920
*Sc*LPMO10D-2b	2b	G81S/D74N	19174.31	7.85	33920
*Sc*LPMO10D-3a	3a	G81S/D74N/N76F/K135P	19176.33	7.11	33920
*Sc*LPMO10D-3b	3b	G81S/D74N/K135P	19143.25	7.11	33920
*Sc*LPMO10D-4a	4a	G81S/D74N/N76F/K135P/T131W	19261.44	7.11	39420
*Sc*LPMO10D-4b	4b	G81S/D74N/K135P/T131Q	19170.28	7.11	33920
*Sc*LPMO10D-5b	5b	G81S/D74N/K135P/T131Q/V130D	19186.24	6.56	33920

4.3 Production of *Sc*LPMO10D mutants

After confirming incorporation of correct point mutations, selected constructs encoding *Sc*LPMO10D mutants were transformed into chemically competent *E. coli* BL21 (DE3) for expression. Three colonies from each transformation were picked and used for protein expression at small scale overnight followed by analysis of protein production using SDS-PAGE (Fig. 4.8) to identify transformants exhibiting adequate expression of the target enzyme.

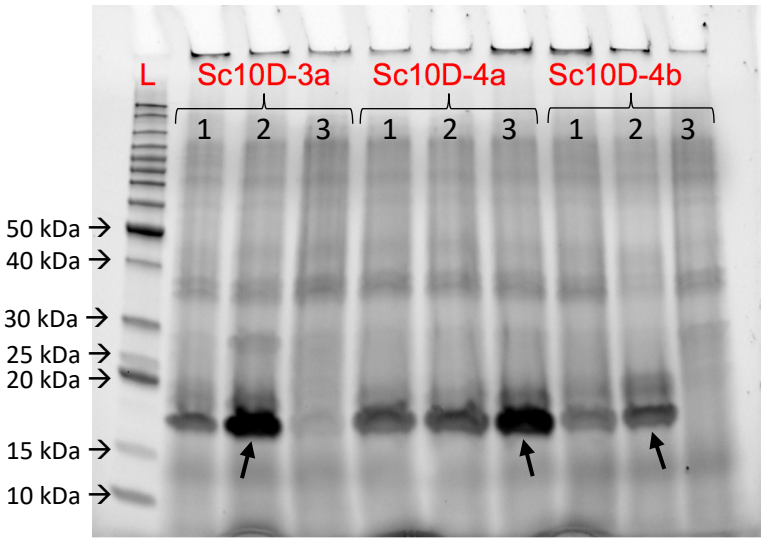

Figure 4.8. SDS-PAGE analysis of transformed constructs of *Sc*LPMO10D mutants. The first lane (L) display a BenchMark™ Protein Ladder, of which bands with molecular sizes ranging from 10 - 50 kDa is indicated on the left of the lane. The remaining lanes display lysed samples from cultures of transformed mutants (i.e. 3a, 4a, and 4b). Transformants exhibiting the highest expression level of the target enzyme (~19 kDa), marked with arrows, were used further in large scale expression and long-time storage (i.e. glycerol stocks stored at -80 °C).

4.3.1 Expression and extraction

For large scale protein expression, fresh cultures or scraps of glycerol stock were utilized to inoculate TB-medium supplemented with 100 µg/ml ampicillin. Elsewise, the same methods and conditions used to express and extract the wild type *Sc*LPMO10D (section 4.1.1) were applied to

produce and extract the mutated enzymes. Figure 4.9 display the results from periplasmic extraction of recombinants 4a and 4b; the other mutants showed similar results. From the expression of all mutants, significant amounts of target enzymes were identified in both the sucrose- and periplasmic fractions, with little remaining in the cell pellets, which have been briefly discussed in Section 4.1.1. The band located right above the target enzyme was displayed by all recombinants and can correspond to the molecular weight of non-mature ScLPMO10D mutants with the N-terminal signal peptide still attached. If so, the molecular weight would be around 3 kDa heavier than the mature proteins (~22 kDa). Of note, this additional band was not observed after the periplasmic extraction of the wild type enzyme.

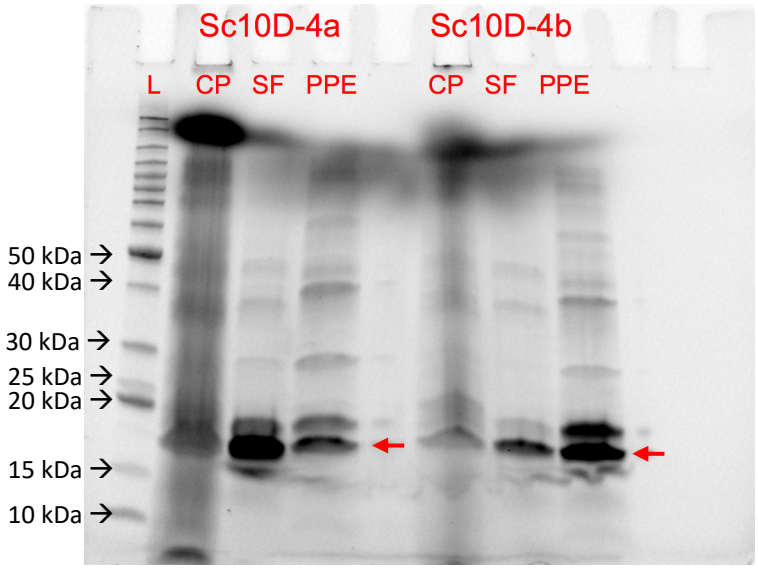

Figure 4.9. SDS-PAGE analysis of periplasmic extraction of 4a and 4b. The first lane (L) shows the BenchMark™ Protein Ladder, of wich molecular sizes ranging from 10-50 kDa are indicated to the left of the lane. Wile the lanes marked with CP display samples of the cytoplasmic frations (i.e. remaining cell pellets), SF display samples from the collected sucrose fractions (i.e. supernatant), and PPE show samples from the periplasmic fractions. Bands corresponding to the molecular weight of *Sc*LPMO10D (i.e. 19 kDa) are indicated by red arrows.

4.3.2 Purification

After extraction, all sucrose fractions went through buffer exchange to remove sugar and other contaminating chemicals from the spheroplast buffer (e.g. EDTA). The sucrose and periplasmic fractions were pulled together before purification to save time, if the protein concentration from did not appear extremely high when analyzed with SDS-PAGE. Wild type *Sc*LPMO10D and recombinants were purified in two steps, starting with anion-exchange chromatography (AEC) (section 3.3.5), followed by size exclusion chromatography (SEC) (section 3.3.6). The purpose of AEC-chromatography is normally to ensure that target proteins bind to the positively changed stationary phase (e.g. quaternary amine) by employing mobile phase conditions (i.e. pH) that gives the target a negative net charge. Elution of bound proteins can thereafter be controlled by applying a gradient of either pH, ionic strength (e.g. salt concentration), or both, which allow different proteins to be eluted into separate fractions based on their charge at a particular pH. Here however, a procedure developed to allow the target protein flow through the column without binding, while other proteins bind, was utilized to purify *Sc*LPMO10D and its recombinants (Fig. 4.10a).

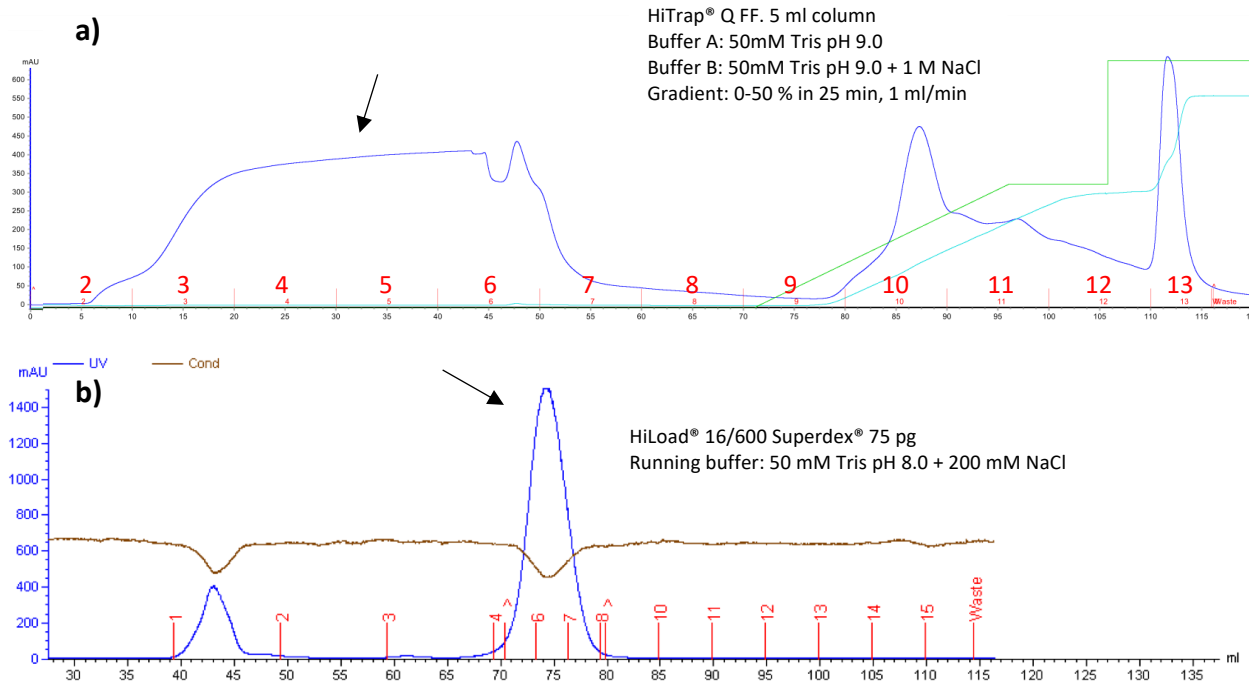

Figure 4.10. Two-step purification of wild type and its mutants. Fraction numbers are shown in red. The X-axes show volume (ml) of buffer passed through the column, while the Y-axes show measurement of UV absorbance at A_{280}. Both chromatograms display eluted proteins detected by real-time monitoring of absorbance at A_{280} (blue lines). The upper chromatogram (a) show the result from AEC purification of *Sc*LPMO10D-4b, which serves as a representative result of all the other *Sc*LPMO10D enzymes (i.e. wild type and mutants). The broad peak arising at the beginning of the chromatogram (arrow) contains the target enzyme, while subsequent peaks eluted by the rising conductivity (cyan) contain contaminating proteins, which was verified by gel electrophoresis (Fig. 4.11a). The lower chromatogram (b) displays a representative result from SEC purifications, featuring *Sc*LPMO10D-4b. The tall peak arising at the beginning of fraction nr. 4 contains the target enzyme (arrow), while the earlier peak contains contaminating proteins, verified by gel electrophoresis (Fig. 4.11b).

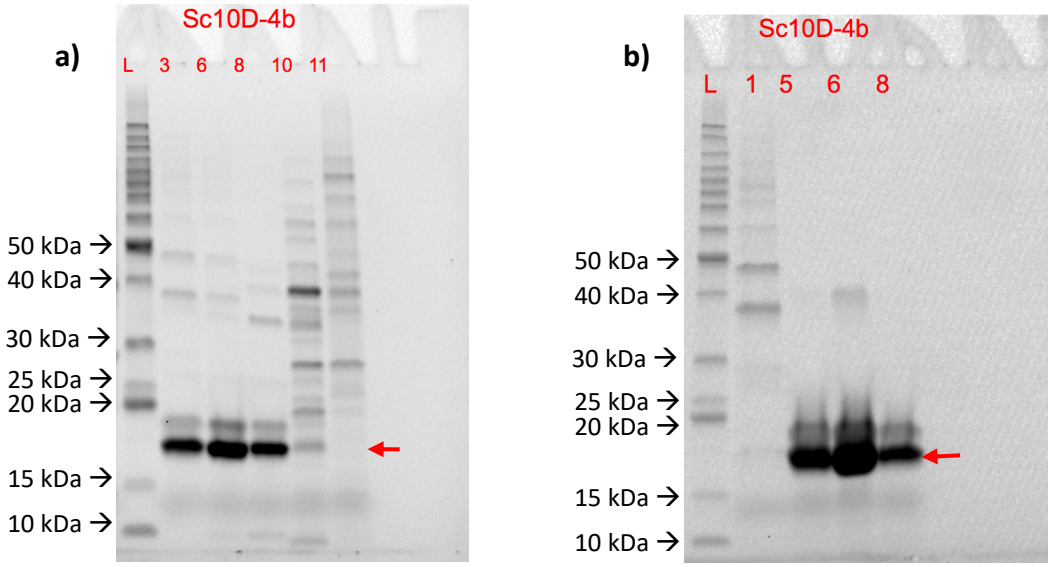

Figure 4.11. SDS-PAGE analysis of the two-step purification. Both gel pictures display analysis of the purification of *Sc*LPMO10D-4b, which serves as representative examples for all the other *Sc*LPMO10D variants. The first lanes (L) show a BenchMark™ Protein Ladder, of which molecular sizes ranging from 10-50 kDa are indicated to the left of the lanes. Numbers over the remaining lanes indicate the fractions of their respective purifications. The red arrows indicate bands of a molecular size corresponding to *Sc*LPMO10D-4b (19 kDa). Gel-picture a) show fractions from the AEC purification, while gel-picture b) display fractions from the SEC purification. The more smudged tendency of the bands observed in the SEC gel-picture relative to the AEC gel, may be caused by the salt content in the SEC running buffer (i.e. 200 mM NaCl).

The theoretical pI of the *Sc*LPMO10D variants were calculated to range from 7.1 - 7.8 (Table 4.1), which means that they should exhibit a negative net charge at pH values above their pI (Stanton, 2004), and thus bind to the strong anion resin (i.e. quaternary amine) at a pH of 9.0. However, all the *Sc*LPMO10D variants appeared in the flow-through, which mean that they should either have a positive or neutral charge at this pH. Therefore, it seems more believable that their true pI must either lie above or be equal 9.0. To check this a simple analysis was manually conducted in PyMOL (Appendix B), using the solved crystal structure of *Sc*LPMO10D. The theoretical electrostatics of the protein surface (i.e. generated in PyMOL) was used to select relevant residues (i.e. non-neutralized charges) among surface exposed residues, which would exhibit charge at pH 9.0 (i.e. Arg, lys, asp, glu, N-terminal and C-terminal residues). Out of 32

charged residues (i.e. at pH 9.0), 9 were estimated to have a negative charge and 23 were seemed to be positively charged. If so, the wild type ScLPMO10D would have approximately 14 more positively charged residues contributing to its net charge at pH 9.0, which may provide a plausible explanation to why it did not bind to the column during the binding step in AEC purification.

Illustrated by the AEC chromatogram of the *Sc*LPMO10D-4b purification (Fig. 4.10a), the broad peaks containing target protein often started with a low shoulder and ended with a long tail, which were found to mostly contain the target protein (including the band suspected to contain the target protein with signal peptide) and some weak bands of higher molecular weights, when analysed with SDS-PAGE (Fig. 4.11a). Notably, the AEC purifications of all proteins displayed an additional peak of variating height at the end of the broad peak (i.e. fraction nr. 6), but this peak did not contain an excessive amount of proteins according to Figure 4.11a. Furthermore, the tall peak in fraction nr. 13 eluted at a 50-100% concentration of buffer B, which were observed for other variants (to a variating extent) too, only displayed slightly visible bonds when analyzed with SDS-PAGE (not analyzed in Fig. 4.11a due to earlier results). The high absorbance of both these peaks could be explained by DNA (e.g. plasmid and genomic), RNA (e.g. tRNA and mRNA), and peptide contamination; released by cell lysis during the periplasmic extraction. Both DNA and RNA will absorb UV at 280 nm (λmax = 260 nm) and exhibit a negative net charge, which makes them bind tightly to the strong anion-exchange resin (i.e. Q Sepharose FF). Thus, DNA and RNA will further need a relatively high salt concentration to be eluted, just like the tall peak observed in fraction 13. Because *Sc*LPMO10D variants most likely have a positive net charge at pH 9.0 (Appendix B), it is likely that they will be able to bind and neutralize the charge of less negatively charged molecules (e.g. proteins, short DNA/RNA oligomers and dNTP molecules), and thereby let them travel freely through the column. However, non-ionic solutes also travel slower through a charged column, which may explain how non-ionic peptides and neutralized LPMOs oligomeric DNA/RNA and dNTP molecules could be accumulated at the end of the bulk flow and contribute to the total absorbance; causing the additional peak at the end of the broader peak (i.e. with target protein). Furthermore, the small shoulder and long tail of the

broad peak may therefore also be caused by the mix of positively charged, neutralized, and non-ionic compounds (i.e. that absorb light at A_{280}), traveling through the column at different speeds.

Fractions 3-8 from the AEC purification of *Sc*LPMO10D-4b was pulled, concentrated and purified further with SEC chromatography. The SEC chromatogram exhibit two peaks. The first peak corresponds to fraction 1 in figure 4.11b, which display various bands of higher molecular weight than the target protein, observed in the pulled fractions from the AEC purification (Fig. 4.11a). The next peak in the SEC chromatogram is tall, symmetrical, and does not display any broad shoulder or long tail, which implies a good separation of homogenous enzymes with good quality (i.e. not denatured or misfolded). In figure 4.11b, this peak is found to mostly contain the target protein, the slightly higher band suspected to represent non-mature enzymes, and a weaker band of ~40 kDa. If the band above the target protein corresponds to the non-mature version of *Sc*LPMO10D-4b, a less symmetrical shape could be expected. However, the column used (i.e. HiTrap® Q FF. 5 ml) does not have the resolution to separate molecules with only 3 kDa difference in molecular weight, and thus might not even show a minor indication of the presence of non-mature protein. The weak band at ~40 kDa was present after SEC purifications of all *Sc*LPMO10D variants and could be a result of dimerization of denatured LPMOs via disulfide bridges. The stock solution of LDS sample buffer which was used to prepare the samples was supplemented with a strong reducing agent (i.e. Dithiothreitol), but at a high protein concentration, the amount of reducing agent might have been inadequate to fully prevent dimerization. However, the band detected at approximately 40 kDa corresponds very well to the molecular weight of the theoretical dimer (i.e. 36 kDa).

Of note, eliminating non-mature *Sc*LPMO10D variants could have been done through in-vitro digestion of the N-terminal signal peptide, using an N-terminal methionine-specific peptidase (Miller et al., 1987). Nevertheless, the purification of all the *Sc*LPMO10D variants could be considered relatively successful.

4.3.3 Copper saturation and final yield

After SEC purification of all *Sc*LPMO10D variants, enzyme containing fractions were pulled and concentrated to ~ 2 ml, before measuring their concentration (Table 4.2; yield). Thereafter, 0.5 mL of each enzyme were incubated with free copper to ensure copper saturation, and further desalted, before measuring the protein concentration again (Table 4.2; Cu-sat.). The measured concentration after copper-saturation were further corrected (Table 4.2; corrected) by multiplying it with an estimated factor of purity (Table 4.2; purity), derived from figure 4.12.

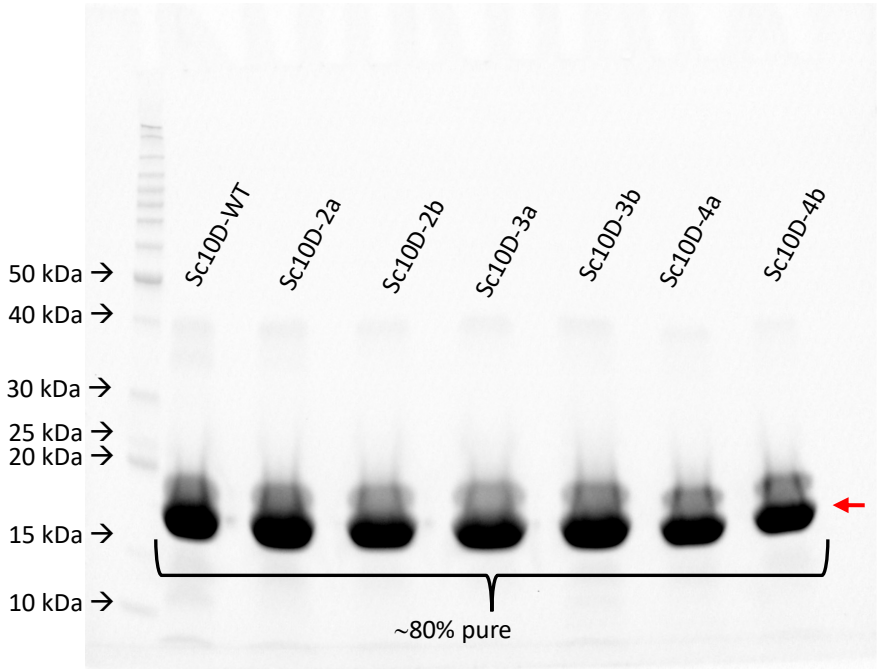

Figure 4.12. Purity of copper-saturated *Sc*LPMO10D variants. The figure show samples from the copper-saturated ScLPMO10D variants, having a molecular weight of 19 kDa and a purity of approximately 80%. The purity of all enzymes were quantified with the Image Lab™ software provided by Bio-Rad.

As seen in figure 4.12, the suspected non-mature protein had suddenly appeared in the sample from the wild type enzyme, which seems strange as it was not observed after the periplasmic extraction (Fig. 4.2) or the two-step purification (not shown). As it seemed difficult to find a logical explanation for this phenomenon at the time, it was momentarily concluded that that the band of non-mature protein had somehow been masked in earlier gel electrophoresis analyses of the wild type enzyme. The theorized purity of functional LPMO enzymes were therefore taken into account throughout the experimental investigation of the mutational effects. However, subsequently, another explanation has been hypothesized and analyzed in Appendix B.

Table 4.2. Production yields of *Sc*LPMO10D variants. The table gives an overview of the measured concentrations of enzyme after purification with SEC (yield), copper-saturated stocks (Cu-saturated), the quantified amounth of functional enzyme (purity), and the corrected concentration of the coppersaturated stocks (Cu-corrected).

ENZYME	YIELD [μM]	Cu-SATURATED [μM]	PURITY (%)	Cu-CORRECTED [μM]
Sc10D-WT SF	3620.3	-	-	-
Sc10D-WT PPE	342.7	176.2	~ 80	141.0
Sc10D-2a	1474.8	581.9	~ 80	465.5
Sc10D-2b	1776.2	597.0	~ 80	477.6
Sc10D-3a	2979.5	882.9	~ 80	706.3
Sc10D-3b	1027.4	606.6	~ 80	485.3
Sc10D-4a	769.3	412.9	~ 80	330.3
Sc10D-4b	766.5	356.0	~ 80	284.8

Notably, when *Sc*LPMO10D-3a was copper saturated some of the enzyme appaired to be stuck in the column, which was discovered when the upper section of the resin was tinted blue (not shown). In retrospect, ScLPMO10-2a, -2b, -3a, and -3b should have been diluted before copper

saturation, as high protein concentration (i.e. >15-20 g/L) tends to become destabilized when excess copper is added to the solution and thereby lead to precipitation (Westereng et al., 2018). Regardless, the other enzymes handled the copper saturation well, and the yield of *Sc*LPMO10D-3a was still relatively high, despite the precipitation.

4.5 Investigation of mutational effects

4.5.1 Activity of wild type *Sc*LPMO10D and its mutants

The activity of all mutants and wild type enzyme were tested on PASC (i.e. phosphoric swollen cellulose), Avicel (i.e. microcrystalline α-cellulose), and BMCC (i.e. bacterial microcrystalline cellulose), but no oxidized products were detected on these cellulosic substrates. When tested on β-chitin however, two out of six mutants still displayed oxidative activity (Fig. 4.13).

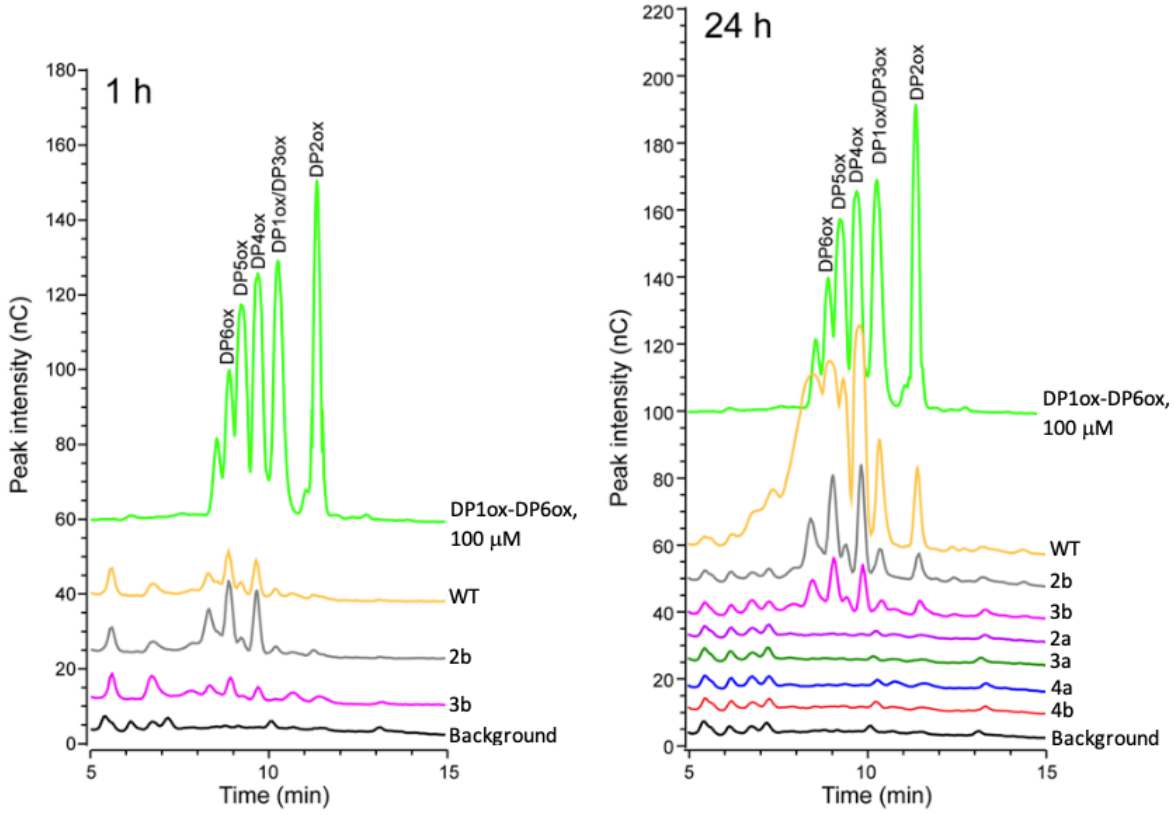

Figure. 4.13. Qualitative analysis of activity on β-chitin, wild type and mutants. Soluble products were analysed with High Performance Anion-Exchange Chromatography (HPAEC) and monitored by Pulsed Amperometric Detection (PAD). The first lane in both chromatogams (1 h & 24 h) display the isocratic elution of N-acetylated chito-oligosaccharides ($GlnNAc_{1\text{-}6}A1$). In the left chromatogram (1h), only enzymes with activity on β-chitin have been displayed, while all enzymes are shown on the right (24 h). Reactions were made with 1 µM enzyme and 10 mg/ml β-chitin, in 50 mM $NaPO_4$ pH 6.0. Reactions were started with adding 1 mM ascorbic acid and incubated at 40 °C, for 24 hours in a shaking incubator (800 rpm). Samples were taken after 1 and 24 hours and the reactions were stopped by filtering the samples.

Notably, *Sc*10D-2a seems to display a higher initial catalytic activity than the wild type. This could be explained by a lower binding affinity to the substrate which possibly allows this mutant to generate more H2O2 than the wild type and thus will have more of the hypothesized co-substrate to drive the reaction at first. Also making it more exposed to autocatalytic events and thus more unstable over time

4.5.1 Apparent melting temperatures

Binding copper is known to have a stabilizing effect LPMOs, the relative difference in melting temperature (Tm in °C) between copper binding and apo enzymes can therefore be used for qualitative analysis of the copper binding ability of mutated LPMOs.

A ThermoFluor assay was applied to study the thermal stability of *Sc*LPMO10D

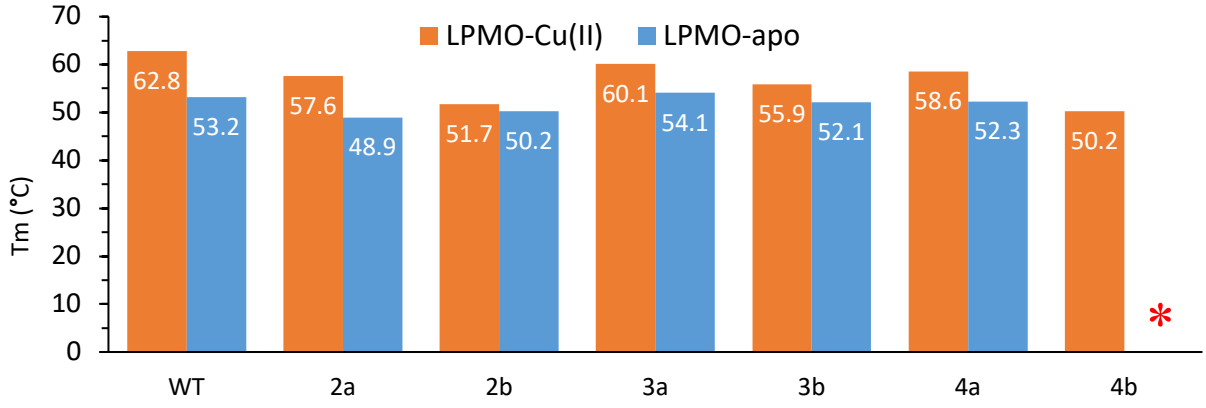

Figure 4.14 Apparent melting temperatures (Tm) of wild type and mutants, in presence or absence of the Cu(II) cofactor. Reactions (n = 5) were made with 1 mg/ml enzyme in 50 mM $NaPO_4$ (pH 0.6), and analyzed with real time PCR using a heating rate of 1 °C min^{-1}, ranging from 25 - 100 °C. Apo reactions were prepared with 10 mM EDTA. Acording to the bar chart, all *Sc*LPMO10D-Cu(II) (i.e. copper associated) variants display a higher Tm than their respective apo enzymes (i.e. withouth copper). The red asterisk referes to the apo reaction of ScLPMO10D-4b, which was lost.

According to the results from the Thermal Shift Assay (Fig 4.14), all mutants and wild type enzyme seems to bind copper (except for the missing value for 4b-apo).

Although the mutants displayed a lower Tm than the wild type, there is not a significant difference in melting temperature between them. The results from Thermal Shift Assay are dependent on many factors which can be

4.5.2 Binding β-chitin

Gallic acid was used instead of ascorbic acid in a. attempt to reduce the enzyme-inactivation over time.

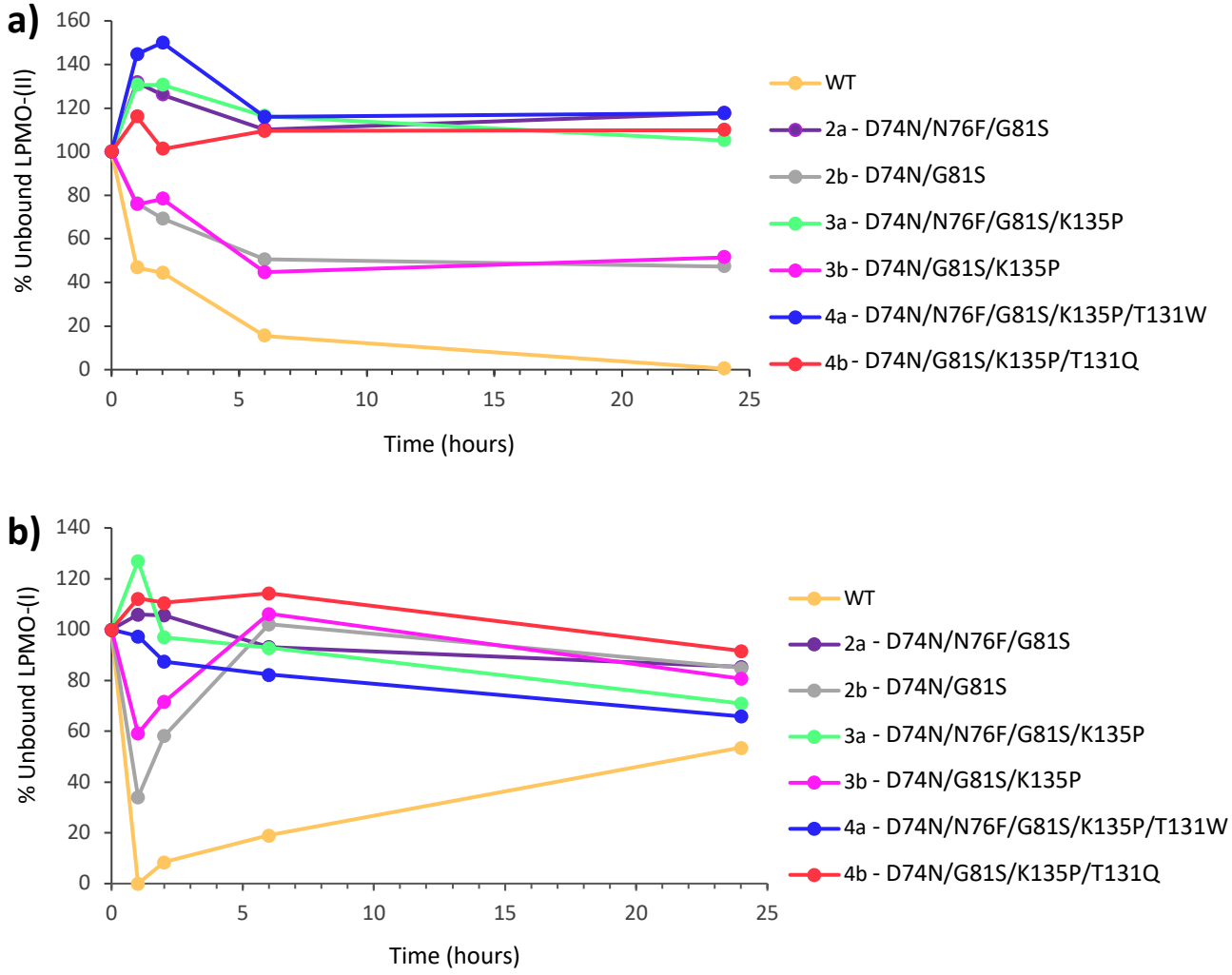

Figure 4.15. Binding β-chitin with and without reductant. Reactions with 2 uM *Sc*LPMO10D and 10 mg/ml β-chitin in 50mM NaPO4 pH 6.0, were incubated at 22 °C and 1000 rpm, either in absence (a) or presence (b) of a reducing agent. Samples taken after 1, 2, 6, and 24 hours, were filtrated immediately after collection and the amount of unbound protein were measured using Bradford assay (A_{595}). Here, the results are shown as the percentage of unbound protein in filtrated samples.

The binding (Fig. 1.15) seems to correlate with the lack of an or reduced activity on beta-chitin.

Interestingly, according to results published by Forsberg et al. (2016) and the results in Figure 4.15, the catalytic domain of the wild type *Sc*LPMO10D seems to bind more specifically to chitin than the truncated version of *Cj*LPMO10A (Forsberg et al., 2016). The native *Cj*LPMO10A display two chitin binding modules, CBM5 and a C-terminal CBM73. They share a relatively similar structure and conserved motifs, and both are chitin-oxidizing enzymes.

4.5.3 H_2O_2 production

In 2012, Kittl et al. reported that reduced LPMOs will react with O_2 and generate H_2O_2 in the absence of substrate. It was further proposed that this side reaction could be used to measure the catalytic activity of LPMOs, in an assay involving Amplex red and horseradish peroxygenase (Kittl et al., 2012). Despite multiple pitfalls, this assay is still considered as a useful and fast method for qualitative detection of LPMO-activity, especially in light of that H_2O_2 was recently identified as a possible cosubstrate (Bissaro et al., 2017).

The wild type enzyme and all mutants were probed in a horseradish peroxygenase/Amplex red assay to investigate if the active site of the mutants had been affected by the directed mutations. The amount of H_2O_2 produced by the wild type and mutants were measured over time (Fig. 4.16), the initial production rates are were displayed in Fig. 4.X and 4.X.

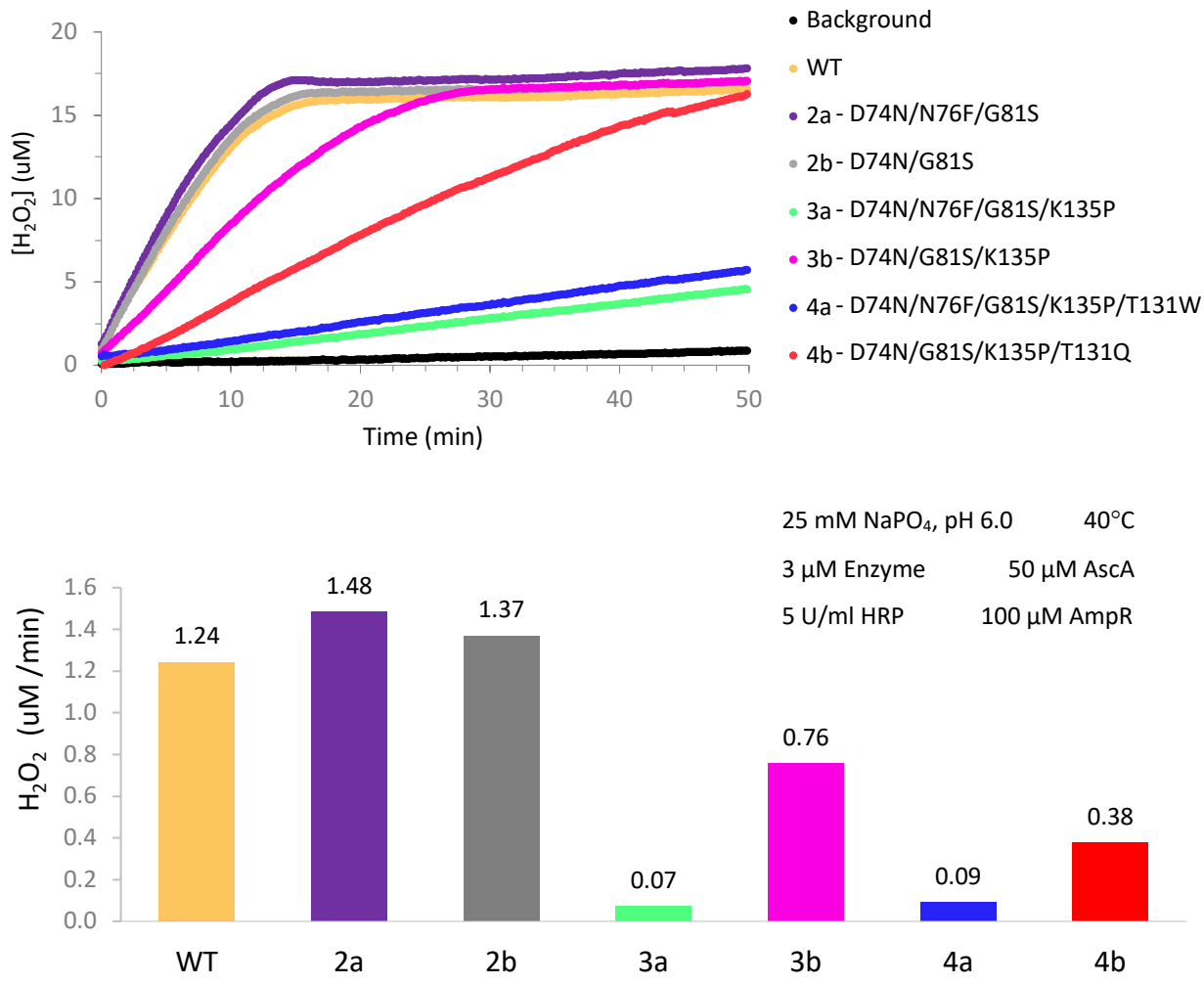

Figure 4.16. H_2O_2 production of wild type and mutant versions of *Sc*LPMO10D. See section 3.4.7, for more information about the assay.

Here Fig. 4.16, a significant difference is seen between the some of the mutants and the wild type. While the lack of activity on PASC (not shown) and beta-chitin correlates with some of the results here, namely WT, 2b, 3a, 4a, and 4b. It is interesting that 2a apparently display a higher

production of H2O2 com paired to the other in-active enzymes. However, there is many possible explanations which is not necessarily related to catalytic activity

4.5.5 H_2O_2 supplemented activity

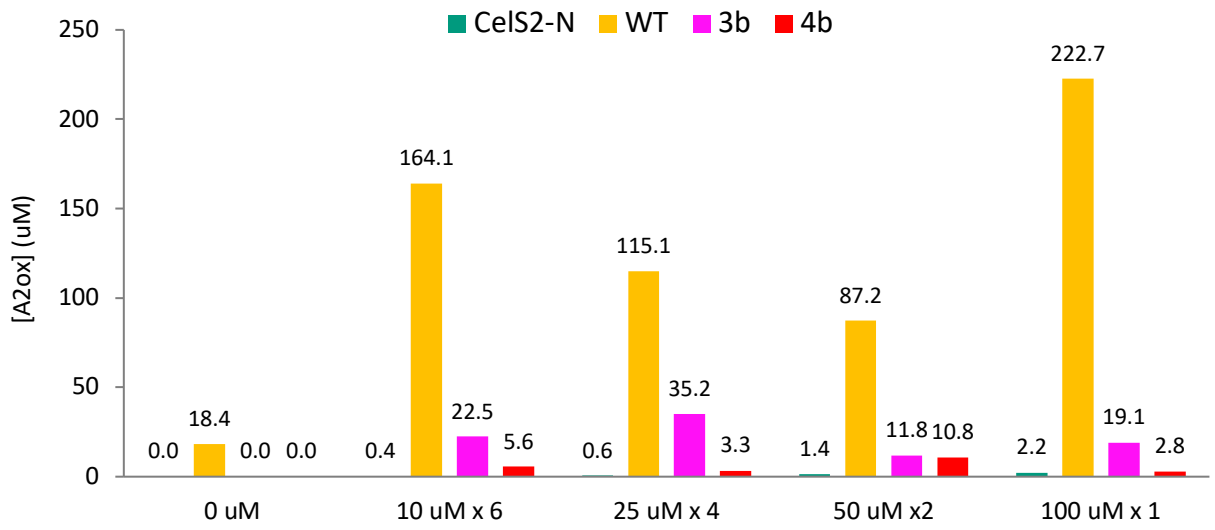

Figure 4.17 Activity on β-chitin in reactions supplemented with H_2O_2. The figure shows the total amount of oxidized products produced in H2O2-driven reactions. CelS2 was used as a negative control

The results from Figure 4.17 seems somewhat inconclusive. The "ugly" results can be explained by the high concentration of the H2O2 stock solution used and the small pipette volumes added which results in very low accuracy. On the other hand, 4b seems to display some oxidative

activity when probed with hydrogen peroxide. However, it cannot be considered especially significant, compared to the wild type enzyme

ScLPMO10D

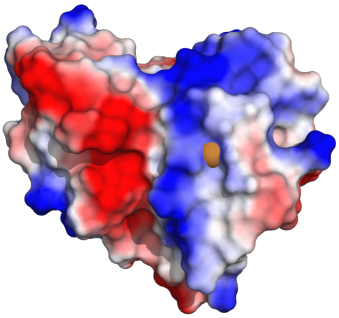

ScLPMO10B

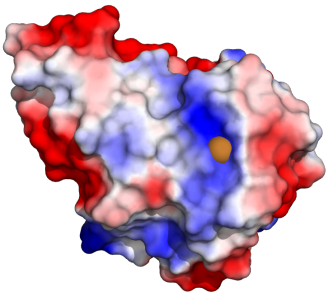

ScLPMO10C

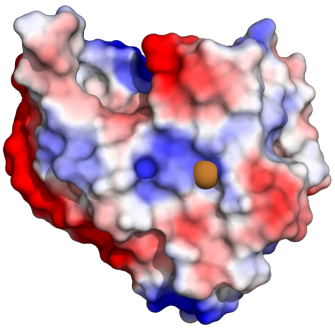

Sc10C-2b

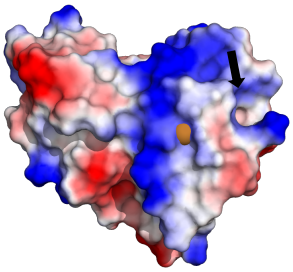

Sc10C-4b

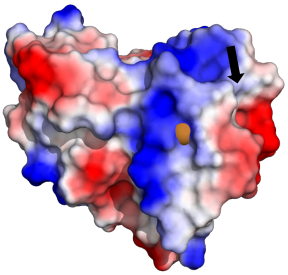

Sc10C-4a

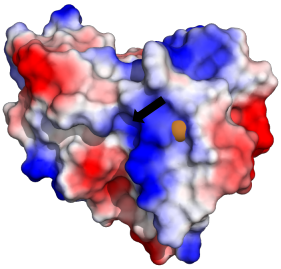

SmLPMO10A (CBP21)

SmLPMO10A (CBP21)

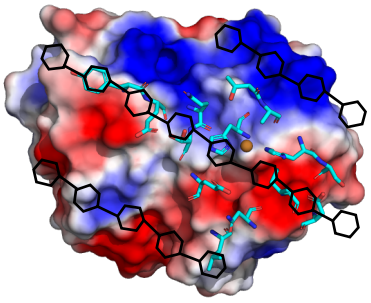

ScLPMO10D

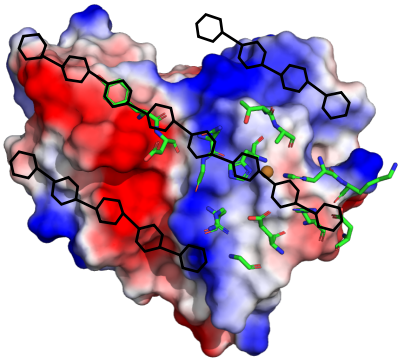

6. REFERENCES

AACHMANN, F. L., SØRLIE, M., SKJÅK-BRÆK, G., EIJSINK, V. G., & VAAJE-KOLSTAD, G. (2012). NMR structure of a lytic polysaccharide monooxygenase provides insight into copper binding, protein dynamics, and substrate interactions. *Proceedings of the National Academy of Sciences of the United States of America, 109*(46), 18779–18784. doi:10.1073/pnas.1208822109

AGGER, J. W., ISAKSEN, T., VÁRNAI, A., VIDAL-MELGOSA, S., WILLATS, W. G., LUDWIG, R., … WESTERENG, B. (2014). Discovery of LPMO activity on hemicelluloses shows the importance of oxidative processes in plant cell wall degradation. *Proceedings of the National Academy of Sciences of the United States of America, 111*(17), 6287–6292. doi:10.1073/pnas.1323629111

AGOSTONI, M., HANGASKY, J. A., & MARLETTA, M. A. (2017). Physiological and Molecular Understanding of Bacterial Polysaccharide Monooxygenases. *Microbiology and molecular biology reviews: MMBR, 81*(3), e00015-17. doi:10.1128/MMBR.00015-17

AGILENT TECHNOLOGIES. (2016). *QuikChange II Xl Site-Directed Mutagenesis Kit.* Available from: https://www.agilent.com/cs/library/usermanuals/public/200521.pdf

ALVIRA, P., BALLESTEROS, M., & NEGRO, M. J. (2013). Progress on Enzymatic Saccharification Technologies for Biofuels Production. In V. K. Gupta & M. G. Tuohy (Eds.), *Biofuel Technologies: Recent Developments,* 145-169. Berlin, Heidelberg: Springer Berlin Heidelberg. doi:10.1007/978-3-642-34519-7_6

ANITHA, A., SOWMYA, S., KUMAR, P. T. S., DEEPTHI, S., CHENNAZHI, K. P., EHRLICH, H., . . . JAYAKUMAR, R. (2014). Chitin and chitosan in selected biomedical applications. *Progress in Polymer Science, 39*(9), 1644-1667. doi:10.1016/j.progpolymsci.2014.02.008

ARMESILLA, A. L., THURSTON, C. F., & YAGÜE, E. (1994). CEL1: a novel cellulose binding protein secreted by Agaricus bisporus during growth on crystalline cellulose. *FEMS Microbiology Letters, 116*(3), 293-299. doi:10.1111/j.1574-6968.1994.tb06718.x

BALAN, V. (2014). Current challenges in commercially producing biofuels from lignocellulosic biomass. *ISRN Biotechnology, 2014*, 31. doi:10.1155/2014/463074

BAPTISTA, A., FERREIRA, I. & BORGES, J. (2013). Cellulose-Based Bioelectronic. In Van De Ven, T. G. M. (Ed), *Devices, Cellulose - Medical, Pharmaceutical and Electronic Applications*. doi: 10.5772/56721.

BANERJEE, G., CAR, S., SCOTT-CRAIG, J. S., BORRUSCH, M. S., & WALTON, J. D. (2010). Rapid optimization of enzyme mixtures for deconstruction of diverse pretreatment/biomass feedstock combinations. *Biotechnology for biofuels, 3*, 22. doi:10.1186/1754-6834-3-22

BARNES, D. K. A., GALGANI, F., THOMPSON, R. C., & BARLAZ, M. (2009). Accumulation and fragmentation of plastic debris in global environments. *Philosophical Transactions of the Royal Society B: Biological Sciences, 364*(1526), 1985-1998. doi:10.1098/rstb.2008.0205

BECKHAM, G. T., MATTHEWS, J. F., PETERS, B., BOMBLE, Y. J., HIMMEL, M. E., & CROWLEY, M. F. (2011). Molecular-Level Origins of Biomass Recalcitrance: Decrystallization Free Energies for Four Common Cellulose Polymorphs. *The Journal of Physical Chemistry B, 115*(14), 4118-4127. doi:10.1021/jp1106394

BECKHAM, G. T., STÅHLBERG, J., KNOTT, B. C., HIMMEL, M. E., CROWLEY, M. F., SANDGREN, M., . . . PAYNE, C. M. (2014). Towards a molecular-level theory of carbohydrate processivity in

glycoside hydrolases. *Current Opinion in Biotechnology, 27*, 96-106. doi:https://doi.org/10.1016/j.copbio.2013.12.002

BEESON, W. T., PHILLIPS, C. M., CATE, J. H. D., & MARLETTA, M. A. (2012). Oxidative Cleavage of Cellulose by Fungal Copper-Dependent Polysaccharide Monooxygenases. *Journal of the American Chemical Society, 134*(2), 890-892. doi:10.1021/ja210657t

BEESON, W. T., VU, V. V., SPAN, E. A., PHILLIPS, C. M., & MARLETTA, M. A. (2015). Cellulose Degradation by Polysaccharide Monooxygenases. *Annual Review of Biochemistry, 84*(1), 923-946. doi:10.1146/annurev-biochem-060614-034439

BENJAMIN, A. M., & TAMHANE, D. V. (1966). Observations on the formation of a pigment by strains of escherichia coli. *Archiv für Mikrobiologie, 53*(3), 242-247. doi:10.1007/bf00446670

BENKERT, P., BIASINI, M., & SCHWEDE, T. (2010). Toward the estimation of the absolute quality of individual protein structure models. *Bioinformatics, 27*(3), 343-350. doi:10.1093/bioinformatics/btq662

BERTRAN, M. S., & DALE, B. E. (1985). Enzymatic hydrolysis and recrystallization behavior of initially amorphous cellulose. *Biotechnology and Bioengineering, 27*(2), 177-181. doi:10.1002/bit.260270212

BHATNAGAR, A., & SILLANPÄÄ, M. (2009). Applications of chitin- and chitosan-derivatives for the detoxification of water and wastewater — A short review. *Advances in Colloid and Interface Science, 152*(1), 26-38. doi:10.1016/j.cis.2009.09.003

BISCHOF, R. H., RAMONI, J., & SEIBOTH, B. (2016). Cellulases and beyond: the first 70 years of the enzyme producer Trichoderma reesei. *Microbial cell factories, 15*(1), 106. doi:10.1186/s12934-016-0507-6

BISSARO, B., ISAKSEN, I., VAAJE-KOLSTAD, G., EIJSINK, V. G. H., & RØHR, Å. K. (2018a). How a Lytic Polysaccharide Monooxygenase Binds Crystalline Chitin. *Biochemistry, 57*(12), 1893-1906. doi:10.1021/acs.biochem.8b00138

BISSARO, B., RØHR, Å. K., MÜLLER, G., CHYLENSKI, P., SKAUGEN, M., FORSBERG, Z., . . . EIJSINK, V. G. H. (2017). Oxidative cleavage of polysaccharides by monocopper enzymes depends on H2O2. *Nature Chemical Biology, 13,* 1123. doi:10.1038/nchembio.2470

BISSARO, B., VÁRNAI, A., RØHR, Å. K., & EIJSINK, V. G. H. (2018b). Oxidoreductases and Reactive Oxygen Species in Conversion of Lignocellulosic Biomass. *Microbiology and Molecular Biology Reviews, 82*(4), e00029-00018. doi:10.1128/MMBR.00029-18

BJURSELL, M.K., MARTENS, E.C., GORDON, J.I. (2006). Functional genomic and metabolic studies of the adaptations of a prominent adult human gut symbiont, Bacteroides thetaiotaomicron, to the suckling period. *J Biol Chem, 281*(47), 36269-36279. doi:10.1074/jbc.M606509200

BOEKHORST, J., DE BEEN, M. W., KLEEREBEZEM, M., & SIEZEN, R. J. (2005). Genome-wide detection and analysis of cell wall-bound proteins with LPxTG-like sorting motifs. *Journal of bacteriology, 187*(14), 4928–4934. doi:10.1128/JB.187.14.4928-4934.2005

BOOK, A. J., YENNAMALLI, R. M., TAKASUKA, T. E., CURRIE, C. R., PHILLIPS, G. N., & FOX, B. G. (2014). Evolution of substrate specificity in bacterial AA10 lytic polysaccharide monooxygenases. *Biotechnology for Biofuels, 7*(1), 109. doi:10.1186/1754-6834-7-109

BRADFORD, M. M. (1976). A rapid and sensitive method for the quantitation of microgram quantities of protein utilizing the principle of protein-dye binding. *Analytical Biochemistry, 72*(1), 248-254. doi:10.1016/0003-2697(76)90527-3

BROWN JR., R. M. (2004). Cellulose structure and biosynthesis: What is in store for the 21st century? *Journal of Polymer Science Part A: Polymer Chemistry, 42(3)*, 487-495. doi:10.1002/pola.10877

BUSK, P. K., & LANGE, L. (2015). Classification of fungal and bacterial lytic polysaccharide monooxygenases. *BMC genomics, 16*(1), 368. doi:10.1186/s12864-015-1601-6

CANNELLA, D., MÖLLERS, K. B., FRIGAARD, N. U., JENSEN, P. E., BJERRUM, M. J., JOHANSEN, K. S., & FELBY, C. (2016). Light-driven oxidation of polysaccharides by photosynthetic pigments and a metalloenzyme. *Nature Communications, 7*, 11134. doi:10.1038/ncomms11134

CANTAREL, B. L., COUTINHO, P. M., RANCUREL, C., BERNARD, T., LOMBARD, V., & HENRISSAT, B. (2009). The Carbohydrate-Active EnZymes database (CAZy): an expert resource for Glycogenomics. *Nucleic acids research, 37*(Database issue), D233–D238. doi:10.1093/nar/gkn663

CARLSTRÖM, D. (1957). The crystal structure of α-chitin (poly-N-acetyl-D-glucosamine) *The Journal of Biophysical and Biochemical Cytology, 3*(5), 669-683. doi:10.1083/jcb.3.5.669

CAZy (CARBOHYDRATE ACTIVE ENZYMES) DATABASE. (2019a, 17/04) Auxiliary Activity Family 11. Retrieved from: http://www.cazy.org/AA11_bacteria.html

CAZy (CARBOHYDRATE ACTIVE ENZYMES) DATABASE. (2019b, 17/04) Auxiliary Activity Family 10. Retrieved from: http://www.cazy.org/AA10_archaea.html

CHAPLIN, A. K., WILSON, M. T., HOUGH, M. A., SVISTUNENKO, D. A., HEMSWORTH, G. R., WALTON, P. H., … WORRALL, J. A. (2016). Heterogeneity in the Histidine-brace Copper Coordination Sphere in Auxiliary Activity Family 10 (AA10) Lytic Polysaccharide Monooxygenases. *The Journal of biological chemistry, 291*(24), 12838–12850. doi:10.1074/jbc.M116.722447

CHARREZ, B., QIAO, L., & HEBBARD, L. (2015). *The role of fructose in metabolism and cancer,* (0). doi:10.1515/hmbci-2015-0009

CHIU, E., HIJNEN, M., BUNKER, R. D., BOUDES, M., RAJENDRAN, C., AIZEL, K., … COULIBALY, F. (2015). Structural basis for the enhancement of virulence by viral spindles and their in vivo crystallization. *Proceedings of the National Academy of Sciences of the United States of America, 112*(13), 3973–3978. doi:10.1073/pnas.1418798112

CHU, H. H., HOANG, V., HOFEMEISTER, J., & SCHREMPF, H. (2001). A Bacillus amyloliquefaciens ChbB protein binds β- and α-chitin and has homologues in related strains. *Microbiology, 147*(7), 1793-1803. doi:10.1099/00221287-147-7-1793

CHYLENSKI, P., BISSARO, B., SØRLIE, M., RØHR, Å. K., VÁRNAI, A., HORN, S. J., & EIJSINK, V. G. H. (2019). Lytic Polysaccharide Monooxygenases in Enzymatic Processing of Lignocellulosic Biomass. *ACS Catalysis, 9*(6), 4970-4991. doi:10.1021/acscatal.9b00246

CORRADINI, C., CAVAZZA, A., & BIGNARDI, C. (2012). High-Performance Anion-Exchange Chromatography Coupled with Pulsed Electrochemical Detection as a Powerful Tool to Evaluate Carbohydrates of Food Interest: Principles and Applications. *International Journal of Carbohydrate Chemistry, 2012*, 13. doi:10.1155/2012/487564

COURTADE, G., FORSBERG, Z., HEGGSET, E. B., EIJSINK, V., & AACHMANN, F. L. (2018). The carbohydrate-binding module and linker of a modular lytic polysaccharide monooxygenase promote localized cellulose oxidation. *The Journal of biological chemistry, 293*(34), 13006–13015. doi:10.1074/jbc.RA118.004269

COURTADE, G., WIMMER, R., RØHR, Å. K., PREIMS, M., FELICE, A. K. G., DIMAROGONA, M., . . . AACHMANN, F. L. (2016). Interactions of a fungal lytic polysaccharide monooxygenase with β-glucan substrates and cellobiose dehydrogenase. *Proceedings of the National Academy of Sciences, 113*(21), 5922. doi:10.1073/pnas.1602566113

COUTURIER, M., LADEVÈZE, S., SULZENBACHER, G., CIANO, L., FANUEL, M., MOREAU, C., . . . BERRIN, J.-G. (2018). Lytic xylan oxidases from wood-decay fungi unlock biomass degradation. *Nature Chemical Biology, 14*, 306. doi:10.1038/nchembio.2558

COX, K. D., COVERNTON, G. A., DAVIES, H. L., DOWER, J. F., JUANES, F., & DUDAS, S. E. (2019). Human Consumption of Microplastics. *Environmental Science & Technology, 53*(12), 7068-7074. doi:10.1021/acs.est.9b01517

DAVIES, G., & HENRISSAT, B. (1995). Structures and mechanisms of glycosyl hydrolases. *Structure, 3*(9), 853-859. doi:10.1016/S0969-2126(01)00220-9

DELANO, W. L., & LAM, J. W. (2005). PyMOL: A communications tool for computational models. *Abstracts of Papers of the American Chemical Society, 230*, 1371-1372.

DEPRISTO, M. A., ZILVERSMIT, M. M., & HARTL, D. L. (2006). On the abundance, amino acid composition, and evolutionary dynamics of low-complexity regions in proteins. *Gene, 378*, 19-30. doi:10.1016/j.gene.2006.03.023

DEVI, R., & DHAMODHARAN, R. (2018). Pretreatment in Hot Glycerol for Facile and Green Separation of Chitin from Prawn Shell Waste. *ACS Sustainable Chemistry & Engineering, 6*(1), 846-853. doi:10.1021/acssuschemeng.7b03195

EDGAR, ROBERT C. (2004), MUSCLE: multiple sequence alignment with high accuracy and high throughput*, Nucleic Acids Research 32*(5), 1792-1797.

EIJSINK, V., PETROVIC, D., FORSBERG, Z., MEKASHA, S., RØHR, Å. K., VÁRNAI, A., … VAAJE-KOLSTAD, G. (2019). On the functional characterization of lytic polysaccharide monooxygenases (LPMOs). *Biotechnology for biofuels, 12*, 58. doi:10.1186/s13068-019-1392-0

ELIEH-ALI-KOMI, D., & HAMBLIN, M. R. (2016). Chitin and Chitosan: Production and Application of Versatile Biomedical Nanomaterials. *International journal of advanced research, 4*(3), 411–427.

ERIKSSON, K.-E., PETTERSSON, B., & WESTERMARK, U. (1974). Oxidation: An important enzyme reaction in fungal degradation of cellulose. *FEBS Letters, 49*(2), 282-285. doi:10.1016/0014-5793(74)80531-4

FERNANDEZ-FUENTES, N., RAI, B. K., MADRID-ALISTE, C. J., EDUARDO FAJARDO, J., & FISER, A. (2007). Comparative protein structure modeling by combining multiple templates and optimizing sequence-to-structure alignments. *Bioinformatics, 23*(19), 2558-2565. Retrieved from https://doi.org/10.1093/bioinformatics/btm377. doi:10.1093/bioinformatics/btm377

FILIATRAULT-CHASTEL, C., NAVARRO, D., HAON, M., GRISEL, S., HERPOËL-GIMBERT, I., CHEVRET, D., . . . BERRIN, J.-G. (2019). AA16, a new lytic polysaccharide monooxygenase family identified in fungal secretomes. *Biotechnology for Biofuels, 12*(1), 55. doi:10.1186/s13068-019-1394-y

FOLDERS, J., TOMMASSEN, J., VAN LOON, L. C., & BITTER, W. (2000). Identification of a chitin-binding protein secreted by Pseudomonas aeruginosa. *Journal of bacteriology, 182*(5), 1257–1263.

FORSBERG, Z., BISSARO, B., GULLESEN, J., DALHUS, B., VAAJE-KOLSTAD, G., & EIJSINK, V. (2018). Structural determinants of bacterial lytic polysaccharide monooxygenase functionality. *The Journal of biological chemistry, 293*(4), 1397–1412. doi:10.1074/jbc.M117.817130

FORSBERG, Z., MACKENZIE, A. K., SØRLIE, M., RØHR, Å. K., HELLAND, R., ARVAI, A. S., … EIJSINK, V. G. (2014a). Structural and functional characterization of a conserved pair of bacterial cellulose-oxidizing lytic polysaccharide monooxygenases. *Proceedings of the National Academy of Sciences of the United States of America, 111*(23), 8446–8451. doi:10.1073/pnas.1402771111

FORSBERG, Z., NELSON, C. E., DALHUS, B., MEKASHA, S., LOOSE, J. S., CROUCH, L. I., … VAAJE-KOLSTAD, G. (2016). Structural and Functional Analysis of a Lytic Polysaccharide Monooxygenase Important for Efficient Utilization of Chitin in Cellvibrio japonicus. *The Journal of biological chemistry, 291*(14), 7300-7312. doi:10.1074/jbc.M115.700161

FORSBERG, Z., SØRLIE, M., PETROVIĆ, D., COURTADE, G., AACHMANN, F. L., VAAJE-KOLSTAD, G., . . . EIJSINK, V. G. H. (2019). Polysaccharide degradation by lytic polysaccharide monooxygenases. *Current Opinion in Structural Biology, 59*, 54-64. doi:https://doi.org/10.1016/j.sbi.2019.02.015

FORSBERG, Z., RØHR, Å. K., MEKASHA, S., ANDERSSON, K. K., EIJSINK, V. G. H., VAAJE-KOLSTAD, G., & SØRLIE, M. (2014b). Comparative Study of Two Chitin-Active and Two Cellulose-Active AA10-Type Lytic Polysaccharide Monooxygenases. *Biochemistry, 53*(10), 1647-1656. doi:10.1021/bi5000433

FORSBERG, Z., VAAJE-KOLSTAD, G., WESTERENG, B., BUNÆS, A. C., STENSTRØM, Y., MACKENZIE, A., … EIJSINK, V. G. (2011). Cleavage of cellulose by a CBM33 protein. *Protein science: a publication of the Protein Society, 20*(9), 1479–1483. doi:10.1002/pro.689

FRANCA, E. F., FREITAS, L. C. G., & LINS, R. D. (2011). Chitosan molecular structure as a function of N-acetylation. *Biopolymers, 95*(7), 448-460. doi:10.1002/bip.21602

FRANCA, E. F., LINS, R. D., FREITAS, L. C. G., & STRAATSMA, T. P. (2008). Characterization of Chitin and Chitosan Molecular Structure in Aqueous Solution. *Journal of Chemical Theory and Computation, 4*(12), 2141-2149. doi:10.1021/ct8002964

FRANDSEN, K. E., SIMMONS, T. J., DUPREE, P., POULSEN, J. C., HEMSWORTH, G. R., CIANO, L., … WALTON, P. H. (2016). The molecular basis of polysaccharide cleavage by lytic polysaccharide monooxygenases. *Nature chemical biology, 12*(4), 298–303. doi:10.1038/nchembio.2029

FROMMHAGEN, M., KOETSIER, M. J., WESTPHAL, A. H., VISSER, J., HINZ, S. W., VINCKEN, J. P., . . . GRUPPEN, H. (2016). Lytic polysaccharide monooxygenases from Myceliophthora thermophila C1 differ in substrate preference and reducing agent specificity. *Biotechnol Biofuels, 9*(1), 186. doi:10.1186/s13068-016-0594-y

FROMMHAGEN, M., SFORZA, S., WESTPHAL, A. H., VISSER, J., HINZ, S. W. A., KOETSIER, M. J., . . . KABEL, M. A. (2015). Discovery of the combined oxidative cleavage of plant xylan and cellulose by a new fungal polysaccharide monooxygenase. *Biotechnology for Biofuels, 8*(1), 101. doi:10.1186/s13068-015-0284-1

FROMMHAGEN, M., WESTPHAL, A. H., HILGERS, R., KOETSIER, M. J., HINZ, S., VISSER, J., … KABEL, M. A. (2018a). Quantification of the catalytic performance of C1-cellulose-specific lytic polysaccharide monooxygenases. *Applied microbiology and biotechnology, 102*(3), 1281–1295. doi:10.1007/s00253-017-8541-9

FROMMHAGEN, M., WESTPHAL, A. H., VAN BERKEL, W., & KABEL, M. A. (2018b). Distinct Substrate Specificities and Electron-Donating Systems of Fungal Lytic Polysaccharide Monooxygenases. *Frontiers in microbiology, 9*, 1080. doi:10.3389/fmicb.2018.01080

GASTEIGER, E. et al. (2005) Protein Identification and Analysis Tools on the ExPASy Server. In: Walker J.M. (eds) The Proteomics Protocols Handbook. Humana Press

GEYER, R., JAMBECK, J. R., & LAW, K. L. (2017). Production, use, and fate of all plastics ever made. *Science Advances, 3(7)*. doi:ARTN e1700782 10.1126/sciadv.1700782

GILBERT, R. D., & KADLA, J. F. (1998). Polysaccharides — Cellulose. In D. L. Kaplan (Ed.), *Biopolymers from Renewable Resources,* 47-95. Berlin, Heidelberg: Springer Berlin Heidelberg. doi:10.1007/978-3-662-03680-8_3

GOODAY, G. W. (1990). The ecology of chitin degradation. In K. C. Marshall (Ed.), *Advances in Microbial Ecology,* 387-340. New York: Plenum press. doi:10.1007/978-1-4684-7612-5_10

GOUFFI, K., PICA, N., PICHEREAU, V., & BLANCO, C. (1999). Disaccharides as a new class of nonaccumulated osmoprotectants for Sinorhizobium meliloti. *Applied and environmental microbiology*, 65(4), 1491–1500.

HANGASKY, J. A., DETOMASI, T. C., & MARLETTA, M. A. (2019). Glycosidic Bond Hydroxylation by Polysaccharide Monooxygenases. *Trends in Chemistry, 1*(2), 198-209. doi:10.1016/j.trechm.2019.01.007

HANGASKY, J. A., IAVARONE, A. T., & MARLETTA, M. A. (2018). Reactivity of O_2 versus H_2O_2 with polysaccharide monooxygenases. Proceedings of the National Academy of Sciences, 115(19), 4915. doi:10.1073/pnas.1801153115

HARISH PRASHANTH, K. V., & THARANATHAN, R. N. (2007). Chitin/chitosan: modifications and their unlimited application potential—an overview. *Trends in Food Science & Technology, 18*(3), 117-131. doi:https://doi.org/10.1016/j.tifs.2006.10.022

HARRIS, P. V., WELNER, D., MCFARLAND, K. C., RE, E., NAVARRO POULSEN, J.-C., BROWN, K., . . . LO LEGGIO, L. (2010). Stimulation of Lignocellulosic Biomass Hydrolysis by Proteins of Glycoside Hydrolase Family 61: Structure and Function of a Large, Enigmatic Family. *Biochemistry, 49*(15), 3305-3316. doi:10.1021/bi100009p

HEGNAR, O. A., PETROVIC, D. M., BISSARO, B., ALFREDSEN, G., VÁRNAI, A., & EIJSINK, V. (2019). pH-Dependent Relationship between Catalytic Activity and Hydrogen Peroxide Production Shown via Characterization of a Lytic Polysaccharide Monooxygenase from Gloeophyllum trabeum. *Applied and environmental microbiology, 85*(5), e02612-18. doi:10.1128/AEM.02612-18

HEIN, L., & LEEMANS, R. (2012). The impact of first-generation biofuels on the depletion of the global phosphorus reserve. *Ambio, 41*(4), 341–349. doi:10.1007/s13280-012-0253-x

HEMSWORTH, G. R., HENRISSAT, B., DAVIES, G. J., & WALTON, P. H. (2014). Discovery and characterization of a new family of lytic polysaccharide monooxygenases. *Nature chemical biology, 10*(2), 122–126. doi:10.1038/nchembio.1417

HEMSWORTH, G. R., TAYLOR, E. J., KIM, R. Q., GREGORY, R. C., LEWIS, S. J., TURKENBURG, J. P., … WALTON, P. H. (2013). The copper active site of CBM33 polysaccharide oxygenases. *Journal of the American Chemical Society, 135*(16), 6069–6077. doi:10.1021/ja402106e

HENRISSAT, B. (1991). A classification of glycosyl hydrolases based on amino acid sequence similarities. *The Biochemical journal, 280*(Pt 2)(Pt 2), 309–316. doi:10.1042/bj2800309

HON, D.N.S. (1994). Cellulose: a random walk along its historical path. *Cellulose, 1*, 1-25. doi:10.1007/BF00818796

HORN, S. J., VAAJE-KOLSTAD, G., WESTERENG, B., & EIJSINK, V. (2012). Novel enzymes for the degradation of cellulose. *Biotechnology for Biofuels, 5*(1), 45. doi:10.1186/1754-6834-5-45

HU, J., TIAN, D., RENNECKAR, S., & SADDLER, J. N. (2018). Enzyme mediated nanofibrillation of cellulose by the synergistic actions of an endoglucanase, lytic polysaccharide monooxygenase (LPMO) and xylanase. *Scientific reports, 8*(1), 3195. doi:10.1038/s41598-018-21016-6

ILLERGÅRD, K., ARDELL, D. H., & ELOFSSON, A. (2009). Structure is three to ten times more conserved than sequence—A study of structural response in protein cores. *Proteins: Structure, Function, and Bioinformatics, 77*(3), 499-508. doi:10.1002/prot.22458

INTERNATIONAL ENERGY AGENCY (2018). *Key world energy statistics.* Retrieved from: https://webstore.iea.org/download/direct/2291?fileName=Key_World_2018.pdf

ISAKSEN, T., WESTERENG, B., AACHMANN, F. L., AGGER, J. W., KRACHER, D., KITTL, R., … HORN, S. J. (2014). A C4-oxidizing lytic polysaccharide monooxygenase cleaving both cellulose and cello-oligosaccharides. *The Journal of biological chemistry, 289*(5), 2632–2642. doi:10.1074/jbc.M113.530196

JENSEN, M. S., KLINKENBERG, G., BISSARO, B., CHYLENSKI, P., VAAJE-KOLSTAD, G., KVITVANG, H. F., . . . EIJSINK, V. G. H. (2019). Engineering chitinolytic activity into a cellulose-active lytic polysaccharide monooxygenase provides insights into substrate specificity. *Journal of Biological Chemistry.* doi:10.1074/jbc.RA119.010056

KAMEDA, T., MIYAZAWA, M., ONO, H., & YOSHIDA, M. (2005). Hydrogen Bonding Structure and Stability of α-Chitin Studied by 13C Solid-State NMR. *Macromolecular Bioscience, 5*(2), 103-106. doi:10.1002/mabi.200400142

KARKEHABADI, S., HANSSON, H., KIM, S., PIENS, K., MITCHINSON, C., & SANDGREN, M. (2008). The First Structure of a Glycoside Hydrolase Family 61 Member, Cel61B from Hypocrea jecorina, at 1.6 Å Resolution. *Journal of Molecular Biology, 383*(1), 144-154. doi:https://doi.org/10.1016/j.jmb.2008.08.016

KARLSSON, J., SALOHEIMO, M., SIIKA-AHO, M., TENKANEN, M., PENTTILÄ, M., & TJERNELD, F. (2001). Homologous expression and characterization of Cel61A (EG IV) of Trichoderma reesei. *European Journal of Biochemistry, 268*(24), 6498-6507. doi:10.1046/j.0014-2956.2001.02605.x

KATO, S., HARUTA, S., CUI, Z. J., ISHII, M., & IGARASHI, Y. (2004). Effective cellulose degradation by a mixed-culture system composed of a cellulolytic Clostridium and aerobic non-cellulolytic bacteria. *FEMS Microbiology Ecology, 51*(1), 133-142. doi:10.1016/j.femsec.2004.07.015

KHATTAK, S., WAHID, F., LIU, L.-P., JIA, S.-R., CHU, L.-Q., XIE, Y.-Y., . . . ZHONG, C. (2019). Applications of cellulose and chitin/chitosan derivatives and composites as antibacterial materials: current state and perspectives. *Applied Microbiology and Biotechnology*, 103(5), 1989-2006. doi:10.1007/s00253-018-09602-0

KITTL, R., KRACHER, D., BURGSTALLER, D., HALTRICH, D., & LUDWIG, R. (2012). Production of four Neurospora crassa lytic polysaccharide monooxygenases in Pichia pastoris monitored by a fluorometric assay. *Biotechnology for biofuels, 5*(1), 79. doi:10.1186/1754-6834-5-79

KJAERGAARD, C. H., QAYYUM, M. F., WONG, S. D., XU, F., HEMSWORTH, G. R., WALTON, D. J., … SOLOMON, E. I. (2014). Spectroscopic and computational insight into the activation of O2 by the mononuclear Cu center in polysaccharide monooxygenases. *Proceedings of the National Academy of Sciences of the United States of America, 111*(24), 8797–8802. doi:10.1073/pnas.1408115111

KLINMAN, J. P. (2006) The copper-enzyme family of dopamine beta-monooxygenase and peptidylglycine alpha-hydroxylating monooxygenase: resolving the chemical pathway for substrate hydroxylation. *Journal of Biological Chemistry, 281*, 3013-3016. doi: 10.1074/jbc.R500011200

KOLBE, S., FISCHER, S., BECIREVIC, A., HINZ, P., & SCHREMPF, H. (1998). The Streptomyces reticuli α-chitin-binding protein CHB2 and its gene. *Microbiology, 144*(5), 1291-1297. doi:10.1099/00221287-144-5-1291

KRACHER, D., ANDLAR, M., FURTMÜLLER, P. G., & LUDWIG, R. (2018). Active-site copper reduction promotes substrate binding of fungal lytic polysaccharide monooxygenase and reduces stability. *The Journal of biological chemistry, 293*(5), 1676–1687. doi:10.1074/jbc.RA117.000109

KRACHER, D., SCHEIBLBRANDNER, S., FELICE, A. K. G., BRESLMAYR, E., PREIMS, M., LUDWICKA, K., . . . LUDWIG, R. (2016). Extracellular electron transfer systems fuel cellulose oxidative degradation. *Science, 352*(6289), 1098. doi:10.1126/science.aaf3165

KRAVANJA, G., PRIMOŽIČ, M., KNEZ, Ž., & LEITGEB, M. (2019). Chitosan-based (Nano)materials for Novel Biomedical Applications. *Molecules (Basel, Switzerland), 24*(10), 1960. doi:10.3390/molecules24101960

KURITA, K. (2001). Controlled functionalization of the polysaccharide chitin. *Progress in Polymer Science, 26*(9), 1921-1971. doi:10.1016/S0079-6700(01)00007-7

KUUSK, S., BISSARO, B., KUUSK, P., FORSBERG, Z., EIJSINK, V., SØRLIE, M., & VÄLJAMÄE, P. (2018). Kinetics of H2O2-driven degradation of chitin by a bacterial lytic polysaccharide monooxygenase. *The Journal of biological chemistry, 293*(2), 523–531. doi:10.1074/jbc.M117.817593

LAEMMLI, U. K. (1970). "Cleavage of Structural Proteins during the Assembly of the Head of Bacteriophage T4". *Nature. 227* (5259): 680–685. doi:10.1038/227680a0

LANGSTON, J. A., SHAGHASI, T., ABBATE, E., XU, F., VLASENKO, E., & SWEENEY, M. D. (2011). Oxidoreductive cellulose depolymerization by the enzymes cellobiose dehydrogenase and glycoside hydrolase 61. *Applied and environmental microbiology, 77*(19), 7007–7015. doi:10.1128/AEM.05815-11

LAVALL, R. L., ASSIS, O. B. G., & CAMPANA-FILHO, S. P. (2007). β-Chitin from the pens of Loligo sp.: Extraction and characterization. *Bioresource Technology, 98*(13), 2465-2472. doi:https://doi.org/10.1016/j.biortech.2006.09.002

LESCHINE, S.B. (1995). Cellulose degradation in anaerobic environments. *Annual Review of Microbiology*. 49 (1). pp. 399–426

LEVASSEUR, A., DRULA, E., LOMBARD, V., COUTINHO, P. M., & HENRISSAT, B. (2013). Expansion of the enzymatic repertoire of the CAZy database to integrate auxiliary redox enzymes. *Biotechnology for biofuels, 6*(1), 41. doi:10.1186/1754-6834-6-41

LI, X., BEESON, W. T., 4TH, PHILLIPS, C. M., MARLETTA, M. A., & CATE, J. H. (2012). Structural basis for substrate targeting and catalysis by fungal polysaccharide monooxygenases. *Structure, 20*(6), 1051–1061. doi:10.1016/j.str.2012.04.002

LO LEGGIO, L., SIMMONS, T. J., POULSEN, J.-C. N., FRANDSEN, K. E. H., HEMSWORTH, G. R., STRINGER, M. A., . . . WALTON, P. H. (2015). Structure and boosting activity of a starch-degrading lytic polysaccharide monooxygenase. *Nature Communications, 6*, 5961. doi:10.1038/ncomms6961

LOMBARD, V., GOLACONDA RAMULU, H., DRULA, E., COUTINHO, P. M., & HENRISSAT, B. (2013). The carbohydrate-active enzymes database (CAZy) in 2013. *Nucleic acids research, 42*(Database issue), D490–D495. doi:10.1093/nar/gkt1178

LOOSE, J. S. M., ARNTZEN, M. Ø., BISSARO, B., LUDWIG, R., EIJSINK, V. G. H., & VAAJE-KOLSTAD, G. (2018). Multipoint Precision Binding of Substrate Protects Lytic Polysaccharide Monooxygenases from Self-Destructive Off-Pathway Processes. *Biochemistry, 57*(28), 4114-4124. doi:10.1021/acs.biochem.8b00484

LOOSE, J. S. M., FORSBERG, Z., FRAAIJE, M. W., EIJSINK, V. G. H., & VAAJE-KOLSTAD, G. (2014). A rapid quantitative activity assay shows that the Vibrio cholerae colonization factor GbpA is an active lytic polysaccharide monooxygenase. *FEBS Letters, 588*(18), 3435-3440. doi:10.1016/j.febslet.2014.07.036

LOOSE, J. S., FORSBERG, Z., KRACHER, D., SCHEIBLBRANDNER, S., LUDWIG, R., EIJSINK, V. G., & VAAJE-KOLSTAD, G. (2016). Activation of bacterial lytic polysaccharide monooxygenases with cellobiose dehydrogenase. *Protein science: a publication of the Protein Society, 25*(12), 2175–2186. doi:10.1002/pro.3043

MARRAFFINI, L. A., DEDENT, A. C., & SCHNEEWIND, O. (2006). Sortases and the art of anchoring proteins to the envelopes of gram-positive bacteria. *Microbiology and molecular biology reviews: MMBR, 70*(1), 192–221. doi:10.1128/MMBR.70.1.192-221.2006

LYND, L. R., WEIMER, P. J., VAN ZYL, W. H., & PRETORIUS, I. S. (2002). Microbial cellulose utilization: fundamentals and biotechnology. *Microbiology and molecular biology reviews : MMBR, 66*(3), 506–577. doi:10.1128/MMBR.66.3.506-577.2002

MARTENS, E. C., CHIANG, H. C., & GORDON, J. I. (2008). Mucosal glycan foraging enhances fitness and transmission of a saccharolytic human gut bacterial symbiont. *Cell host & microbe, 4*(5), 447–457. doi:10.1016/j.chom.2008.09.007

MAZMANIAN, S. K., LIU, G., TON-THAT, H., & SCHNEEWIND, O. (1999). Staphylococcus aureus sortase, an enzyme that anchors surface proteins to the cell wall. Science (New York, N.Y.), 285(5428), 760-763. doi:10.1126/science.285.5428.760

MEIER, K. K., JONES, S. M., KAPER, T., HANSSON, H., KOETSIER, M. J., KARKEHABADI, S., … KELEMEN, B. (2018). Oxygen Activation by Cu LPMOs in Recalcitrant Carbohydrate Polysaccharide Conversion to Monomer Sugars. *Chemical reviews, 118*(5), 2593–2635. doi:10.1021/acs.chemrev.7b00421

MENG, F., & KURGAN, L. (2016). DFLpred: High-throughput prediction of disordered flexible linker regions in protein sequences. *Bioinformatics (Oxford, England), 32*(12), i341–i350. doi:10.1093/bioinformatics/btw280

MILLER, C. G., STRAUCH, K. L., KUKRAL, A. M., MILLER, J. L., WINGFIELD, P. T., MAZZEI, G. J., . . . MOVVA, N. R. (1987). N-terminal methionine-specific peptidase in Salmonella typhimurium. *Proc Natl Acad Sci U S A, 84*(9), 2718-2722. doi:10.1073/pnas.84.9.2718

MINKE, R., & BLACKWELL, J. (1978). The structure of α-chitin. *Journal of Molecular Biology, 120*(2), 167-181. doi:10.1016/0022-2836(78)90063-3

MOREAU, C., TAPIN-LINGUA, S., GRISEL, S., GIMBERT, I., LE GALL, S., MEYER, V., . . . VILLARES, A. (2019). Lytic polysaccharide monooxygenases (LPMOs) facilitate cellulose nanofibrils production. *Biotechnology for Biofuels, 12*(1), 156. doi:10.1186/s13068-019-1501-0

MÜLLER, G., CHYLENSKI, P., BISSARO, B., EIJSINK, V. G. H., & HORN, S. J. (2018). The impact of hydrogen peroxide supply on LPMO activity and overall saccharification efficiency of a commercial cellulase cocktail. Biotechnology for Biofuels, 11(1), 209. doi:10.1186/s13068-018-1199-4

MÜLLER, G., VÁRNAI, A., JOHANSEN, K. S., EIJSINK, V. G. H., & HORN, S. J. (2015). Harnessing the potential of LPMO-containing cellulase cocktails poses new demands on processing conditions. *Biotechnology for Biofuels, 8*(1), 187. doi:10.1186/s13068-015-0376-y

NEU, H. C., & HEPPEL, L. A. (1965). The release of enzymes from Escherichia coli by osmotic shock and during the formation of spheroplasts. *The Journal of biological chemistry, 240*(9), 3685-3692. Retrieved from: http://europepmc.org/abstract/MED/4284300.

NISHIYAMA, Y., LANGAN, P., & CHANZY, H. (2002). Crystal Structure and Hydrogen-Bonding System in Cellulose Iβ from Synchrotron X-ray and Neutron Fiber Diffraction. *Journal of the American Chemical Society, 124*(31), 9074-9082. doi:10.1021/ja0257319

NISHIYAMA, Y., SUGIYAMA, J., CHANZY, H., & LANGAN, P. (2003). Crystal Structure and Hydrogen Bonding System in Cellulose Iα from Synchrotron X-ray and Neutron Fiber Diffraction. *Journal of the American Chemical Society, 125*(47), 14300-14306. doi:10.1021/ja037055w

O'SULLIVAN, A. C. (1997). Cellulose: the structure slowly unravels. *Cellulose, 4*(3), 173-207. doi:10.1023/a:1018431705579

PARK, Y. B., KAFLE, K., LEE, C. M., COSGROVE, D. J., & KIM, S. H. (2015). Does cellulose II exist in native alga cell walls? Cellulose structure of Derbesia cell walls studied with SFG, IR and XRD. *Cellulose, 22*(6), 3531-3540. doi:10.1007/s10570-015-0750-8

PASPALIARI, D. K., LOOSE, J. S. M., LARSEN, M. H., & VAAJE-KOLSTAD, G. (2015). Listeria monocytogenes has a functional chitinolytic system and an active lytic polysaccharide monooxygenase. *The FEBS Journal, 282*(5), 921-936. doi:10.1111/febs.13191

PAYNE, C. M., BABAN, J., HORN, S. J., BACKE, P. H., ARVAI, A. S., DALHUS, B., … VAAJE-KOLSTAD, G. (2012). Hallmarks of processivity in glycoside hydrolases from crystallographic and computational studies of the Serratia marcescens chitinases. *The Journal of biological chemistry, 287*(43), 36322–36330. doi:10.1074/jbc.M112.402149

PERERA, F. (2017). Pollution from Fossil-Fuel Combustion is the Leading Environmental Threat to Global Pediatric Health and Equity: Solutions Exist. *International journal of environmental research and public health, 15*(1), 16. doi:10.3390/ijerph15010016

PETROVIĆ, D. M., BISSARO, B., CHYLENSKI, P., SKAUGEN, M., SØRLIE, M., JENSEN, M. S., … EIJSINK, V. (2018). Methylation of the N-terminal histidine protects a lytic polysaccharide monooxygenase from auto-oxidative inactivation. *Protein science: a publication of the Protein Society, 27*(9), 1636–1650. doi:10.1002/pro.3451

PHILLIPS, C. M., BEESON, W. T., CATE, J. H., & MARLETTA, M. A. (2011). Cellobiose Dehydrogenase and a Copper-Dependent Polysaccharide Monooxygenase Potentiate Cellulose Degradation by Neurospora crassa. *ACS Chemical Biology, 6*(12), 1399-1406. doi:10.1021/cb200351y

POLGE, C., SMITH, A. U., & PARKES, A. S. (1949). Revival of Spermatozoa after Vitrification and Dehydration at Low Temperatures. *Nature, 164(*4172), 666-666. doi:10.1038/164666a0

QUINLAN, R. J., SWEENEY, M. D., LO LEGGIO, L., OTTEN, H., POULSEN, J. C., JOHANSEN, K. S., … WALTON, P. H. (2011). Insights into the oxidative degradation of cellulose by a copper metalloenzyme that exploits biomass components. *Proceedings of the National Academy of Sciences of the United States of America, 108*(37), 15079–15084. doi:10.1073/pnas.1105776108

RAABE, D., SACHS, C., & ROMANO, P. (2005). The crustacean exoskeleton as an example of a structurally and mechanically graded biological nanocomposite material. *Acta Materialia, 53*(15), 4281-4292. doi:10.1016/j.actamat.2005.05.027

RAGUZ, S., YAGUEA, E., WOOD, D. A., & THURSTON, C. F. (1992). Isolation and characterization of a cellulose-growth-specific gene from Agaricus bisporus. *Gene, 119*(2), 183-190. doi:10.1016/0378-1119(92)90270-Y

REESE, E. T., SIU, R. G., & LEVINSON, H. S. (1950). The biological degradation of soluble cellulose derivatives and its relationship to the mechanism of cellulose hydrolysis. *Journal of bacteriology, 59*(4), 485–497.

REGUERA, G., & LESCHINE, S. B. (2001). Chitin degradation by cellulolytic anaerobes and facultative aerobes from soils and sediments. *FEMS Microbiology Letters, 204*(2), 367-374. doi:10.1111/j.1574-6968.2001.tb10912.x

RINAUDO, M. (2006). Chitin and chitosan: Properties and applications. *Progress in Polymer Science, 31*(7), 603-632. doi:https://doi.org/10.1016/j.progpolymsci.2006.06.001

ROBERTS, G. A. F. (1992). *Chitin Chemistry,* (1). Palgrave, London. doi:10.1007/978-1-349-11545-7

ROHRER, J. S., THAYER, J., WEITZHANDLER, M., & AVDALOVIC, N. (1998). Analysis of the N-acetylneuraminic acid and N-glycolylneuraminic acid contents of glycoproteins by high-pH anion-exchange chromatography with pulsed amperometric detection (HPAEC/PAD). *Glycobiology, 8*(1), 35-43. doi:10.1093/glycob/8.1.35

RULLI, M. C., BELLOMI, D., CAZZOLI, A., DE CAROLIS, G., & D'ODORICO, P. (2016). The water-land-food nexus of first-generation biofuels. *Scientific Reports, 6*, 22521. doi:10.1038/srep22521

SABBADIN, F., HEMSWORTH, G. R., CIANO, L., HENRISSAT, B., DUPREE, P., TRYFONA, T., . . . MCQUEEN-MASON, S. J. (2018). An ancient family of lytic polysaccharide monooxygenases with roles in arthropod development and biomass digestion. *Nature Communications, 9*(1), 756. doi:10.1038/s41467-018-03142-x

SAGNÉ, C., ISAMBERT, M. F., HENRY, J. P., & GASNIER, B. (1996). SDS-resistant aggregation of membrane proteins: application to the purification of the vesicular monoamine transporter. *The Biochemical journal, 316* (Pt 3)(Pt 3), 825–831. doi:10.1042/bj3160825

SAINI, A., AGGARWAL, N. K., SHARMA, A., & YADAV, A. (2015). Actinomycetes: A Source of Lignocellulolytic Enzymes. *Enzyme research, 2015*, 279381. doi:10.1155/2015/279381

SAITO, Y., OKANO, T., GAILL, F., CHANZY, H., & PUTAUX, J.-L. (2000). Structural data on the intra-crystalline swelling of β-chitin. *International Journal of Biological Macromolecules, 28*(1), 81-88. doi:https://doi.org/10.1016/S0141-8130(00)00147-1

SALOHEIMO, M., NAKARI-SETÄLÄ, T., TENKANEN, M., & PENTTILÄ, M. (1997). cDNA Cloning of a Trichoderma reesei Cellulase and Demonstration of Endoglucanase Activity by Expression in Yeast. *European Journal of Biochemistry, 249*(2), 584-591. doi:10.1111/j.1432-1033.1997.00584.x

SARKO, A., SOUTHWICK, J., & HAYASHI, J. (1976). Packing Analysis of Carbohydrates and Polysaccharides. 7. Crystal Structure of Cellulose IIII and Its Relationship to Other Cellulose Polymorphs. *Macromolecules, 9*(5), 857-863. doi:10.1021/ma60053a028

SCHNELLMANN, J., ZELTINS, A., BLAAK, H., & SCHREMPF, H. (1994). The novel lectin-like protein CHB1 is encoded by a chitin-inducible Streptomyces olivaceoviridis gene and binds specifically to crystalline α-chitin of fungi and other organisms. *Molecular Microbiology, 13*(5), 807-819. doi:10.1111/j.1365-2958.1994.tb00473.x

SCHREMPF, H. (1999). Characteristics of chitin-binding proteins from Streptomycetes. *EXS, 87*, 99-108.

SCHWARZ, W. (2001). The cellulosome and cellulose degradation by anaerobic bacteria. *Applied Microbiology and Biotechnology, 56*(5), 634-649. doi:10.1007/s002530100710

SCOTT, B. R., HUANG, H. Z., FRICKMAN, J., HALVORSEN, R., & JOHANSEN, K. S. (2016). Catalase improves saccharification of lignocellulose by reducing lytic polysaccharide monooxygenase-associated enzyme inactivation. *Biotechnology letters, 38*(3), 425–434. doi:10.1007/s10529-015-1989-8

SHARP, R. G. (2013). A Review of the Applications of Chitin and Its Derivatives in Agriculture to Modify Plant-Microbial Interactions and Improve Crop Yields. *Agronomy, 3*(4), 757-793. doi:10.3390/agronomy3040757

SHEN, T., & GNANAKARAN, S. (2009). The stability of cellulose: a statistical perspective from a coarse-grained model of hydrogen-bond networks. *Biophys J, 96*(8), 3032-3040. doi:10.1016/j.bpj.2008.12.3953

SOLOMON, B. D. (2010). Biofuels and sustainability. *Annals of the New York Academy of Sciences, 1185*(1), 119-134. doi:10.1111/j.1749-6632.2009.05279.x

SOLOMON, E. I., GINSBACH, J. W., HEPPNER, D. E., KIEBER-EMMONS, M. T., KJAERGAARD, C. H., SMEETS, P. J., … WOERTINK, J. S. (2011). Copper dioxygen (bio)inorganic chemistry. *Faraday discussions, 148*, 11–108. doi:10.1039/C005500J

SOLOMON, E. I., HEPPNER, D. E., JOHNSTON, E. M., GINSBACH, J. W., CIRERA, J., QAYYUM, M., … TIAN, L. (2014). Copper active sites in biology. *Chemical reviews, 114*(7), 3659–3853. doi:10.1021/cr400327t

STANTON, P. (2004). Ion-Exchange Chromatography. In M.-I. Aguilar (Ed.), *HPLC of Peptides and Proteins: Methods and Protocols*, 23-43. Totowa, NJ: Springer New York.

SUZUKI, K., SUZUKI, M., TAIYOJI, M., NIKAIDOU, N., & WATANABE, T. (1998). Chitin Binding Protein (CBP21) in the Culture Supernatant of Serratia marcescens 2170. *Bioscience, Biotechnology, and Biochemistry, 62*(1), 128-135. doi:10.1271/bbb.62.128

SWIONTEK BRZEZINSKA, M., JANKIEWICZ, U., BURKOWSKA, A., & WALCZAK, M. (2013). Chitinolytic microorganisms and their possible application in environmental protection. *Current microbiology, 68*(1), 71–81. doi:10.1007/s00284-013-0440-4

TANGHIN, M., DANNEELS, B., LAST, M., BEERENS, K., STALS, I., & DESMET, T. (2017). Disulfide bridges as essential elements for the thermostability of lytic polysaccharide monooxygenase LPMO10C from Streptomyces coelicolor. *Protein Engineering, Design and Selection, 30*(5), 401-408. doi:10.1093/protein/gzx014

TAKASUKA, T. E., BOOK, A. J., LEWIN, G. R., CURRIE, C. R., & FOX, B. G. (2013). Aerobic deconstruction of cellulosic biomass by an insect-associated Streptomyces. *Scientific Reports, 3,* 1030. doi:10.1038/srep01030

TERMINOLOGY OF BIOANALYTICAL METHODS (IUPAC Recommendations 2018). (2018). In *Chemistry International 40*, 34. doi:10.1515/ci-2018-0319

THERMO FISHER SCIENTIFIC. 2017. Invitrogen™ pRSET A, B and C - For high-level expression of recombinant proteins in E.coli. Cat. no. V351-20. Available from: https://tools.thermofisher.com/content/sfs/manuals/prset_man.pdf

TORATANI, T., SHOJI, T., IKEHARA, T., SUZUKI, K., & WATANABE, T. (2008). The importance of chitobiase and N-acetylglucosamine (GlcNAc) uptake in N,N′-diacetylchitobiose [(GlcNAc)2] utilization by Serratia marcescens 2170. *Microbiology, 154*(5), 1326-1332. doi:10.1099/mic.0.2007/016246-0

TORRES PAZMIÑO, D. E., WINKLER, M., GLIEDER, A., & FRAAIJE, M. W. (2010). Monooxygenases as biocatalysts: Classification, mechanistic aspects and biotechnological applications. *Journal of Biotechnology, 146*(1), 9-24. doi:https://doi.org/10.1016/j.jbiotec.2010.01.021

VAAJE-KOLSTAD, G., BØHLE, L. A., GÅSEIDNES, S., DALHUS, B., BJØRÅS, M., MATHIESEN, G., & EIJSINK, V. G. H. (2012). Characterization of the Chitinolytic Machinery of Enterococcus faecalis V583 and High-Resolution Structure of Its Oxidative CBM33 Enzyme. *Journal of Molecular Biology, 416*(2), 239-254. doi:https://doi.org/10.1016/j.jmb.2011.12.033

VAAJE-KOLSTAD, G., FORSBERG, Z., LOOSE, J. S. M., BISSARO, B., & EIJSINK, V. G. H. (2017). Structural diversity of lytic polysaccharide monooxygenases. *Current Opinion in Structural Biology, 44*, 67-76. doi:https://doi.org/10.1016/j.sbi.2016.12.012

VAAJE-KOLSTAD, G., HORN, S. J., SØRLIE, M., & EIJSINK, V. G. H. (2013). The chitinolytic machinery of Serratia marcescens – a model system for enzymatic degradation of recalcitrant polysaccharides. *The FEBS Journal, 280*(13), 3028-3049. doi:10.1111/febs.12181

VAAJE-KOLSTAD, G., HORN, S. J., VAN AALTEN, D. M. F., SYNSTAD, B., & EIJSINK, V. G. H. (2005b). The Non-catalytic Chitin-binding Protein CBP21 from Serratia marcescens Is Essential for Chitin Degradation. *Journal of Biological Chemistry, 280*(31), 28492-28497. doi:10.1074/jbc.M504468200

VAAJE-KOLSTAD, G., HOUSTON, D. R., RIEMEN, A. H. K., EIJSINK, V. G. H., & VAN AALTEN, D. M. F. (2005a). Crystal Structure and Binding Properties of the Serratia marcescens Chitin-binding Protein CBP21. *Journal of Biological Chemistry, 280*(12), 11313-11319. doi:10.1074/jbc.M407175200

VAAJE-KOLSTAD, G., WESTERENG, B., HORN, S. J., LIU, Z., ZHAI, H., SØRLIE, M., & EIJSINK, V. G. H. (2010). An Oxidative Enzyme Boosting the Enzymatic Conversion of Recalcitrant Polysaccharides. *Science, 330*(6001), 219-222. doi:10.1126/science.1192231

VANDERHART, D. L., & ATALLA, R. H. (1984). Studies of microstructure in native celluloses using solid-state carbon-13 NMR. *Macromolecules, 17*(8), 1465-1472. doi:10.1021/ma00138a009

VANHOLME, B., DESMET, T., RONSSE, F., RABAEY, K., VAN BREUSEGEM, F., DE MEY, M., SOETAERT, W. & BOERJAN, W. (2013). Towards a carbon-negative sustainable bio-based economy. *Frontiers in Plant Scienceant science. 4*(174). doi:10.3389/fpls.2013.00174

VÁRNAI, A., SIIKA-AHO, M., & VIIKARI, L. (2013). Carbohydrate-binding modules (CBMs) revisited: reduced amount of water counterbalances the need for CBMs. *Biotechnology for Biofuels, 6*(1), 30. doi:10.1186/1754-6834-6-30

VENTURA, M., CANCHAYA, C., TAUCH, A., CHANDRA, G., FITZGERALD, G. F., CHATER, K. F., & VAN SINDEREN, D. (2007). Genomics of Actinobacteria: tracing the evolutionary history of an ancient phylum. *Microbiology and molecular biology reviews: MMBR, 71*(3), 495–548. doi:10.1128/MMBR.00005-07

VOSHOL, G. P., VIJGENBOOM, E., & PUNT, P. J. (2017). The discovery of novel LPMO families with a new Hidden Markov model. *BMC research notes, 10*(1), 105. doi:10.1186/s13104-017-2429-8

VU, V. V., BEESON, W. T., PHILLIPS, C. M., CATE, J. H. D., & MARLETTA, M. A. (2014). Determinants of Regioselective Hydroxylation in the Fungal Polysaccharide Monooxygenases. *Journal of the American Chemical Society, 136*(2), 562-565. doi:10.1021/ja409384b

WADA, M., CHANZY, H., NISHIYAMA, Y., & LANGAN, P. (2004). Cellulose IIII Crystal Structure and Hydrogen Bonding by Synchrotron X-ray and Neutron Fiber Diffraction. *Macromolecules, 37*(23), 8548-8555. doi:10.1021/ma0485585

WAGNER, A., LACKNER, N., MUTSCHLECHNER, M., PREM, E., MARKT, R., & ILLMER, P. (2018). Biological Pretreatment Strategies for Second-Generation Lignocellulosic Resources to Enhance Biogas Production. *Energies, 11*(7), 1797. doi:10.3390/en11071797

WALTON, P. H., & DAVIES, G. J. (2016). On the catalytic mechanisms of lytic polysaccharide monooxygenases. *Current Opinion in Chemical Biology, 31*, 195-207. doi:10.1016/j.cbpa.2016.04.001

WANG B, JOHNSTON EM, LI P, SHAIK S, DAVIES GJ, WALTON PH, ROVIRA C. (2018). QM/MM studies into the H2O2-dependent activity of lytic polysaccharide monooxygenases: evidence for the formation of a caged hydroxyl radical intermediate. *ACS Catal 8*, 1346–1351. doi:10.1021/acscatal.7b03888.

WATANABE, T., KIMURA, K., SUMIYA, T., NIKAIDOU, N., SUZUKI, K., SUZUKI, M., … REGUE, M. (1997). Genetic analysis of the chitinase system of Serratia marcescens 2170. *Journal of bacteriology, 179*(22), 7111-7117.

WATERHOUSE, A., BERTONI, M., BIENERT, S., STUDER, G., TAURIELLO, G., GUMIENNY, R., . . . SCHWEDE, T. (2018). SWISS-MODEL: homology modelling of protein structures and complexes. *Nucleic Acids Research, 46*(W1), W296-W303. doi:10.1093/nar/gky427

WESTERENG, B., ARNTZEN, M. Ø., AGGER, J. W., VAAJE-KOLSTAD, G., & EIJSINK, V. G. H. (2017). Analyzing Activities of Lytic Polysaccharide Monooxygenases by Liquid Chromatography and Mass Spectrometry. In D. W. Abbott & A. Lammerts van Bueren (Eds.), *Protein-Carbohydrate Interactions: Methods and Protocols*, 71-92. New York, NY: Springer New York.

WESTERENG, B., CANNELLA, D., WITTRUP AGGER, J., JØRGENSEN, H., LARSEN ANDERSEN, M., EIJSINK, V. G., & FELBY, C. (2015). Enzymatic cellulose oxidation is linked to lignin by long-range electron transfer. *Scientific reports, 5*, 18561. doi:10.1038/srep18561

WESTERENG, B., ISHIDA, T., VAAJE-KOLSTAD, G., WU, M., EIJSINK, V. G., IGARASHI, K., … SANDGREN, M. (2011). The putative endoglucanase PcGH61D from Phanerochaete chrysosporium is a metal-dependent oxidative enzyme that cleaves cellulose. *PloS one, 6*(11), e27807. doi:10.1371/journal.pone.0027807

WESTERENG, B., LOOSE, J. S. M., VAAJE-KOLSTAD, G., AACHMANN, F. L., SØRLIE, M., & EIJSINK, V. G. H. (2018). Analytical Tools for Characterizing Cellulose-Active Lytic Polysaccharide Monooxygenases (LPMOs). In M. Lübeck (Ed.), *Cellulases: Methods and Protocols,* 219-246. New York, NY: Springer New York. doi:10.1007/978-1-4939-7877-9_16

WILKE, M. S., LOVERING, A. L., & STRYNADKA, N. C. J. (2005). β-Lactam antibiotic resistance: a current structural perspective. *Current Opinion in Microbiology, 8*(5), 525-533. doi:https://doi.org/10.1016/j.mib.2005.08.016

WOLFENDEN, R., LU, X., & YOUNG, G. (1998). Spontaneous Hydrolysis of Glycosides. *Journal of the American Chemical Society, 120*(27), 6814-6815. doi:10.1021/ja9813055

WOOD, T. M. (1988). Preparation of crystalline, amorphous, and dyed cellulase substrates. *Methods in Enzymology, 160*, 19-25. doi:10.1016/0076-6879(88)60103-0

WOOD, T. M., & GARCIA-CAMPAYO, V. (1990). Enzymology of cellulose degradation. *Biodegradation, 1*(2), 147-161. doi:10.1007/bf00058833

WU, M., BECKHAM, G. T., LARSSON, A. M., ISHIDA, T., KIM, S., PAYNE, C. M., … SANDGREN, M. (2013). Crystal structure and computational characterization of the lytic polysaccharide monooxygenase GH61D from the Basidiomycota fungus Phanerochaete chrysosporium. *The Journal of biological chemistry, 288*(18), 12828–12839. doi:10.1074/jbc.M113.459396

YADAV, S. K., ARCHANA, SINGH, R., SINGH, P. K., & VASUDEV, P. G. (2019). Insecticidal fern protein Tma12 is possibly a lytic polysaccharide monooxygenase. *Planta, 249*(6), 1987-1996. doi:10.1007/s00425-019-03135-0

YOUNES, I., & RINAUDO, M. (2015). Chitin and chitosan preparation from marine sources. Structure, properties and applications. *Marine drugs, 13*(3), 1133–1174. doi:10.3390/md13031133

ZELTINS, A., & SCHREMPP, H. (1997). Specific Interaction of the Streptomyces Chitin-Binding Protein Chb1 with α-Chitin. *European Journal of Biochemistry, 246*(2), 557-564. doi:10.1111/j.1432-1033.1997.t01-1-00557.x

7. Appendices

Appendix A

The provided gene encoding the catalytic N-terminal domain of *Sc*LPMO10D had beforehand been optimized for expression in *E. coli* (Fig. A.1). A sequence derived from CBP21 encoding a signal peptide had also been added to the sequence, to ensure that the protein would be transported to the periplasm. The resulting amino acid sequence is displayed in Fig. A.2

```
ATGCCGGCGCCGAGCGCGAGCCGTCGTGCGGCGGCGGTGGCGGTTGCGGGCCTGGCGCCGCTGGCGCTGACCACC
CTGGCTGCGGCGCCGGCGAGCGCGCACGGTAGCATGGGCGACCCGGTGAGCCGTGTTAGCCAGTGCCACGCGGAG
GGTCCGGAAAACCCGAAGAGCGCGGCGTGCCGTGCGGCGGTGGCGGCGGGTGGCACCCAGGCGCTGTACGATTGG
AACGGTATCCGTATTGGCAACGCGGCGGGTAAACACCAAGAGCTGATTCCGGATGGCCGTCTGTGCAGCGCGAAC
GATCCGGCGTTCAAAGGTCTGGACCTGGCGCGTGCGGATTGGCCGGCGACCGGCGTTAGCAGCGGTAGCTACACC
TTCAAGTATCGTGTGACCGCGCCGCACAAGGGCACCTTTAAAGTTTACCTGACCAAGCCGGGTTATGACCCGAGC
AAACCGCTGGGTTGGGGCGACCTGGATCTGAGCGCGCCGGTTGCGACCAGCACCGATCCGGTTGCGAGCGGTGGC
TTCTATACCTTTAGCGGCACCCTGCCGGAGCGTAGCGGTAAACACCTGCTGTACGCGGTGTGGCAACGTAGCGAC
AGCCCGGAAGCGTTCTATAGCTGTAGCGATGTTACCTTTGGTTAA
```

Figure A.1. Optimized DNA sequence for *E. coli* expression. The picture shows the optimized sequence of *Sc*LPMO10 D, provided by GenScript.

MPAPSASRRAAAVAVAGLAPLALTTLAAAPASAHGSMGDPVSRVSQCHAEGPENPKSAACRAAVAAGGTQALYDWNGIRIGNAA
GKHQELIPDGRLCSANDPAFKGLDLARADWPATGVSSGSYTFKYRVTAPHKGTFKVYLTKPGYDPSKPLGWGDLDLSAPVATSTDPV
ASGGFYTFSGTLPERSGKHLLYAVWQRSDSPEAFYSCSDVTFGGDGDGDGDGGSGSGAATGDDTASGDAEAGAAPAPEASAPSEE
QLAAAAEKSTIEHHGHGDQDAATTTDPTDPAAAPEEAPGTAAEPHQVKAAGGGTENLAETGGDSTTPYIAVGGAAALALGAAVLF
ASVRRRATTGGRHGH

Figure A.2. Amino acid sequence of ScLPMO10D with altered signal peptide. The picture displays the amino acid sequence, in which the signal peptide (SP) derived from CBP21 is indicated with white background (residues 1-33), the catalytic domain is indicated by gray background (residues 34-214), and the truncated C-terminal domain including the linker region is indicated with white background and gray colored letters (residues 215-365). Notably, the naïve signal peptide of *Sc*LPMO10D is 34 residues long, which means that the residue positions referred to in this thesis (e.g. D74) will have positions of one number higher (e.g. D75) in the native enzyme, which exhibit the wild type SP.

Appendix B

Investigation the of surface charge and disulfide bridges of ScLPMO10D to better understand purification results.

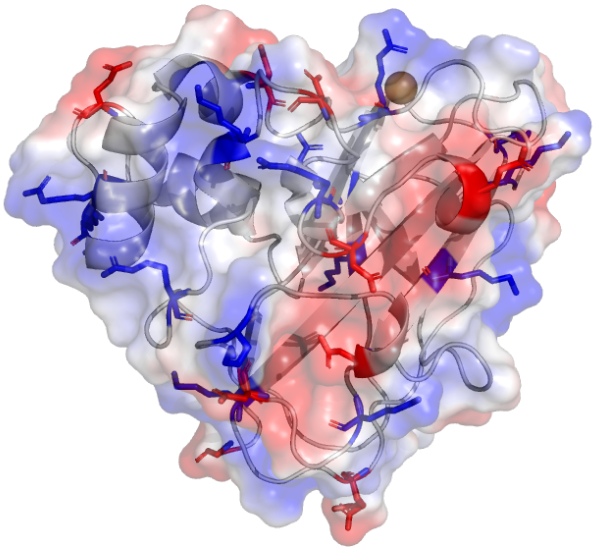

Figure B.1. Solvent exposed residues of ScLPMO10D which exhibit charge at pH 8-9.0. The figure was made in PyMOL, using the "Generate vacuum electrostatics" function to target all surface exposed residues that theoretically would contribute to the net charge at pH 8-9.0. Positively charged residues are colored blue; K56, R61, R79, K86, R95, K105, R111, K127, R129, K135, K139, K144, K151, and K189. Negatively charged residues are colored red; E53, D74, E89, D93, D101, D148, D157, E185, and the C-terminal G214. Notably, the NH_2 group of the N-terminal histidine was not included, as it would not be solvent exposed and further engaged in copper binding in the mature protein, at least according to the model investigated in PyMOL.

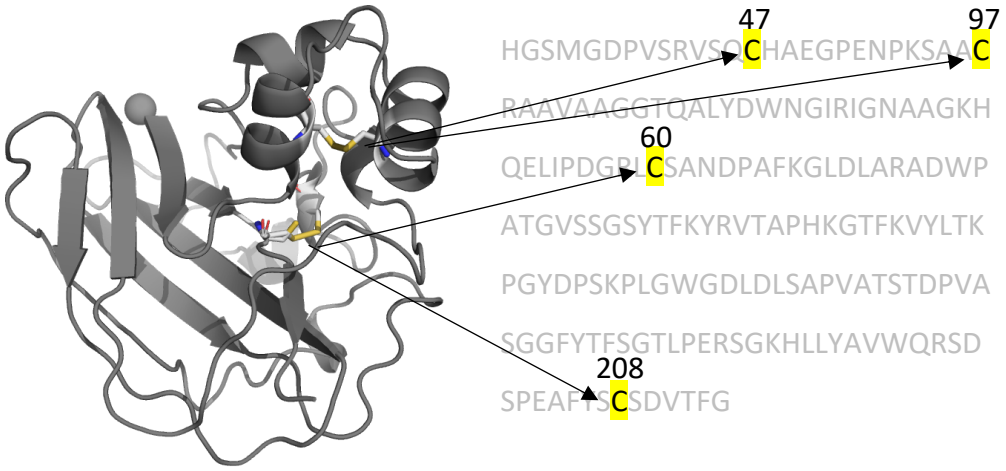

Figure B.2. Disulfide bridges of ScLPMO10D. As displayed in the picture, ScLPMO10D have two disulfide bridges. The first consists of the cysteine residues found in position 47 and 60, and the second, position 97 and 208. The first disulfide bond connects two alpha helices in loop 2, which are found relatively close to each other in the sequence. The second disulfide bond residues are over 110 residues apart and connects loop 2 to the beta-sandwich.

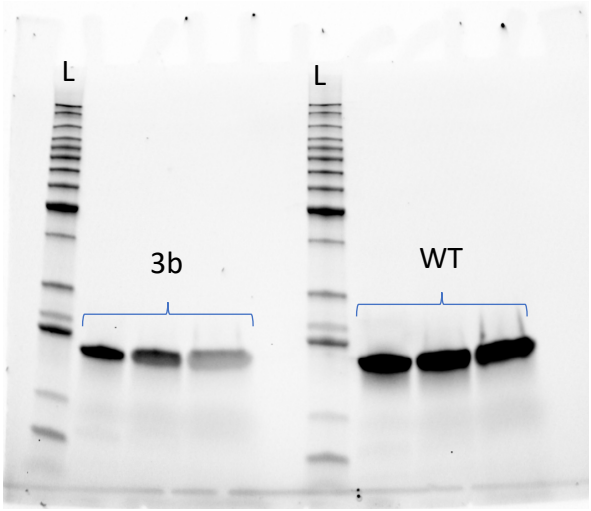

Figure A.3 SDS-PAGE analysis of ScLPMO10D, 3b and wild type (WT). An analysis of purified protein were conducted with freshly prepared LDS sample buffer. Here, both the dimer (40 kDa) and the additioal band previously observerd right above the target enzymes is abcent. Three samples were prepared with different concentration of enzyme relative to sample buffer, with a increasing propotion of LDS sample buffer from left to right (i.e. 1:5, 1:3, and 1:2 ratios of LDS to protein solution).

Norges miljø- og biovitenskapelige universitet
Noregs miljø- og biovitskapelege universitet
Norwegian University of Life Sciences

Postboks 5003
NO-1432 Ås
Norway